UNIVERSITY OF OKLAHOMA

GRADUATE COLLEGE

A DECISION-FRAMEWORK FOR BUILDING PORTFOLIOS TOWARDS ENHANCED RESILIENCE AND SUSTAINABILITY OF COMMUNITIES UNDER NATURAL HAZARDS

A DISSERTATION

SUBMITTED TO THE GRADUATE FACULTY

in partial fulfillment of the requirements for the

Degree of

DOCTOR OF PHILOSOPHY

By

YINGJUN WANG
Norman, Oklahoma
2019

A DECISION-FRAMEWORK FOR BUILDING PORTFOLIOS TOWARDS ENHANCED RESILIENCE AND SUSTAINABILITY OF COMMUNITIES UNDER NATURAL HAZARDS

A DISSERTATION APPROVED FOR THE
SCHOOL OF CIVIL ENGINEERING AND ENVIRONMENTAL SCIENCE

BY

Dr. Naiyu Wang, Co-chair

Dr. Kanthasamy Muraleetharan, Co-chair

Dr. Deven Carlson

Dr. Yang Hong

Dr. Philip Scott Harvey

Prof. Kathrina Simonen

I dedicate this research to my family for their love and support

Acknowledgements

I would like to express my deepest gratitude to Dr. Naiyu Wang, for her endless support and warm encouragement throughout my journey of Ph.D. study. Her keen insight in research areas, enthusiasm in work, and invaluable guidance have had a fundamental influence in my studies at OU and my future career. I also would like to express my gratitude to Dr. Kanthasamy Muraleetharan, for his outstanding insights, thoughtful advices and kind guidance. I am so grateful for their tremendous help and guidance and have been so fortunate to have them as my advisors. Without them, I would not have finished my Ph.D. study and written this dissertation.

I would like to express my appreciation to my committee members - Dr. Yang Hong, Dr. P. Scott Harvey, Dr. Deven Carlson (Political Science, OU), and Prof. Kathrina Simonen (Architecture, University of Washington) – for their insight, advice, and guidance from the beginning to the end of my Ph.D. study. My appreciation is extended to Dr. Bruce Ellingwood (Colorado State University), Prof. Kathrina Simonen, Dr. Hussam Mahmoud (Colorado State University), Dr. John van de Lindt (Colorado State University), and Dr. Amy Cerato for their thought-provoking discussions, fruitful collaborations in the U.S. National Science Foundation project as well as in the co-authored papers.

I also would like to thank my colleagues and fellow students for their support and friendship: Dr. Xianwu Xue, Dr. Jun He, Dr. Weifeng Tao, Dr. Fuyu Hu, Dr. Huiquan Miao, Dr. Peihui Lin, Dr. Weili Zhang, Mohammad Hadikhan Tehrani, Alexander

Rodriguez, Paul Calle Contreras, Dr. Changlong Chen, Shang Yan, Chen Xu, PoChun Huang, and Qian Wang.

Finally, I am truly indebted to my parents and other family members, their love and support are and would always be my harbor. I would also like to thank my wife Yuan for her love, patience, and sacrifice, and my son Leonardo for bringing so much joy.

The research is supported by the U.S. National Science Foundation (NSF) through Grant No. CMMI-1452708. This support is gratefully acknowledged.

Table of Contents

List of Tables

List of Figures

Abstract

In recent years, communities in the U.S. and other countries have experienced several catastrophic natural hazards (e.g. Hurricane Katrina in 2005 and the Christchurch Earthquake in 2011). The unproportioned social, political impact and economic loss from these events and the fact that such events will continue to occur have highlighted the vulnerability of typical communities, and more importantly, emphasized the significance of considering the performance of communities as a whole under extreme natural and man-made events over a long-time horizon. The physical built environment and the decision-making on them plays a critical role in determining the extent to which the community will perform immediately after the hazard events, the recovery trajectory afterward as well as the long-term financial health, environmental protection, and prosperity. Some communities in the U.S. began or about to implement large-scale, community-level engineering strategies. However, such strategies generally suffer from lacking quantitative support. While some studies have been done to explore the large-scale decision-making, they might be not sufficient to address the problem systematically. A uniform decision support framework for various strategies across different stages of infrastructure systems must be developed.

This dissertation focuses on developing a risk-informed decision-making framework for building portfolios under the threat of natural hazards, with particular emphasis on exploring optimal strategies supporting the engineering enhancement measures in different stages of building portfolios over their lifetime. In this study, three

categories of large-scale engineering strategies are discussed in depth: new construction, pre-hazard retrofitting, and post-hazard reconstruction that communities may adopt to enhance the performance of the residential building cluster, and thus the whole community in future hazards. Decision-making is explored under seismic and tornado hazards as examples and reveals that communities can and must make engineering decisions from the perspective of the resilience performance of communities and simultaneously consider the sustainability requirements (by employing the economic metric of life-cycle cost as an example). The study demonstrates that the resilience and sustainability goals could be achieved at the same time without compromising one or the other. The proposed decision-making framework could assist community leaders in designing mandatory/voluntary policies or financial incentives to let owners invest in an organized manner and collectively enable the community to achieve its pre-defined resilience and sustainability goals in the long-term.

Chapter 1 Introduction

1.1 Background and Motivation

Recent catastrophic natural hazards in the United States and around the world, e.g. Hurricane Katrina (2005), the Great East Japan Earthquake and Tsunami (2011), and Hurricane Sandy (2012), have highlighted the enormous socio-economic consequences of such extreme events on the highly developed and interconnected modern societies. Such consequences are anticipated to increase given the continued economic and population growth in hazard-prone regions. These impacts from natural hazards have raised concerns regarding the current system of hazard prevention and mitigation, that is, structural engineers analyze and design, retrofit, and reconstruct buildings to ensure life safety under rare hazards according to codes and standards which, however, usually do not include systematic community-level considerations on functionalities of community as a whole, let alone the calibration of the performance of communities against the anticipation of their stakeholders.

The *resilience* of a community is defined by its ability to adapt to changing conditions and to return to a level of normalcy within a reasonable time. The resilience of a community depends on the performance of the built environment and on supporting social, economic and public institutions which are essential for immediate response and long-term recovery within the community following a disaster (NIST, 2015b). The resilience of a community's building portfolio as a functionally integrated system, in particular, plays a critical role in mitigating the negative impact from natural hazards, promoting rapid

recovery, and supporting the sustainable development of the community (NIST, 2015b). The concept of resilience provides brand-new perspectives to community leaders, engineers, and other stakeholders for hazard preparedness and mitigation. To enhance the resilience of their building portfolios, communities can gradually implement voluntary or mandatory portfolio-level enhancement programs, such as elevated new construction requirements (Wang et al., 2018), retrofitting programs for existing building categories with poor performance before disasters (e.g. City and County of San Francisco, 2013; HCIDLA, 2015; FDEM, 2016) and reconstruction program for damaged buildings following a disaster. However, such large-scale plans often suffer from lack of quantitative measurements which link the extent to which the resilience performance gap (between current and target performance) being filled, and from the inconsistency between different enhancement plans. In addition, current community-level plans often do not have a perspective on long-term planning, thus miss the opportunity of balancing short-term resilience planning with the long-term sustainable development of the community.

On the other hand, *sustainability* aims at fulfilling the needs of the present generation without compromising the ability of future generations to meet their own needs (Brundtland 1987). More and more scientific studies have shown that the accumulation of greenhouse gas (GHG) from human activities since the industrial revolution has caused significant global warming and climate change, which could lead to re-distribution of precipitation and more severe climate-related hazards (e.g. Brooks (2013)). The concept of sustainability emerged at a time when the public and countries gradually realized the importance of the above-mentioned environmental issues, equity, and long-term

development. The built environment, especially the construction and operation of building portfolios, contribute significantly to the financial investment and environmental impact, therefore has attracted more and more attention from researchers, engineers, and decision-makers, who try to develop decisions based on sustainability indicators and sustainable development philosophy.

Resilience and sustainability ultimately should be inextricably linked and mutually reinforcing in engineering decision-making in a community (Czajkowski, 2015). Recently, some studies have attempted to unify the resilience and sustainability quantification for community's infrastructure systems due to their similarities in metrics (both include economic and social dimensions), scope, and ultimate goals (Padgett & Tapia, 2013; Bocchini et al., 2014). However, few attempts have been made to incorporate a quantitative and unified framework in decision-making involving community-scale, portfolio-level building new design, retrofitting, and reconstruction to fulfill both resilience and sustainability goals of the community.

Considering the unproportioned social and economic loss from hazard events, the extended time horizon of future hazard exposure, public's expectations on communities' functional performance under such events, there is an urgent need to develop a decision framework that can support portfolio-level, systematic new design, pre-hazard retrofitting and post-hazard reconstruction strategies that would enable communities to achieve a higher, pre-defined resilience performance goal as well as fulfilling requirement for sustainable development in the long-term. As an essential infrastructure system of a community, the performance of its building portfolio under various hazards is critical to its

hazard resilience. Generally, a community may achieve higher resilience in the long term by setting a higher design requirement for new constructions, retrofitting existing portfolio before hazard events, or strategically rebuilding damaged portfolio after hazard events. However, currently, there is no community level, systematic decision tool that can support these procedures.

1.2 Objectives, Scope and Assumptions

The overall aim of this Ph.D. research is to develop a risk-informed and unified decision-making methodology that could ultimately help a community achieve its pre-defined resilience and sustainability goals. This decision-making process will require a fundamental change to current engineering practices by adjusting the new design, pre-hazard retrofitting, and post-hazard reconstruction strategies. The intention is to assess the social and economic consequences from extreme events (related to Resilience) and in overall life-cycle (related to Sustainability) and to derive optimal decisions for building portfolios, in which the performance under rare hazard events are guaranteed and at the minimum life-cycle cost (or maximum value). To achieve the above objectives, the following tasks are to be conducted:

(1) Reviewing and critically appraising existing literature related to decision-making including community resilience, sustainability, and their relationship, hazard characterization and uncertainty propagation, life-cycle assessment under hazards, and multi-criteria decision making.

(2) Performing the hazard characterization for building portfolios according to the hazard type, and requirement of resilience and sustainability assessment.
(3) Investigating the propagation of uncertainties from hazard event generation, transmission, local amplification, building response, and damage.
(4) Assessing the performance of building portfolios under hazards for rare hazards events and for all events within the life-cycle in resilience and sustainability indicators.
(5) Identifying the minimum design requirement of new building construction from de-aggregating the resilience performance goals of building portfolios.
(6) Developing the retrofit strategy for the existing, vulnerable building portfolios prior to major hazard events with the aim to enhance future performance in terms of economic loss and social well-being.
(7) Developing the reconstruction strategy for the damaged building portfolios after major devastating hazard events from the perspective of the life-cycle measures of the building portfolio over the long term in the future.
(8) Implementing the proposed decision-making framework to testbed communities under different hazard types.

The assumptions for this study are:

(1) It is possible to quantify resilience and sustainability performances of a community, and it is possible to employ these measurements to identify optimal pre-hazard and post-hazard enhancement strategies for community building portfolios.

(2) While the resilience and sustainability performance of a community is collectively defined by its physical, social, economic, and political systems, as well as the interdependencies among them, in this study only the physical infrastructure system will be considered from an engineering perspective.

(3) It is not the focus of this study to pursue the absolute measurement of resilience and sustainability metrics of a community, rather this study will focus on quantifying the resilience and sustainability in a way that can support decision-making related to design, retrofit and reconstruction of building portfolios.

(4) While the concept of sustainability embodies ecological, economic, and social dimensions, this study will only explore the economic aspect of sustainability as economic metric is also connected with resilience.

1.3 Organization of Dissertation

The dissertation is organized as follows:

Chapter 2 appraises current literature on risk-informed decision-making related to civil infrastructures, including resilience, sustainability, and their unification, hazard characterization, life-cycle assessment, and multi-criteria decision-making methodologies.

Chapter 3 identifies the minimum design requirement for new building constructions through a risk de-aggregation algorithm. A new design philosophy is needed to support a communities' functionality preservation and quick recovery under extreme events. Thus, it is proposed that the performance target of individual buildings under hazards should be ultimately related to the resilience goal(s) of the community as a whole

in a quantitative manner. This task will invert the minimum performance objective for new building constructions by de-aggregating the community resilience goals expressed in terms of multiple metrics. Part of this chapter (new construction under tornado hazards) has been published in a journal paper (Wang et al., 2018), where I developed the methodology, performed the case study, and wrote the draft paper.

Chapter 4 develops a pre-hazard retrofit strategy for existing building portfolios. There is a growing trend in recent years for communities to implement large-scale community-level retrofit programs to enhance the resilience of under-performing community building inventories. Such community-level retrofit activities are expected to be common as more communities have started to incorporate resilience concepts in their strategic development planning. This task will seek to develop the portfolio-level retrofit framework that provides optimal retrofit strategies for enhancing a community's existing building portfolio before the hazard event. Part of this chapter has been published in a conference paper (Wang & Wang, 2017), where I developed the methodology, performed the case study, and wrote the draft paper.

Chapter 5 develops a post-hazard reconstruction strategy for damaged building portfolios. Following a catastrophic natural hazard, communities seek strategies to rebuild their severely damaged building portfolios, which can be opportunities to enhance their resilience and sustainability under future hazards. The large-scale investment and long-lasting impact of reconstruction practices require that the decision-making should be constructed on the analysis of the building portfolio over its whole life-cycle. A quantitative methodology is needed that could handle each of the phases that a building

portfolio need to face after a severe hazard event, and further provide decision support to best enhance the performance of the portfolio in future hazards. This task will propose a post-hazard reconstruction decision framework that can support Build Back Better based on portfolio level life-cycle analysis.

Lastly, Chapter 6 summarizes the major findings and conclusions of this dissertation as well as points out future research needs and possible directions.

Chapter 2 Literature Review

In this section, literature in relevant research areas is reviewed and arranged according to topics. A critical appraisal is given at the end to discuss research needs and, more importantly, to provide insights and the motivation for the present study.

2.1 The Concept of Resilience and Sustainability

2.1.1 Resilience

The word resilience derives from the Latin word *resilio* (the ability to rebound or spring back) (Klein et al., 2003), and its concept was firstly developed by researchers in the ecological study to describe how an ecological system withstand and recover from the external perturbations (Holling, 1973). Timmerman (1981) defined resilience as the ability of a system to withstand and recover from external shock or perturbation to the infrastructure. Such definition contains two key aspects: 1) resilience focuses on systems as a whole rather than individual components; 2) resilience does not only consider the ability to withstand shocks, but also the ability to recover from the disturbed state in a prompt manner.

In the context of the built environment under hazards, Bruneau et al. (2003) proposed four core properties of resilience: robustness, rapidity, redundancy, and resourcefulness. *Robustness* refers to the ability of an individual component or system to withstand the external pressure or distraction without physical damage or functionality loss. *Rapidity* refers to the ability of an individual component or system to recover

promptly from physical damage or functionality loss. *Redundancy* refers to the ability of an individual component or system to function as before after unprecedented events due to the inclusion of extra components or connections. *Resourcefulness* refers to the capacity to locate problems, setting plans, and organize material and human resources to implement the pre-defined plans and achieve goals.

Bruneau et al. (2003) also conceptualized resilience in four intercorrelated dimensions: technical, organizational, social, and economic. The *technical* dimension of resilience is defined by the ability of systems (including the individual components, sub-systems, and the interactions between components and sub-systems) to have an acceptable/appropriate performance under hazards. The *organizational* dimension of resilience is defined by the ability of organizations to manage the infrastructure system, make decisions, and take actions to enhance the performance of physical systems and achieve their pre-defined performance goals. The *social* dimension of resilience refers to specific measures that could reduce the extent to which the external hazard may bring negative outcomes (e.g. casualties and social disruptions) on the community due to the loss of functionality on critical services. The *economic* dimension of resilience is defined by the ability of systems to reduce the economic impact (both direct and indirect) under hazards.

Recently, the community planning guideline from National Institute of Standards and Technology (NIST, 2015b) defined community resilience as "… the preparedness of the community to include prevention of incidents, mitigation of risk, protection of assets, and pre-event planning for response and recovery". In sum, the concept of community resilience embodies a systemic approach towards hazard mitigation.

Thus, a holistic and interdisciplinary perspective is required to quantify community resilience. At the time of introducing the seismic resilience to civil engineering, Bruneau et al. (2003) proposed that the resilience performance of systems could be represented by the curve of Quality of infrastructure ($Q(t)$) over time, as illustrated in Figure 2.1. $Q(t)$ ranges from 0% to 100%, i.e. 100% and 0% corresponds to no degradation in service and no service available, respectively. Accordingly, the resilience of a community can be measured by loss of resilience, R

$$R = \int_{t_0}^{t_1} \big(100 - Q(t)\big) dt \tag{1}$$

where t_0 and t_1 denote the time of hazard event and complete recovery, respectively. Such definition of resilience could easily be appreciated by non-expert audience, however, it does not answer the question of how to measure the $Q(t)$ at the time immediately after the hazard event and the time to complete recovery as well as how to obtain the curve of $Q(t)$. Further, the loss of resilience measure, R quantified in this way is criticized for its lack of physical meaning and for hard to form the basis for developing trackable enhancement plans.

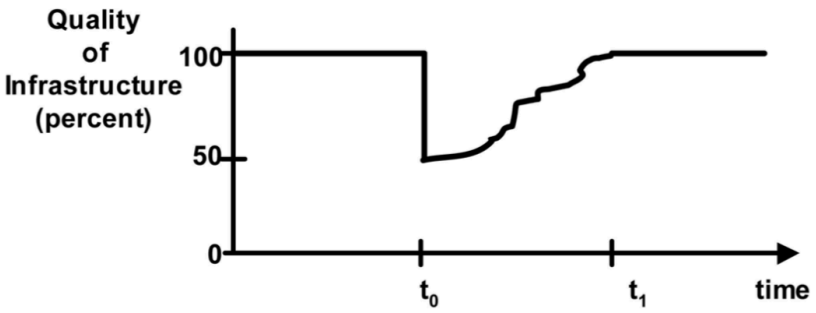

Figure 2.1: Measure of resilience—conceptual definition (Bruneau et al., 2003)

In the past decades, the focus of community resilience research in civil engineering has switched to the quantification of community resilience performance, the interdependency between sub-systems, and decision-making to relate the resilience gap (between goals and current state) with specific engineering enhancement strategies. It is generally agreed that the resilience of a community can be quantitatively described as the time-varying performance of certain community metrics (e.g. economic loss or recovery time) conditioned on interested hazard levels (e.g. a hazard with a 2500-year return period) or scenarios (e.g. the scenario that contributes most to a community's hazard risk). Generally, community resilience metrics can be categorized into three kinds: (1) recovery time, (2) economic metrics, and (3) social well-being metrics (NIST, 2015a). *Recovery time*, which provides a measure of how long an individual infrastructure or system is unfunctional or operates at reduced capacity (Lin & Wang, 2017), is selected as the major metric of community resilience by NIST guide (NIST, 2015b), SPUR (SPUR, 2009) and REDi (2013). *Economic-based metrics* measures how hazards affect the properties and economic activities of communities, including the direct and indirect economic loss, jobs,

tax base, poverty, and income distribution. (NIST, 2015a). Direct economic loss (e.g., structural and non-structural failure-induced repair cost) and indirect economic loss (e.g., cost due to the loss of functionality) are the most widely employed economic metrics.

Social well-being metrics reflect human needs, including survival, safety/security, sense of belonging, and growth/achievement. So far, systematic approaches are needed to define and quantify these social metrics. Some metrics reflect the combined effects of several basic resilience metric categories. For instance, the dislocation of the population is a complex social and economic process where the performance of infrastructures, social and economic demographic characteristics, the performance of other community services all affect the dislocation. Lin and Wang (2016) developed two dislocation related metrics: Immediate Occupancy Ratio (IOR) and Household Dislocation Ratio (HDR), where the former is the ratio of building portfolio that can provide safe occupancy immediately following a disaster and the latter is the ratio of total household displaced due to loss of housing habitability and short-term shelter needs. Figure 2.2 gives an example of system performance measures for a community with four key infrastructure elements: hospital, power, water, and local emergency management systems.

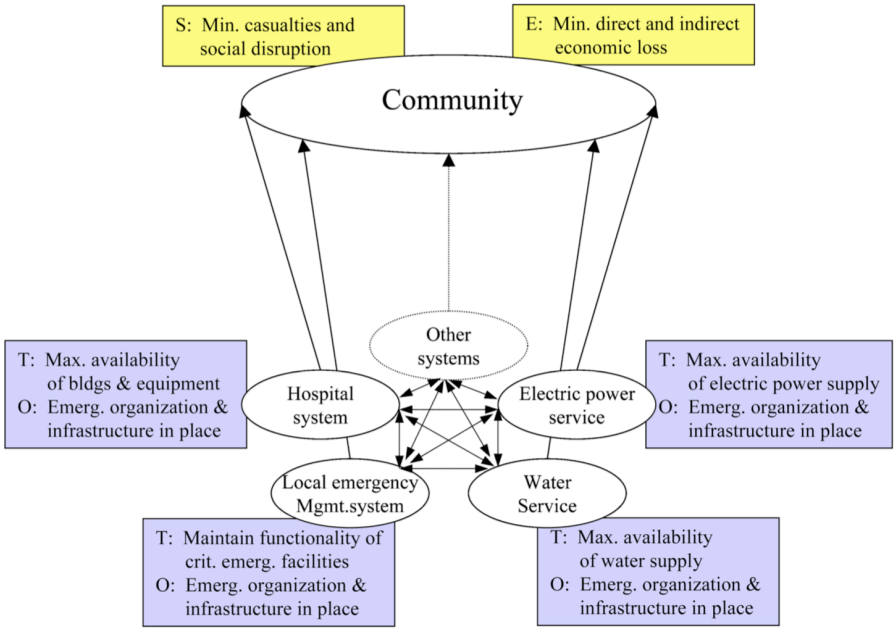

Figure 2.2: System and community performance measures in community resilience (Bruneau et al., 2003)

Another ingredient of community resilience definition is the selection of the appropriate hazard level(s) or scenario(s). Some frameworks assess and guide their resilience planning and enhancement based on specific hazard level(s). For instance, The NIST community resilience planning guideline encourages communities to select three hazard levels for resilience goals setting in terms of the hazard return period (NIST, 2015b), thus the performance of communities under different hazard levels can be addressed explicitly and communities can improve own resilience more confidently and economically. Typically for earthquakes and hurricanes, the return period of the three levels are selected as 50 to 100 years for the routine, 500 to 700 years for the expected, and 2500 to 3000 years for the extreme level (SPUR, 2009; REDi, 2013; ASCE, 2016). On the

other hand, some frameworks rest their methodology on specific hazard scenario(s) to assess and improve resilience, e.g. the SPUR Framework and the Oregon Resilience Plan. More discussion on hazard consideration will be provided in Section 2.2.

Various conceptual guideline and methodologies have been proposed to assess communities' resilience. HAZUS (FEMA/NIBS, 2003) is a standard natural hazard risk assessment methodology developed by FEMA that incorporates a geographic information system (GIS) to quantify the impact from multiple hazards (including earthquake, wind, flood, and tsunami) to communities' physical infrastructures, economic development, and social structure within the U.S. HAZUS focuses on assessing the direct and indirect impacts immediately after natural hazards with less consideration in the post-hazard functionality recovery. Though HAZUS includes modules for multiple hazard types, it cannot analyze the true risk of communities threatened by multiple hazards. Nevertheless, HAZUS's detailed database and scientific analysis framework form the basis for other sophisticated research. Some frameworks assess the community resilience from multiple indicators that combine the basic socioeconomic character of the community, the possible hazard scenarios, and the anticipated functionality loss and recovery time given by experts and government agencies. For instance, UNISDR Disaster Resilience Scorecard for Cities (Williams et al., 2014) helps cities recognize their resilience performance under natural hazards and forms the basis for developing future investment plan from a resilience scorecard system, where sub-indicator scores are aggregated by weighted sum method to obtain scores in each dimension. Similarly, the City Resilience Index (CRI) (Arup, 2014), developed by Arup and funded by Rockefeller Foundation 100 Resilient Cities initiative,

includes 4 categories, 12 key indicators, and 52 basic indicators. It integrates economic, social, and physical aspects and considers the human-driven factors as a key component. CRI is not hazard specific, rather, it provides an insight into the performance of cities under external pressure as well as facilitates the planning process. Some frameworks evaluate communities' resilience based on statistical data. For example, Baseline Resilience Indicators for Communities (BRIC) is an empirically-based assessment framework (Cutter et al., 2010), which employs 49 metrics from 6 areas (social, economic, housing and infrastructure, organization, community capital, and environment). BRIC evaluates the overall resilience performance of communities based on publicly accessible census data, other than the assessment of performance under hazards.

Zhang et al. (2018) proposed a framework for probabilistically assessing the post-hazard building portfolio functionality loss, in which, the functionality of buildings is affected by both the damage of buildings themselves and the availability of utility systems. The disruption of the utility system in their study considers the interdependenc of power and water network system. Cutler et al. (2016) proposed a dynamic spatial computable general equilibrium (DSCGE) model that integrate both the engineering and economic models to assess the economic, demographic, and fiscal impact of disasters. The detailed dynamic economic-wide effects are simulated with consideration of infrastructure physical damage and adjustment of the economic behavior of agents. Lin and Wang (2017) proposed a simulation-based, stochastic post-hazard building portfolio recovery model, where the functionality state transformation of an individual building over time is modeled by a discrete state, continuous time Markov Chain. The recovery model can predict the

recovery time as well as the recovery trajectory of a community building portfolio after an earthquake scenario. The effect of building portfolio pre-hazard retrofitting as well as the insurance coverage on the recovery process are considered. Masoomi and van de Lindt (2017) proposed a methodology to assess the infrastructure functionality loss and restoration under tornado hazard. Their study models water network, power network, school buildings, residential buildings, and business considering their spatial distribution and dependency.

Other notable assessment frameworks include PEOPLES (Cimellaro et al., 2016), SPUR framework (2009), and Oregon Resilience Plan (OSSPAC, 2013).

2.1.2 Sustainability

Literally, sustainability implies the ability to sustain, maintain, and continue previous status, condition, and relation (Kajikawa, 2008). The earliest contents on sustainability appeared at the beginning of the 20th century together with the environmentalism (Pepper, 2005). The discussion of sustainability emerged in the 1970s and 1980s when the issue of environmental pollution and resource consumption related problems became more and more inevitable. Meadow et al. (1972) asserted that the world economy will fail in the next 100 years if the development pattern at that time remains and no additional interventions are made, after analyzing the world economic growth and consumption of resource at that time. The Brundtland report (United Nations World Commission on Environment and Development, UNWCED) (Brundtland, 1987), for the first time in history, gave the definition of sustainable development-"the needs of the present without compromising the ability of future generations to meet their own needs" -

and how it might be achieved. Sustainability is frequently related to the policy discussion and decision in the political context as a way of addressing the increasing pressure on environment pollution, resource consumption from economic growth within and between countries all over the world, especially after the publication of the Brundtland report. For instance, United Nations Framework Convention on Climate Change in Kyoto in 1997 (UN, 1998) determined obligatory targets for each country in limitation of environmental impacts, e.g. reduction of CO_2 emissions in the following decades. Some scholars suggested that sustainability has the just and equality in its meaning, and sustainable development is the one that combines economic growth, environmental protection, and social equity (Agyeman et al., 2002). The social equity here includes equity in different groups/countries as well as equity in inter-generation (Rackwitz et al., 2005; Nishijima et al., 2007; Lee & Ellingwood, 2017).

Sustainability can be measured in three dimensions: economy, ecology, and society, each can be further measured by one or more lower-level related criteria or indicators (Otto, 2007). A conceptual categorization is illustrated in Figure 2.3. To quantify infrastructures' sustainability performance, considerable assessment methodologies have been proposed. One category of methods assess sustainability performance based on rating. The British Building Research Establishment Environmental Assessment Method (BREEAM) system (BRE, 2010) launched in 1990, is the first sustainability rating system for buildings. The American Leadership in Energy and Environmental Design (LEED) system (USGBC, 2012), published in 1998, is applicable to individual buildings, multiple buildings, and communities. BREEAM and LEED are the

most widely accepted green building rating system in the world. Both BREEAM and LEED have a strong focus on the environmental issues, while in German DGNB system (GCSB, 2009) sustainability is quantified more broadly and holistically. All of these assessment methodologies employ pre-defined weights to combine indicators in the lower level to upper-level indicators. Such simplified aggregation, although necessary for practical use by consultants and decision-makers, causes difficulties in explaining the meaning and in advising enhancement decisions.

Rating-based methods cannot directly measure the absolute impact of a building or an infrastructure. On the other hand, Life-cycle assessment (LCA) (ISO, 1997) could quantify the impacts associated with a product or building throughout its life (from cradle to grave). When applying to buildings, LCA typically considers multiple phases of the life-cycle from construction to service to demolishment. LCA could help: 1) identify the critical phases of a product or building's life-cycle that improvement can be made; 2) make decisions to select the alternative with lowest impacts throughout life-cycle; 3) select relevant performance indicators; and 4) market the product/building (e.g. environmental claim, ecolabelling). Initially developed for quantifying environmental impacts, however, LCA's scope can be extended to economic and social aspects. More discussion on LCA will be given in Section 2.3.1.

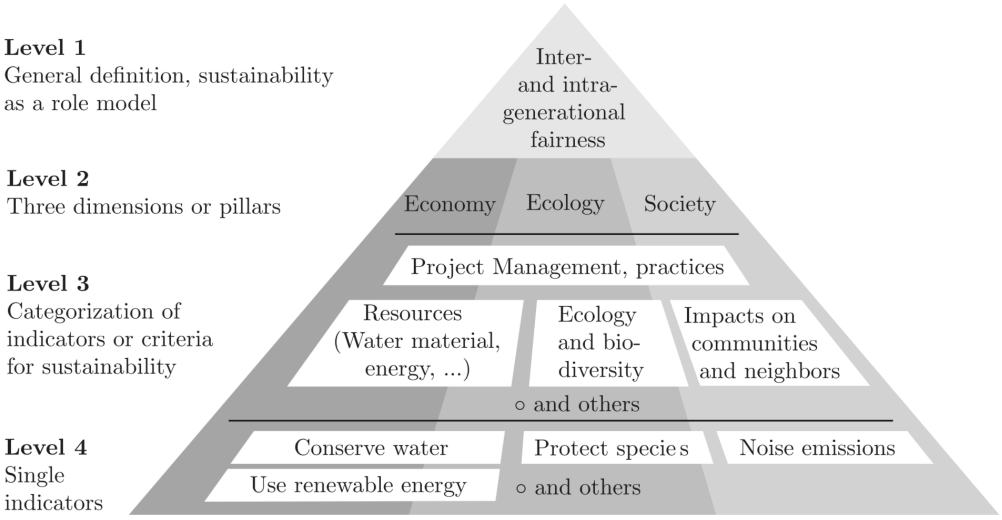

Figure 2.3: Aspects of Sustainability (Bocchini et al., 2014)

2.1.3 Unified Consideration of Resilience and Sustainability

The above literature review reveals that the concept of resilience and sustainability are developed from distinct motivations and backgrounds. *Resilience* relates to the performance of community under hazard events and the ability to withstand unprecedented impacts and recover rapidly from it, while *Sustainability* concerns the long-term cumulative impact of a single structure or project, with emphasis on the impact to environmental aspects and long-lasting effects. However, some similarities could be found between these two concepts (Bocchini et al., 2014). Both resilience and sustainability (1) can deal with the infrastructure system; (2) take a holistic point of view on the infrastructure system; (3) contain social and economic aspects; (4) try to optimize the civil engineering system and support decision-making.

Some studies and reports have made tentative progress to unify resilience and sustainability through the LCA. For example, Ghosh et al. (2011) proposed a life-cycle energy assessment (LCEA) approach that takes into account the embodied energy from hazard exposure in the LCA of bridges by considering the hazard occurrence probability. Rose (2011) selected several sustainability indicators in the post-hazard rehabilitation measures to achieve resilient and sustainable infrastructures. The Report Card on American's Infrastructure defined resilience and sustainability together as one of the three key factors to enhance infrastructures' performance and grade (ASCE, 2013). Bocchini et al. (2014) provided a detailed review of the concept of community resilience and sustainability, and further proposed a unified approach to combine these two concepts in the well-established risk assessment framework. Padgett and colleagues (Padgett & Tapia, 2013; Padgett & Li, 2014) developed a Life-cycle Sustainability Analysis (LCS-A) framework that can consider the role of natural hazard risk on the sustainability assessment of bridges and buildings and emphasized the importance of disaster resilience and sustainability in the structural design. They extended the metrics of traditional performance-based engineering paradigm to embodied energy, CO_2 emission, human casualties, and functionality downtime besides the monetary cost.

2.2 Hazard Characterization

A major challenge of community-level resilience assessment and decision-making lies in how to characterize natural hazards, specifically at the community scale. Hazard characterization refers to how the spatial and temporal characteristics of the hazard are

modeled and how the uncertainties involved are properly addressed. Two types of natural hazard will be considered in this research, i.e. seismic and tornado hazards; existing methodologies in literature will be discussed and grouped for earthquakes and tornadoes, respectively.

2.2.1 Seismic Hazard

Seismic hazard is one of the major natural hazards in the U.S. and many other countries in the world. Among various earthquake characterization approaches, scenario-based methods have been widely employed by researchers in recent years in community resilience assessment and decision-making. In scenario-based methods, the ground motion field and corresponding assessment are derived from pre-defined one (or few) scenario(s) described by magnitude and location, which is usually obtained from probabilistic seismic hazard analysis (PSHA) followed by a hazard de-aggregation (McGuire, 2004). The scenario-based methods are comparable to the deterministic methods in quantifying the design ground motion in traditional risk-assessment and design of a single building/facility (ASCE, 2016). However, in scenario-based methods designed for resilience study, the emphasis is usually given in modeling the spatial correlation of ground motion field, which is essential for the analysis of spatially distributed systems, such as building portfolios, utilities, and transportation networks and the interdependency between systems. Scenario-based method is the dominant in current community resilience studies, including resilience planning (e.g. SPUR, 2009), pre-hazard retrofit (Zhang et al., 2016), functionality loss assessment (Zhang et al., 2018), and post-hazard recovery (Bocchini & Frangopol, 2010; Lin & Wang, 2017; Zhang et al., 2017). However, scenario-based methods lack

information on the true risk under these scenarios, in which case the following resilience analysis and optimal decisions could be very sensitive to the initial selection of the scenario(s). An example of scenario-based characterization in the seismic hazard is illustrated in Figure 2.4.

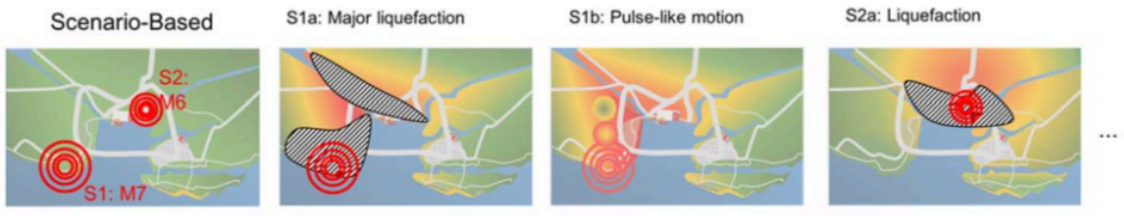

Figure 2.4: Scenario-based approach in characterizing seismic hazard (ASCE IRD, 2017)

By contrast, intensity-based methods quantify the potential impact on the community functionality under any event of a specific level of ground motion metric (e.g. peak ground acceleration, PGA with 10% exceedance probability in 50 years) in community scale (NIST, 2015b). They can explicitly represent the ground motion in probability form and consider the spatial variation and correlation of ground motion within the community. The target ground motion level (e.g. PGA) is found by making the exceedance probability of (mean) ground motion metric equal to some probability level (e.g. 10% in 50 years). These targeted ground motions can be employed as the input of resilience-based pre-hazard design and retrofit of buildings/facilities. It is comparable to the Probabilistic Seismic Hazard Analysis (PSHA) in treatment of ground motions, where the final product is the probability distribution of ground motion metrics and the combined response spectrum of single-site (McGuire, 2004), while in intensity-based method, the

final product is a set of correlated ground motion fields for a group of geological closed-related sites in a community. The intensity-based methods are recommended in ASCE IRD report (ASCE IRD, 2017), however, currently few studies have employed the intensity-based method, due to the complexity and computational cost in deriving the ground motion fields and application in resilience analysis.

Regarding the temporal characteristics, the occurrence of seismic events traditionally has been modeled as a Poisson process, and the inter-arrival time as an exponential distribution (e.g. Ellingwood & Wen, 2005; Gencturk et al., 2016;), which imply that the occurrence rate of earthquakes distributes evenly by time. However, historical records analysis (Wesnousky, 1994; Tuttle et al., 2002) along with the elastic rebound theory (Reid, 1911) suggest that the occurrence of earthquakes in a certain seismic source is related to previous seismic history. *Characteristic earthquake model* states that individual fault (segment) periodically generates earthquakes with near maximum magnitude (typically within one-half to one magnitude unit), while small to moderate earthquakes occur near randomly in time. For the New Madrid Seismic Zone (NMSZ) (Toro & Silva, 2001; Hebden & Stein, 2009) as well as the most active faults in California (Petersen et al., 2007) and Japan (Ishibe & Shimazaki, 2012), large-magnitude earthquakes can be modeled as *characteristic earthquake* (CE). Various non-Poisson hazard models (NPHM) have been proposed, for example, Semi-Markov model (Anagnos & Kiremidjian, 1984), Markov renewal model (Kiremidjian & Anagnos, 1984), and Brownian Passage Time (BPT) model (Matthews et al., 2002).

2.2.2 Tornado Hazard

Tornado hazard is significant in the Central U.S. (Goliger & Milford, 1998) and has a disproportionate impact on low-rise residential buildings in wood frame structures (Maloney et al., 2018). Tornadoes cause, on average, 70 deaths annually in the U.S. (NOAA, 2015) and $1 billion in economic losses (Changnon, 2009). For instance, tornadoes have brought $2.92B, $2.56B, and $2.09B direct economic loss and 72, 162, and 25 fatalities to Joplin (2011), Tuscaloosa (2011), and Moore (2013) respectively.

During a tornado event, the wind speed near the tornado vortex center is very high (>200 mph for an EF-5 tornado) (Texas Tech University, 2011), yet the wind speed close to the edge is relatively lower. Further, for a specific site, the annual occurrence probability of tornadoes is very low, in the order of $10^{-6} \sim 10^{-4}$ depending on the location (Reinhold & Ellingwood, 1982; Standohar-Alfano & van de Lindt, 2014). The Low-probability/High-consequence (LPHC) nature of the tornado hazard poses a significant challenge in characterizing the hazard itself and assessing the risk of individual buildings, communities, and regions.

Over the past decades, some notable research has been done on modeling the tornado risk for regions across the U.S. For instance, Reinhold and Ellingwood (1982) proposed a methodology that considers the variation of intensity along the path of tornado to evaluate the tornado risk for the design of nuclear structures across broad regions in the U.S. The classification and random errors from misclassification of tornado's intensity are considered. Similarly, Schaefer et al. (1986) developed a tornado risk contour for the entire U.S. in terms of Fujita-scale (F-scale) intensity. However, their hazard assessment fails to

consider the variation of intensity along the tornado path length and path width, resulting in an overestimation of tornado hazard. Recently, Standohar-Alfano and van de Lindt (2014) incorporated the methodologies from Reinhold and Ellingwood (1982) and Schaefer (1986) to generate the empirically-based probabilistic tornado hazard for the U.S. in terms of EF-scale from historical data. They proposed a gradient model for tornado path by estimating the percentage of damage area associated with each Enhanced Fujita-scale (EF-scale) (Texas Tech University, 2011). The wind speed given a certain EF-scale is assumed to be normal distribution due to the lack of sufficient database on the statistics of tornado wind distribution for each EF-scale. It is argued that the normal distribution can capture the classification error associated with the subjective definition of tornado intensity in terms of EF-scale (Lu, 1995). However, the wind distribution model may be modified easily whenever sufficient data is available. The above-mentioned methodologies are designed for generating tornado wind speed for a specific site, the spatial correlation of wind speed fields over a geological space under a tornado event is not properly addressed.

2.3 Analysis and Decision Approaches

2.3.1 Risk De-aggregation

De-aggregation is a common tool in Probabilistic Seismic Hazard Analysis (PSHA), which identifies the contribution of each combination of epicenter distance, magnitude, and epsilon to overall seismic risk (McGuire, 2004). In the field of risk-informed decision-making in engineering, risk de-aggregation was first developed in the nuclear industry to design, analyze, and regulate components within the complex nuclear

power plant to ensure consistent reliability level (IAEA, 2009). It starts from the plant level functionality/reliability target and derives targets for supporting systems and eventually individual components. Mieler et al. (2015) introduced the de-aggregation idea to link the community resilience goals to performance targets for individual components by event tree. The outcome of the framework is the target failure probability of individual buildings under a 500-year earthquake. Lin et al. (2016) proposed a de-aggregation framework that relates the community-level resilience target and individual building performance target by considering the correlation between buildings' performance due to location closeness and similar construction practices.

2.3.2 Life-cycle Analysis

Initially developed for tracking the environmental impact of industrial products (Hunt & Franklin, 1996), life-cycle analysis, aka. life-cycle assessment, (LCA) provides a rigorous tool to support decision-making for products or engineering projects over a long time horizon (e.g. Estes & Frangopol, 1999; Wen & Kang, 2001; Ellingwood & Wen, 2005), and is often measured in terms of the monetary cost (e.g. Bocchini et al., 2014) or the environmental footprint (Carbon, Water etc.) (e.g. Padgett & Tapia, 2013) of a project during its service life. Generally, LCA measures the sum of quantities of all phases within the life-cycle of a product or building in terms of same units (Padgett & Tapia, 2013)

$$LCA(\boldsymbol{X}) = S_{ra}(\boldsymbol{X}) + S_{tf}(\boldsymbol{X}) + S_{p}(\boldsymbol{X}) + S_{c\_i}(\boldsymbol{X}) + S_{c\_r}(\boldsymbol{X}) + S_{op}(\boldsymbol{X}) + S_{m}(\boldsymbol{X}) + S_{h}(\boldsymbol{X}) + S_{d}(\boldsymbol{X}) \quad (2.1)$$

where LCA denotes the life-cycle indicator; S_{ra}, S_{tf}, and S_p, together form cradle-to-gate phases, denote the indicators from raw material acquisition, transportation, and production, respectively; S_{c_i}, S_{c_r}, S_{op}, S_m, S_h, and S_d, together form the gate-to-grave phases, denote the indicators from initial construction, retrofitting, operation, maintenance, future hazard exposure, and demolition phases, respectively. Vector $\boldsymbol{X}$ denotes a group of design parameters.

For cases where more than one indicator is employed, two solutions may be considered, i.e. 1) keep these indicators and employ a multi-criteria decision-making; 2) convert all indicators into monetary or utility (value) terms. While it is still controversial to convert social and environmental consequences into monetary items (Turner, 1992; Ayres et al., 1998), such transformation could greatly facilitate the quantification and the following decision-making. As a simplified version of LCA, the life-cycle cost (LCC) based approach (i.e. minimum expected LCC, in the presence of uncertainties) has been widely applied to optimize the initial design of buildings (Wen & Kang, 2001), pre-hazard retrofit, and post-event reconstruction of bridges (Tapia & Padgett, 2013) exposed to environmental effects (e.g. corrosion) or natural hazards (e.g. earthquakes and hurricanes). While this approach is well-accepted for engineering decision-making, other decision models have been developed to reflect the fact that decision-makers often find it difficult or impossible to monetize risk. Among these models, cumulative prospect theory (CPT) (Tversky & Kahneman, 1992) maps occurrence probabilities and economic consequences into perceived probabilities and values, respectively to reflect the non-linear reception of

probability and value from different decision-makers. Notably, it is ideal to apply in infrastructures exposed to natural hazards as it emphasizes low-probability/high consequences (LPHC) events and de-emphasis high-probability/low consequences (HPLC) events to reflect the risk-aversion of typical decision-makers. CPT has been successfully discussed in civil engineering decision-making in new construction and retrofit applications (e.g. Goda & Hong, 2008; Cha & Ellingwood, 2012).

2.3.3 Multi-criteria Decision Making

Traditionally, decision-making problems are formulated as choosing the best alternative among others or optimizing the design parameters concerning one criterion/objective. However, in reality, we are typically faced with solving decision-making problems under multiple criteria/objectives. In general, there are two categories of decision-making problems in civil engineering risk management: i) choosing one or more alternatives from available options, i.e. multi-attribute decision making (MADM) (Hwang & Yoon, 1981) and ii) designing unknown or undefined prototypes by changing their parameters based on the multiple goals set by the decision makers, i.e. multi-objective decision making (MODM) (Sen & Yang, 1998).

Specifically, for MODM problems, a multi-objective optimization (MOO) is appropriate to address this situation. In the MOO, the Pareto Front approach is often employed to explore the tradeoff surface between different objectives and yield a set of optimal solutions. While traditional operation research approaches such as dynamic programming (Bellman, 1954) and weighting approach (e.g., Saaty, 1977) can obtain the Pareto front, they are not designed for multi-objective application and are generally

inefficient. By contrast, modern heuristic techniques based on population search/optimization such as evolutionary algorithms (EAs) (e.g., NSGA-II (Deb et al., 2001)) and swarm intelligence techniques (e.g., MOPSO (Reddy & Kumar, 2007)) could consider the complex trade-off between several criterions in its function directly.

2.4 Critical Appraisal

Several research needs have been identified through the literature review:

1. The tremendous social, economic, and political impacts on communities from natural hazards demand effective engineering decision-making regarding the communities' building portfolios over different stages of its lifetime, i.e. new construction, retrofitting, and reconstruction. While studies on each of the subject might be abundant, there is no existing decision-framework that can provide a unified approach to enable systematic implementation of new construction, pre-hazard retrofitting, and post-hazard reconstruction of building portfolios in a community in a consistent manner to facilitate communities to achieve their resilience and sustainability goals.
2. Although resilience and sustainability ultimately should be inextricably linked and mutually reinforcing in building portfolio decision-making, they are not at the present time. While a few preliminary attempts have been made to unify these two dimensions in decision-making regarding retrofit and construction of individual structures or engineered facilities, no research has been done to develop, to the best

knowledge, systematically unified decision approach for a community building portfolio as a whole.

3. LCA has been widely applied to measure the overall environmental impact and economic cost of publicly-owned facilities and to provide a rigor basis for their life-cycle management. However, application of LCA to residential building portfolios has not been explored, let alone to form the basis for developers or owners to make decisions regarding design, retrofit, or reconstruction, mainly due to frequent ownership change and little financial incentives through insurance or tax policies. The missing of LCA has led to the failure in quantifying the impact of multiple hazard events in a planning cycle and in balancing the tradeoffs between pre- and post-hazard risk management strategies.
4. Codes have been traditionally developed by different organizations with different objectives and performance expectations. This lack of system perspective and coordination has led to a situation where the performance of individual buildings under demands from extreme natural hazards is not consistent within the performance expectations of the building portfolio as a whole. A fundamental change must occur, as a starting point, in the way that code and standard-writing groups approach the problem of stipulating design requirements for buildings from the community's current condition, resilience requirement, and preference. While some studies in risk de-aggregation have been done to quantitatively relate the individual building performance target with community resilience target, clearly-

defined minimum individual building performance criteria, which can be easily employed in the design of buildings, have yet to be developed.

5. Traditionally, design, retrofit, and reconstruction of individual buildings are mostly implemented by their owners. Implementing portfolio-level strategies will pose a significant challenge in coordinating actions in enhancing the resilience and sustainability of the community, among diverse ownership groups within the building portfolio. MADM and MODM have the potential to systematically address competing objectives in satiations where multiple stakeholders are presented. More studies are needed to explore the application of MADM and MODM in the decision-making problems in buildings portfolios.

2.5 Closure

This review identifies research issues associated with decision-making on building portfolios under natural hazards. The following chapters will address the portfolio level decision making for new construction, pre-hazard retrofitting, and post-hazard reconstruction, respectively. The aim of these studies is to develop a risk-informed decision-making framework that can support designing strategies for communities' building portfolios that consider not only functionality loss and prompt recovery under rare events (resilience) but also long term economic, social, and environmental efficiency (sustainability) in a systematic manner.

Chapter 3 Performance Criteria for New Constructions

Defining the performance criteria for new constructions is of importance as they not only form the basis for the design of new buildings, but also could guide the pre-hazard retrofitting of vulnerable buildings and the post-hazard reconstruction of damaged buildings. The new perspective from resilience performance in community-level suggests that the performance criteria implied by current design codes in the U.S. are unsound and inadequate.

This chapter begins with the introduction of the philosophy of Resilience-based Design (RBD) as compared to traditional engineering design philosophy. The concept of risk de-aggregation is then discussed regarding how it could help develop the performance criteria for individual buildings in a systematic manner that can be matched to the community's socioeconomic resilience goals within the RBD framework. Afterward, the definition of portfolio resilience goals is established, including three ingredients: resilience metrics, hazard characterization, and probabilistic statement of resilience goals. The risk de-aggregation under tornado and seismic hazard is then developed separately due to the distinction in hazard characterization and performance metric setting. This chapter will also discuss how various factors will affect the minimum performance criteria.

3.1 Resilience-based Design

Buildings, as other infrastructures, are traditionally designed according to the minimum requirement from design codes, guidelines, and regulations. The

disproportionate socioeconomic loss from catastrophic hazard events in recent years and the continuous increasing concern from community stakeholders (e.g. government agencies and residents) beg a high-level community planning focusing on the functionality of community as a whole under hazard events. This suggests that the engineering community need to shift their focus to community level to reduce direct and indirect loss, preserve the key functionality, and recover from an interruption in a prompt manner under natural or man-made hazards.

Communities in the U.S. have gradually realized the importance of considering community's performance as a whole and are urging to implement community-level, long-term resilience plans (e.g. San Francisco (SPUR, 2010)) aiming to prepare communities withstanding unprecedented natural and man-made hazards in future. However, those large-scale resilience plans generally lack quantitative measurements to link their resilience performance goals with the performance criteria of sub-systems and eventually of individual buildings.

In addition, a survey shows that the people in hazard-prone regions have high expectation on the performance of buildings/communities and are willing to pay the extra cost, given the tremendous break-through in civil engineering in the past decades and the growing hazard awareness. Ideally, buildings codes, which dictate the minimum design and construction level of buildings, should reflect the expectation of society and citizens on their performance (Porter, 2016). The inconsistency between the high-level community resilience expectation and low-level building design codes suggests deriving the performance criteria from community level rather than calibrate from previous codes and

shifting the design objective from ensuring Life-Safety (LS) to loss reduction, functionality preservation, and recovery promptness.

To achieve higher resilience performance of buildings, Porter (2016) suggested a simple seismic design method which employs an earthquake importance factor of 1.5, i.e. 50% stronger than LS minimum, in which case buildings could achieve 95% shelter-in-place objective for about 1% increase in cost. Masoomi and van de Lindt (2019) proposed a community resilience-based assessment and enhancement methodology, in which improvements are made if the performance gap between the existing community's overall recovery time and the pre-defined performance goal exists. However, the process is based on the specific and existing community, and to achieve specific performance goals, infinite decision combination could be made.

3.1.1 Current Design Codes and Guidelines

Current seismic design codes (e.g. ASCE-7 (2016)) generally concern preventing fatalities and injuries (Life-Safety, LS) related to building collapse under rare earthquakes, which does not necessarily guarantee the functionality of buildings in this and other hazard levels (Bertero & Bertero, 2004). Damage to the buildings are allowed under rare earthquakes, since remaining elastic was believed to be unnecessary and uneconomic (Housner, 1956). FEMA P-695 (FEMA, 2009) suggested a 10% exceedance probability of collapse under maximum considered earthquake (MCE). Luco et al. (2001) proposed a risk-targeted design procedure, which is adopted by ASCE-7, intended to provide a uniform 1% collapse probability in 50 years through risk-targeted MCE, MCE_R. Such 1% collapse probability in 50 years is back-calibrated from buildings designed under previous

seismic design codes (such as ANSI A-58 (ANSI, 1972)), which is further back calibrated (e.g. the work by Ellingwood et al. (1980)) ultimately from the first edition of Uniform Building Code in 1927. The performance level implied by the generations of seismic design code in the U.S. seems arbitrary and lack a rational background (Porter, 2016). Ellingwood et al. (1980) also addressed the low reliability of buildings under seismic load than under gravity load, however, little studies had been done on how to rationally define the appropriate performance level.

Further, in spite of the design requirements in current seismic design codes on structural and non-structural components, which are essential for preserving the functionality of buildings after seismic events, there is no explicit statement on their performance objectives nor the anticipated performance. Lastly, there is a lack of consideration on the performance of the building portfolio as a whole under hazard events.

Regarding tornado hazards, notably, there is no nationwide design code specifying additional requirement for structures under tornadoes in design codes, with the only exemption in the City of Moore, OK, which adopted residential building code that could withstand an EF2 tornado (City of Moore, 2014), however, such a requirement is not directly derived from community-level social, economic goals, and more studies are needed to investigate the community's performance in future hazards under this new code (Simmons et al., 2015).

In sum, the shortcomings of current design codes are:

1. Their aim is to ensure Life-Safety (LS) of occupants under rare hazards. Functionality preservation and loss reduction are either not considered or considered as a secondary by-product from fulfilling LS objective.
2. The performance objective is not defined in a top-down and rational manner from communities' own preference, rather it is obtained by back-calibration from previous design codes.
3. There is no explicitly quantitative statement of the performance objectives in functionality nor performance criteria for structural and non-structural components.
4. There is a lack of consideration on the performance of the building portfolio as a whole under specific hazard levels.

It should be noted that currently the low-rise residential building structures made of wood light-frame are not designed but constructed according to "conventional construction" provisions of building codes (FEMA/NIBS, 2003; IRC, 2015), which are further based on ASCE 7, however, to fulfill higher community resilience goals, a top-down design roadmap is indispensable. The purpose of the study in this chapter is to provide a rational basis in defining the performance level implied by design codes which will align with communities' resilience performance goals.

3.1.2 Proposed Resilience-based Design

Resilience-based Design (RBD) is defined as a design philosophy that considers functionality metrics at community-level as the primary performance objective, which also

forms the basis in deriving the performance requirement of individual buildings according to their occupancy type and importance in the performance of community as a whole.

For a specific community, as illustrated in Figure 3.1, RBD includes four steps: (i) defining the community level resilience goal by a diverse group of stakeholders, such government agencies, residents, engineers; (ii) upper-level de-aggregation (ULD) gives the performance requirement for each sub-system (e.g. building portfolio) from community resilience goal; (iii) lower-level de-aggregation (LLD) establishes the minimum performance criteria for individual components (e.g. buildings) from subsystem performance requirement; (iv) performance-based design (PBD) of individual components of each sub-system according to the previously obtained corresponding performance criteria. Among the steps, risk de-aggregations in step (ii) and (iii) are essential to obtain performance objectives for each sub-system and individual components and relate the RBD to current Performance-based Design (PBD). The risk de-aggregation framework will be discussed in depth in Section 3.2.

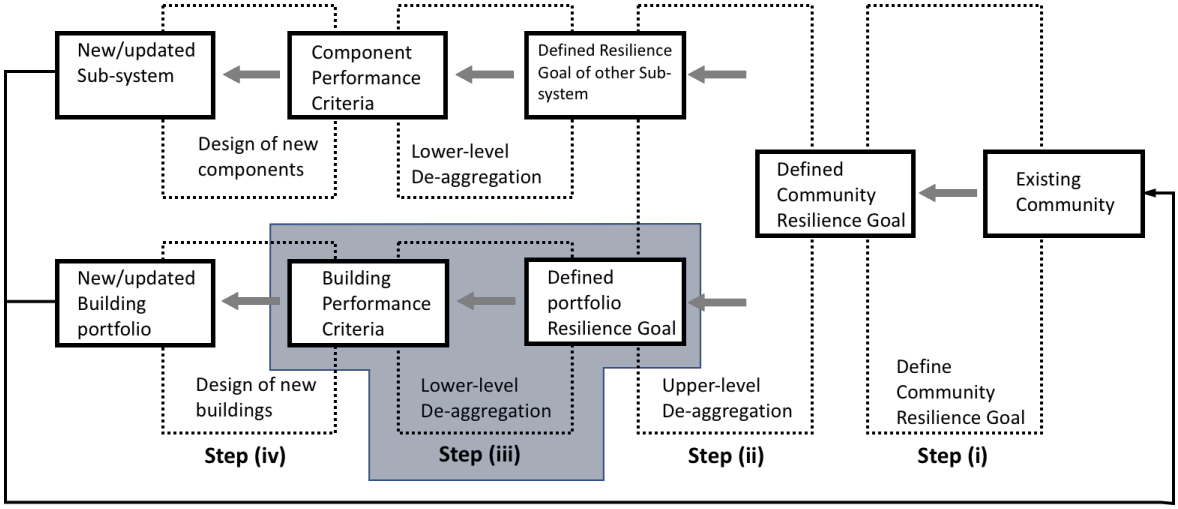

Figure 3.1. Proposed resilience-based design flowchart

Features of proposed Resilience-based Design (RBD)

1. Not LS, but metrics related to functionality and loss are considered as the major performance objectives for individual components (e.g. buildings) under specific hazard levels (see the illustration in Figure 3.2). Generally, the RBD will give higher performance level under specific hazard level.
2. The minimum performance requirement of individual components is derived from portfolio level resilience requirement (LLD), which is further derived from the community's resilience goals defined by community stakeholders (ULD).
3. There is an explicit statement of the performance objectives in individual components, subsystem, and community level expressed in probabilistic form conditioned on design hazard.

4. Communities those construct new individual components and subsystems according to RBD will eventually achieve their pre-defined performance goal under specific hazard level.

Taking the individual building level as an example, the comparison of the performance objectives of current code design and RBDs for individual buildings under seismic hazard is illustrated in Figure 3.2, which emphasizes the performance requirement on the Immediate Occupancy (IO) (will be discussed in Section 3.6.3) of each design method under various hazard level. To be consistent with current seismic design codes (e.g. ASCE 7-16), the occasional, design, and maximum considered hazard are defined as ones with the return period of 72 years, 475 years, and 2475 years, respectively. The details of hazard characterization will be discussed in Section 3.5.2 and 3.6.2 for tornado and seismic hazard, respectively. In the example given in Figure 3.2, buildings following current codes are estimated to be in Restricted-Use state, while buildings following Basic/Enhanced IO-based design will achieve Re-occupancy/Baseline functionality under Design Earthquake (DE). It should be noted that for current design code, Restricted-Use is given approximately since no explicit functionality performance goal, but LS is given in those codes for DE.

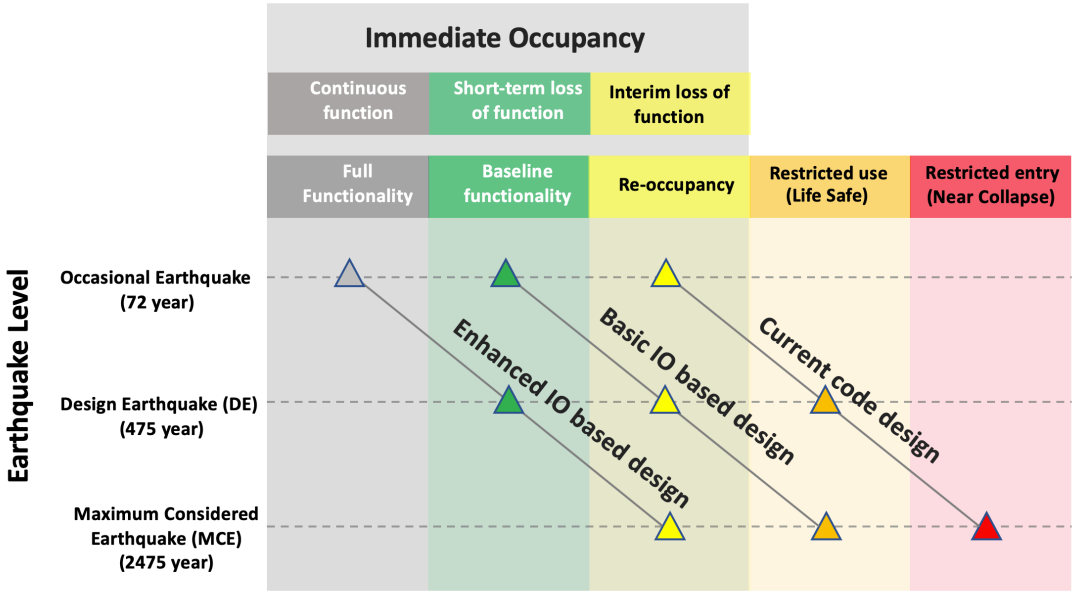

Figure 3.2 Example performance objectives for resilience-based design (metric: Immediate Occupancy (IO)) and that for current code design (approximate)

3.2 Risk De-aggregation Framework

This section will introduce a path forward towards developing performance-based design (PBD) requirements for the built environment aimed at achieving community resilience goals. Specifically, it seeks to transform resilience goals articulated for the whole community into requirements that are practical to implement from an engineering perspective. It will be shown that at its highest level, resilience-driven PBD begins with community resilience goals expressed in terms of social and economic metrics. These goals are then used to differentiate subsystem performance objectives for a spectrum of building clusters and lifeline systems, and ultimately lead to PBD criteria for individual buildings of different occupancies and for system components of lifelines. The overarching aim is to relate engineering design and practices to socioeconomic

performance expectations and to provide a vehicle for risk-informed decision-making in natural hazard events.

The resilience of a community is supported by its physical infrastructure, as illustrated in Figure 3.3. Community resilience assessment (Section 3.4) requires bottom-up, multi-layered analysis at different spatial and temporal resolutions. First, it estimates the performance of individual infrastructure components (e.g. buildings). It then ***aggregates*** the performance of these individual structures on spatial and temporal scales to obtain the performance of the community's physical subsystems - building clusters and infrastructure networks - which are then further ***aggregated*** with the socioeconomic attributes of the community to obtain overall measures of community resilience as a whole.

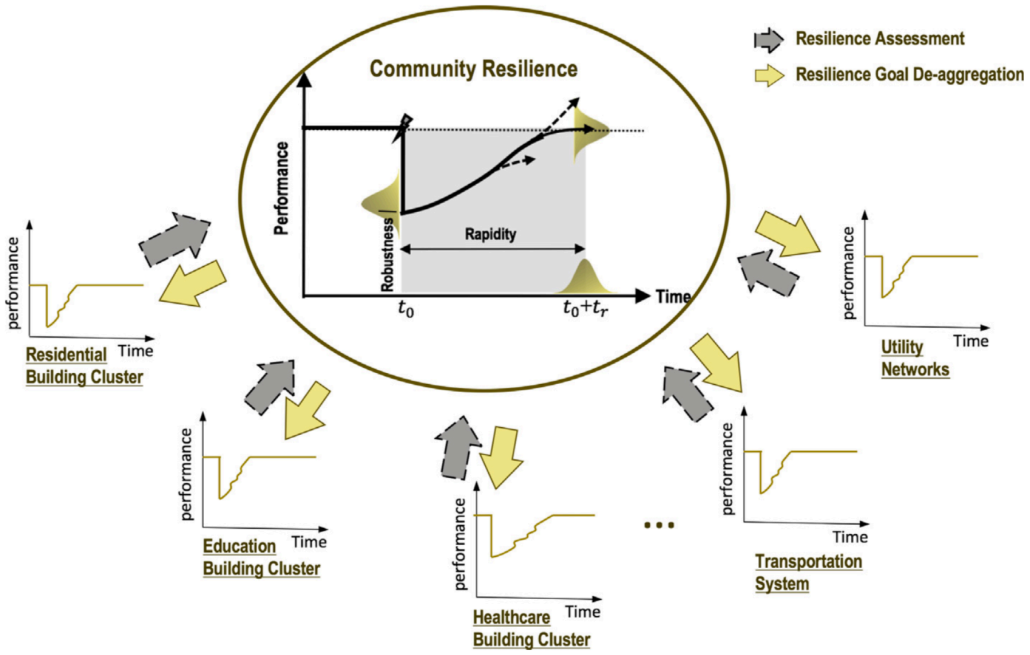

Figure 3.3: Illustration of Resilience Assessment and Goal De-aggregation

Now, to identify the performance objectives for individual buildings and lifeline components that would collectively enable a set of pre-defined overarching community resilience goals to be achieved, the assessment procedure is reversed, creating a top-down, multi-layered cascading "de-aggregation" framework shown in Figure 3.4. Ideally, this multi-layered de-aggregation analysis begins with a policy-driven process that sets the overarching community resilience goals expressed in terms of socioeconomic metrics. Through an ***upper-level de-aggregation*** (ULD), this set of overarching community resilience goals is de-aggregated to a set of performance goals for physical sub-systems (i.e. building inventories and infrastructure networks) that serve the social and economic functions of the community. This ULD can be formulated as an inverse Multi-objective Optimization Problem (MOOP), where we simultaneously search for the minimum performance goals for each subsystem that collectively enable the overarching community resilience goals to be achieved. This optimization must operate on an analysis model that estimates the overarching community resilience metrics of interest using the community's subsystem performances as input. For example, if the overarching community resilience goals are articulated in terms of economic measures, e.g. job, income, gross domestic product, among others, an economic computable general equilibrium (CGE) model (e.g. Rose (2004)) can be integrated into the MOOP for the ULD. This ULD is performed at the community scale, and it decouples the interdependencies among the subsystems for the subsequent analysis. Once the set of minimum resilience goals are obtained for the subsystems, they are de-aggregated further in a ***lower-level de-aggregation*** (LLD) to obtain the minimum performance objectives for the individual components in each

subsystem. The LLD is also formulated as an inverse MOOP and must operate on subsystem analysis models, i.e., residential building cluster resilience assessment model, transportation network resilience assessment model, etc. For example, Lin et al. (2016) developed a cluster analysis model to assess the robustness and recovery of residential building clusters. Such a model can be integrated into MOOP to obtain the minimum performance criteria for individual residential buildings and enable the residential cluster resilience goals obtained from ULD to be achieved. Finally, once the performance objectives for individual structures are established, ***performance-based design*** (PBD) and retrofit (e.g. in Chapter 4) can be implemented at the individual facility scale, in which building (or lifeline component) attributes can be identified and parameterized to meet the performance objectives resulted from the LLD.

As discussed in the NIST Resilience Guide (2015b), community resilience goals include two temporal components - robustness goal and recovery goal. For a community subsystem, the robustness goal usually is an acceptable level of damage or loss due to the immediate impact of a particular hazard level, while the recovery goal, on the other hand, is often stipulated as an acceptable recovery target at selected points in time after a hazard occurrence. The robustness of a community subsystem (e.g. a building cluster, measured in terms of direct loss ratio), is exclusively affected by the existing physical condition of its buildings, which is directly tied to building design code levels. Recovery of a building cluster, however, has been shown to be conditional on initial damage and is collectively determined by the preparedness (e.g. the speed of damage inspection, the process of design and permitting, the availability of finances) and resourcefulness (e.g. contractors,

construction material and equipment) of a community, among many other factors, as systematically modeled in Lin and Wang (2017). Accordingly, it is emphasized that while de-aggregation of the robustness goals yields improvements in design criteria for buildings and lifeline components, de-aggregation of the recovery goals leads to organizational and preparedness guidelines for community resilience planning, such as, target insurance percentage, target inspection speed, etc. The focus of this study is on deriving design criteria for buildings. This study illustrates the feasibility of the Low-level De-aggregation (LLD) by using a residential building cluster as the testbed subsystem.

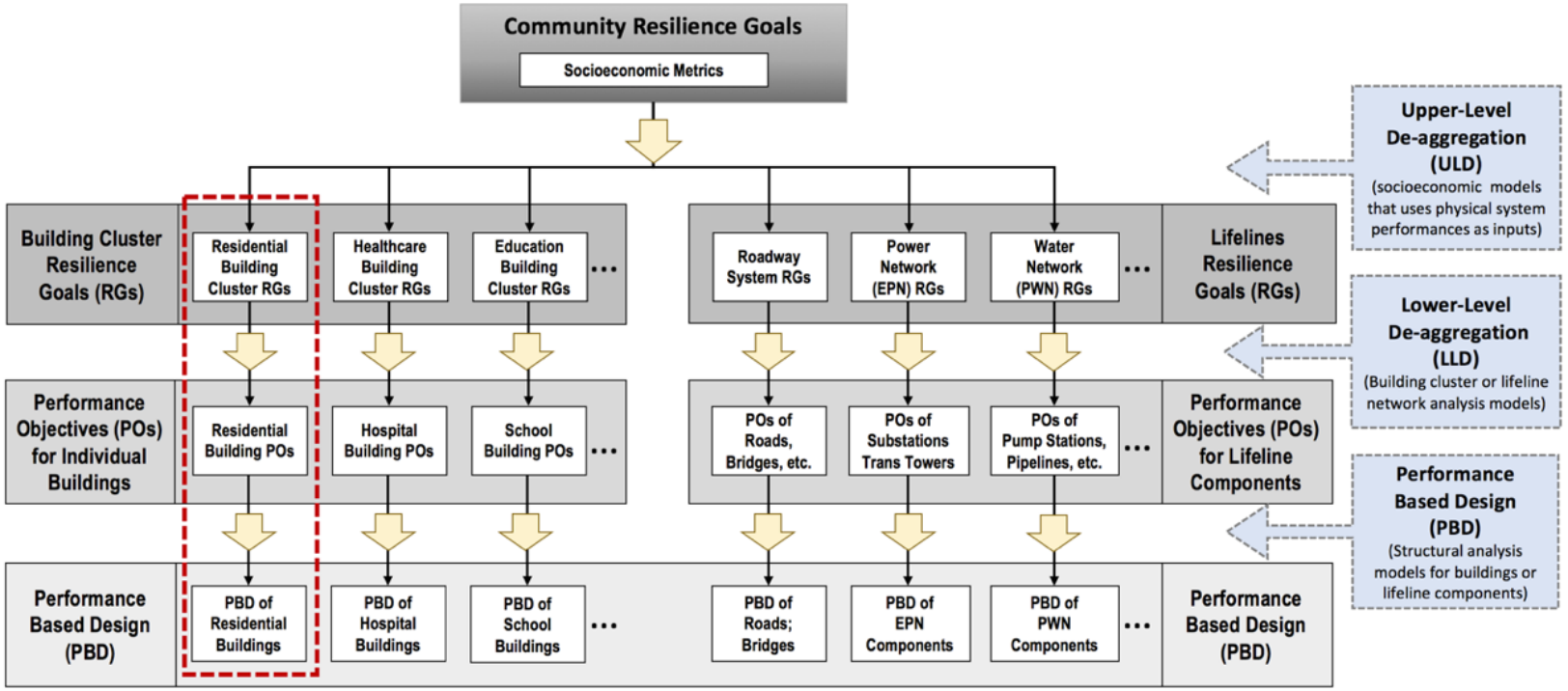

Figure 3.4: The Concept of Cascading De-aggregation

3.3 Building Portfolio Resilience Goals

Well-posed resilience goals should be clearly defined by three key elements: 1) hazard characterizations, 2) resilience metrics, and 3) goal statements articulated probabilistically in terms of the defined metrics conditional on the selected hazard intensity levels.

3.3.1 Hazard Characterization

Due to the distinct nature of tornado and seismic hazard in spatial and temporal characteristics, the hazard characterization for each hazard will be given in of Section 3.5.1 and 3.6.1, respectively.

3.3.2 Resilience Metrics

To illustrate the LLD in developing the minimum performance criteria for residential buildings under hazards, *Direct Loss Ratio* (DLR), *Un-Inhabitable Ratio* (UIR) (Lin & Wang, 2016), and Immediate Occupancy Ratio (IOR) are selected as the resilience metrics measuring the robustness of a residential building cluster. The DLR is defined as the ratio of hazard-induced direct loss of residential buildings to the overall replacement cost of the residential cluster; UIR is defined as the proportion of the dwelling units that are un-inhabitable (only consider building damage) following a hazard event to the total number of dwelling units in the building cluster under investigation. IOR is defined as the ratio of buildings that remained safe to occupy considering damage from structural and non-structural components (more formal definition will be given in Section 3.6.2). The DLR is a damage-control metric and contributes directly to the hazard-induced economic

impact, while the UIR and IOR, both related to population dislocation, are functionality-control metrics relevant to the social well-being of the community following a disaster.

3.3.3 Probabilistic Statement of Resilience Goals

The uncertainties associated with both hazard characterization (H) and metric quantification (M) require community resilience goals to be expressed in a probabilistic form, i.e.:

$$P\left(M_{MTC,h} < G_{MT,h} \,\middle|\, h\right) = a\% \tag{3.1}$$

where $M_{MTC,h}$ represents a community resilience metric of interest MTC (e.g. UIR) evaluated under hazard (e.g. Tornados) with an intensity level h (e.g. EF5), $G_{MTC,h}$ is the prescribed resilience goal corresponding to $M_{MTC,h}$, and the $a\%$ is a prescribed confidence level. The presence of the $a\%$ in the goal statement acknowledges the uncertain nature associated with any community resilience assessment, reflects the risk level that a community is willing to tolerate, and should be aligned with a community's preferences. The cluster resilience goal, $G_{MTC,h}$, might be determined by different approaches or, more likely, a combination of the following: 1) de-aggregation of socioeconomic resilience goals at a higher-level (ULD) using quantitative models (e.g. population outmigration models, computable general equilibrium models) that relate functionally of building clusters to socioeconomic consequences of a disaster; 2) selections made by community resilience officers or a group of private and public stakeholders based on their experience, expertise

and public expectations; or 3) calibration against expected performance of well-performed building clusters.

3.4Resilience Assessment

First developed in earthquake engineering research (Cornell & Krawinkler, 2000), and recently employed by Lin and Wang (2016) in building portfolio resilience assessment, Eq. (3.2) allows the probabilistic estimation of building cluster resilience metrics:

$$P(M \le z|h) = \int\int\int\int_{M<z} f_{\boldsymbol{DV}|\boldsymbol{DS}}(\boldsymbol{u}|\boldsymbol{v}) f_{\boldsymbol{DS}|\boldsymbol{IM}}(\boldsymbol{v}|\boldsymbol{x}) f_{\boldsymbol{IM}|\boldsymbol{S}}(\boldsymbol{x}|\boldsymbol{s}) f_{\boldsymbol{S}|H}(\boldsymbol{s}|h) d\boldsymbol{u} d\boldsymbol{v} d\boldsymbol{x} d\boldsymbol{s} \quad (3.2)$$

where the bold-faced notations denote vector-valued variables; from right to left, $f_{\boldsymbol{HS}|H}(\boldsymbol{s}|h)$ is the Probability Density Function (PDF) of the parameters defining a hazard scenario ($\boldsymbol{S}$) conditioned on hazard intensity, $H = h$; $f_{\boldsymbol{IM}|\boldsymbol{S}}(\boldsymbol{x}|\boldsymbol{s})$ is the PDF of the hazard intensity field $\boldsymbol{IM}$ given $\boldsymbol{S} = \boldsymbol{s}$; $f_{\boldsymbol{DS}|\boldsymbol{IM}}(\boldsymbol{v}|\boldsymbol{x})$ is the PDF of damage state $\boldsymbol{DS}$ of buildings in the cluster conditioned on $\boldsymbol{IM} = \boldsymbol{x}$; $f_{\boldsymbol{DV}|\boldsymbol{DS}}(\boldsymbol{u}|\boldsymbol{v})$ is the PDF of damage value $\boldsymbol{DV}$ conditioned on $\boldsymbol{DS} = \boldsymbol{v}$; and $\boldsymbol{DV}$ is the loss to individual buildings with respect to the resilience metric of interest as a result of its physical damage (Lin & Wang , 2016). The community resilience metric M, i.e. DLR, UIR, and IOR in this study, is a function of $\boldsymbol{HS}$,

$\boldsymbol{IM}$, $\boldsymbol{DS}$ and $\boldsymbol{DV}$. Therefore, the cumulative distribution function (CDF) of M conditioned on H can be estimated by integrating the joint PDF of the four random vectors, namely, $\boldsymbol{HS}$, $\boldsymbol{IM}$, $\boldsymbol{DS}$, and $\boldsymbol{DV}$, over the multi-dimensional region where $M(\boldsymbol{HS}, \boldsymbol{IM}, \boldsymbol{DS}, \boldsymbol{DV}) < z$. The dimension of $\boldsymbol{IM}$, $\boldsymbol{DS}$, and $\boldsymbol{DV}$ is consistent with the number of buildings in the cluster. Eq. (3.2) relates the performance of individual buildings (represented by building fragility functions, $f_{\boldsymbol{DS}|\boldsymbol{IM}}(\boldsymbol{v}|\boldsymbol{y})$) to the resilience metrics of the cluster as a whole (represented by M, measured in terms of DLR or UIR). Generally, Eq. (3.2) cannot be evaluated in a closed-form and a multi-layered Monte Carlo Simulation (MCS) is employed to estimate the probability distributions of M.

De-aggregating resilience goals to obtain the strength criteria for individual buildings and engineered facilities is an inverse process of the resilience metric evaluation procedure. The de-aggregation starts with a set of prescribed cluster resilience goals (and determines the theoretical minimum individual building performance criteria enabling the cluster resilience goals to be achieved). The premise is that the de-aggregation should be independent of the current condition of a building cluster. The cluster resilience goal is a long-term target for a community to strive for; and it is this long-term target (i.e. what is to achieve in future) that governs the de-aggregation, not the existing situations (i.e. where we are now). In other words, de-aggregation answers the question: what is the minimum building performance criteria necessary for a cluster of buildings to achieve the prescribed cluster resilience goals? The process of de-aggregation is illustrated in Figure 3.5.

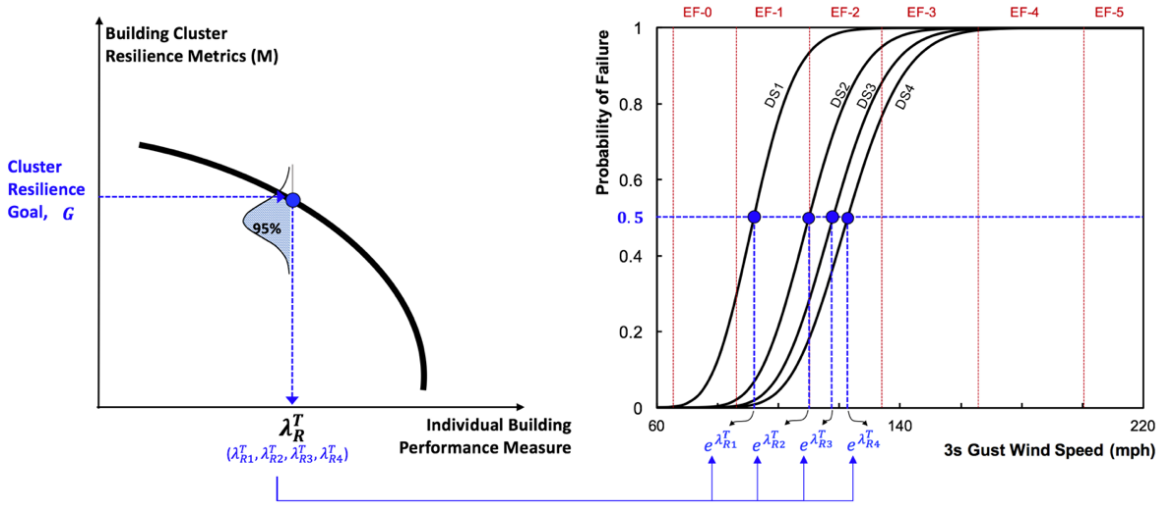

Figure 3.5:Illustration of de-aggregation, demonstrating the relation between (a) the cluster resilience goals and (b) the target building fragility functions

3.5Risk De-aggregation Under Tornado Hazards

In this section, the minimum performance criteria for residential buildings will be derived from direct loss ratio (DLR) and un-inhabitable dwelling ratio (UIR) performance goals of residential building portfolios under EF2 and EF5 tornadoes, which is formulated as a multi-objective optimization problem (MOOP).

3.5.1 Hazard Characterization

Tornadoes have very low probability of occurrence for a specific location (at the order of 10^{-4} or lower for regions in east of rocky mountain of the U.S. (Lu, 1995)), relatively localized impact (compared to other natural hazard, such earthquakes), and spatially varied wind field along and across their path. The Enhanced Fujita (EF) scale (Texas Tech, 2011), modified from the original Fujita (F) scale, is the standard and well-

accepted form of describing the intensity of tornadoes. According to the historical data from 1950 to 2015 (NOAA, 2015), approximately, 90% of tornadoes are categorized as EF2 or below in the U.S. For most cities in the U.S., the current design wind speed for buildings, lies between EF1 and EF2 (van de Lindt et al., 2012), when considering straight winds (ASCE, 2016). EF5 tornadoes, on the other hand, have brought massive economic and social impacts in the U.S. in recent years (e.g. Joplin, MO 2011 and Moore, OK 2013). In this study, EF2 and EF5 are considered as *expected* and *extreme* intensity levels, respectively, in articulating the resilience goals with respect to tornadoes. A spectrum of EF2 and EF5 scenario events will be considered in the LLD formulation.

It begins with generating tornado scenarios given a pre-defined intensity level expressed in EF-scale *(H)*, i.e. $f_{\boldsymbol{HS}|H}(\boldsymbol{s}|h)$ in Eq. (3.2). A tornado path can be effectively determined by four parameters (Strader et al., 2016): initiation point (P), path angle (θ), path length (L) and width (W), as shown in Figure 3.6(a) on a Community A, assumed to be in the State of Oklahoma. In the MCS, a Region B surrounds community A is defined, and its dimension in each direction is 100 miles larger than that of the community A, as illustrated in Figure 3.6(b). It is assumed that the tornado initiation point P is equally likely over Region B, and only tornados initiated in Region B can possibly pass through Community A. A statistical study of the historical tornado records during the period of 1950-2015 (NOAA, 2015), as tabulated in Table 3.1 for the State of Oklahoma, indicates that tornado path angle θ can be described by a normal distribution, approximately with a mean of 35°~45° (measured counterclockwise from due east) and standard deviation (SD) of 31°~37°, while the path length L and width W can be most effectively modeled by

Weibull distributions with parameters tabulated in Table 3.1. According to the probability distributions of the four path parameters, 4,000 tornado scenarios are generated for Community A, 2,000 for each EF2 and EF5 intensity level, in order to obtain a probabilistic quantification of the UIR and DLR.

For each of the simulated tornado scenarios, the wind gradient (the spatial variation of wind speed along and across the path), i.e. $\boldsymbol{f_{IM|HS}(x|s)}$ is established in Eq. (3.2). Further, it employs the approach proposed by Standohar-Alfano and van de Lindt (2014), in which the spatial wind speed gradients take concentric rectangular shapes and the wind speed in each gradient is expressed in terms of EF-scale, as illustrated in Figure 3.6(a). The classification error associated with subjectively defining the wind intensity in terms of EF-scale is captured by a normal distribution (Lu, 1995). Accordingly, uncertainties of the wind speed within the gradients are modeled by a normal distribution, as tabulated in Table 3.2, in which the upper and lower 2nd percentiles of the normal distribution coincide with the upper and lower bounds of the wind speed range for the corresponding gradient associated with an EF-scale. For each of the 4000 simulated tornado scenarios with a determined path and corresponding footprint, a second-layer of MCS with 100 realizations is performed to capture the uncertainties in the wind speed at each of the building sites in the cluster.

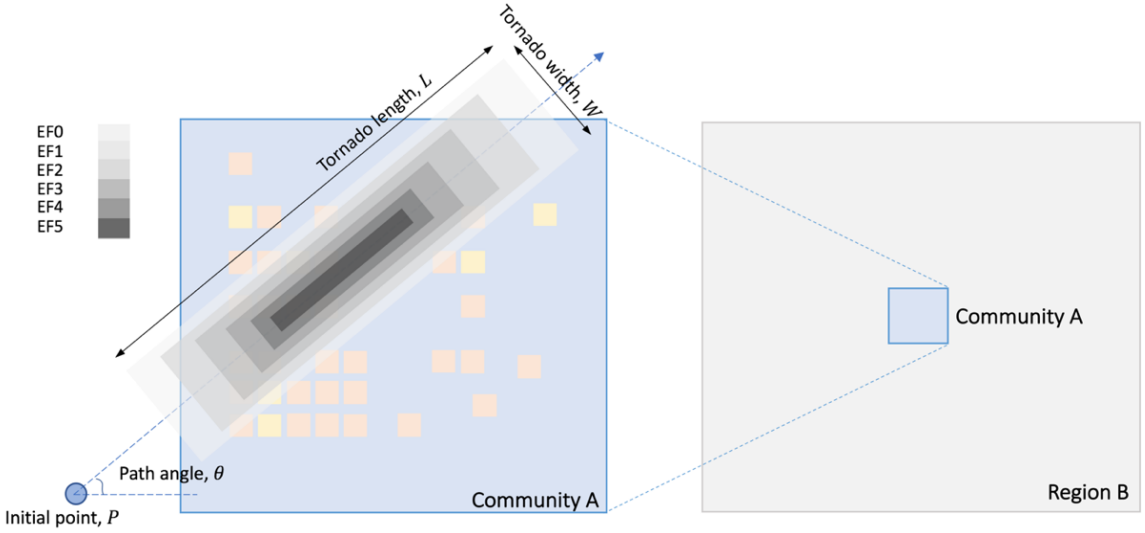

(a) *(b)*

Figure 3.6 Tornado Scenario (TS) simulation using MCS: (a) footprint of one TS and (b) the spatial region for tornado path simulation

Table 3.1 Statistics of the path parameters for tornadoes in Oklahoma

(From the NOAA SPC data (2015), 1950 - 2015, 400 EF2 events and 10 EF5 events)

EF-scale	**Length (m)** $\mathbf{L \sim Weibull(k, \lambda)}$				**Width (m)** $\mathbf{W \sim Weibull(k, \lambda)}$				**Angle (°)** $\boldsymbol{\theta \sim N(\mu, \sigma)}$	
	Sample		Parameters		Sample		Parameter		Sample	
	Mean	S.D.	Shape, k	Scale,	Mean	S.D.	Shape, k	Scale,	Mean	SD
EF2	11,032	12,993	1.125	12,458	287	327	0.945	280	34.6	31.9
EF5	36,305	23,342	1.691	41,451	1,047	564	2.123	1,195	44.9	36.3

Table 3.2 Statistics of wind speed in each EF-scale

EF-scale	**Wind speed (3s gust, mph)**	
	Speed range	**Normal dist.**
	(Texas Tech, 2011)	$\boldsymbol{N(\mu, \sigma)}$
EF0	65-85	$N(75,5.0)$
EF1	86-110	$N(98,6.0)$
EF2	111-135	$N(123,6.0)$
EF3	136-165	$N(151,7.5)$
EF4	166-200	$N(183,8.5)$
EF5	Over 200	$N(220,10.0)$

The simulations of tornado path and spatial gradient of wind speed for each path result in full spatial characterizations of 100 demand fields for each of the 4000 tornado scenario events, HS. Imposing each demand field on a spatially distributed building cluster, the probability of each of the damage states, DS as defined in Table 3.3, can be estimated for each building by fragility functions. Furthermore, the DV, conditional on DS, i.e. DV^{DL} − the loss percentage of a building with respect to its replacement cost and DV^{UI} − the un-inhabitable of a building, is tabulated in Table 3.4.

Table 3.3 Definition of damage state under tornado hazard (Maloney et al., 2018)

Damage State	Damage Description	Roof Cover Failure	Window & Door Failures	Roof Deck	Exterior Wall Damage	Roof Structure	Wall Structure Failure
0	None to Very Minor	0-15% Shingle Failure	No Damage	No Roof Panel Loss	Cracking on 1-2 Sides	No Damage	No Damage
1	Minor	15-50% Shingle Failure	1-3>20%	No Roof Panel Loss	Cracking on 3-4 Sides	No Damage	No Damage
2	Moderate	50%+ Shingle Failure	3≥0% - 50%	1 - 25% Panel Loss	-	No Damage	No Damage
3	Severe	-	≥50%	25% - 50% Panel Loss	-	No Damage	No Damage
4	Destruction	-	-	≥50% Roof Panel Loss	-	Rafter-Sill Failure	Foundation Connection Damage

Table 3.4 Damage Value, DV (FEMA/NIBS, 2003)

Damage Value, DV	Damage State			
	1	2	3	4
DV for direct loss (DV_{DL}^{ds})	0.05	0.2	0.5	1.0
DV for un-inhabitability (DV_{UI}^{ds})	0	0	1.0	1.0

3.5.2 Resilience Metrics

Accordingly, the DLR and UIR can be obtained by aggregating the corresponding *DV* for each building over the entire building cluster, as:

$$M_{DLR,h} = \frac{\sum_{i=1}^{I_N} \mathrm{C}^i \cdot \sum_{ds=1}^{4} DV_{DL}^{ds} \cdot p_h^{i,ds}}{\sum_{i=1}^{I_N} \mathrm{C}^i} \tag{3.3a}$$

$$M_{UIR,h} = \frac{\sum_{i=1}^{I_N} \mathrm{U}^i \cdot \sum_{ds=1}^{4} DV_{UI}^{ds} \cdot p_h^{i,ds}}{\sum_{i=1}^{I_N} \mathrm{U}^i} \tag{3.3b}$$

in which I_N is the number of buildings in the cluster; $p_h^{i,ds}$ is the probability of damage state equal to $ds \in (1,2,3,4)$ of the *i*-th building obtained from fragility functions with respect to tornado intensity level $h \in (EF2, EF5)$; C^i is the total replacement cost of the *i*-th building; U^i is the number of dwelling units in the *i*-th building.

From Eq. (3.3) for all the 4×10^5 simulated tornado demand fields, the full probabilistic distributions of $M_{DLR,h}$ and $M_{UIR,h}$ (the UIR and DLR for T1-T4 tabulated in Table 3.5 are the 95th percentile values estimated using this procedure) are obtained. It should be noted that while each building has its own characteristics with respect to its response to a tornado load, the performance of these buildings during a disaster are positively correlated due to the extended spatial footprint of the common hazard, and the common building design and construction practices within a community. While such positive correlation in hazard demands at all building sites is preserved in this two-layer MCS procedure, this study neglects the positive correlation in building capacities by eliminating a third-layer simulation of building damage states conditional on a demand

field. This simplification reduces the computational effort of the MCS, which is justified by the fact that the uncertainty in M is dominated by the hazard characterization, and comparatively, the impact of uncertainties in building capacities is secondary. This justification will be further illustrated in Section 3.5.3.

3.5.3 Resilience Goals

The uncertainties associated with both hazard characterization (H) and metric quantification (M) require community resilience goals to be expressed in a probabilistic form (has been given in Eq. (3.1)) and is re-written below for tornado hazards. For instance, when the metric of interest is UIR

$$P\left(M_{UIR,h} < G_{UIR,h} \,\middle|\, h\right) = a\% \tag{3.4}$$

where $M_{UIR,h}$ represents a community resilience metric UIR evaluated under tornadoes with an intensity level of $h \in (EF2, EF5)$, $G_{UIR,h}$ is the prescribed resilience goal corresponding to $M_{UIR,h}$, and the $a\%$ is a prescribed confidence level. A similar definition could be easily obtained when the metric of interest is DLR. An example of the goal statement expressed in Eq. (3.4) is $P\left(M_{UIR,EF5} < 2\% \,\middle|\, EF5\right) = 95\%$, meaning "less than 2% of the residential buildings are uninhabitable immediately following any EF5 tornado event with 95% probability.

In this study, the calibration method is employed to establish the cluster resilience goals with respect to UIR and DLR for residential building clusters subjected to tornadoes. Four hypothetical clusters are considered, each consisting of 5000 identical archetype buildings distributed over a 20-mile by 20-mile area. The four archetypes, T1-T4, that employed to populate the four hypothetical clusters are typical well-built, IRC-complied wood residential buildings introduced in Amini and van de Lindt (2013). The basic attributes of the four archetypes and the resilience metrics evaluated for the four hypothetical clusters are tabulated in Table 3.5. The probabilistic analysis procedure to estimate the cluster DLR and UIR has been given in Section 3.5.2. It is observed that for these four clusters the 95th percentile of DLR is in the range of 0.23%~0.42% and 2.64%~2.99% for EF2 and EF5 tornadoes, respectively; and the 95th percentile of UIR is in the range of 0.22%~0.44% and 2.64%~3.08% for EF2 and EF5 tornadoes, respectively. Accordingly, for the subsequent illustration, the resilience goals proposed in the last three columns in Table 3.5 for the 20-mile by 20-mile benchmark residential building cluster will be utilized. The last three columns of Table 3.5 each corresponds to a specific code level: Level 1 – *Baseline Code* (focus on life-safety), Level 2 - *Enhanced Code* (focus on reparability), and Level 3 – *Continued Use* (focus on continued occupancy and use). It is emphasized that when the community area (A_C) varies from 20 mile^2 to 600 mile^2, the DLR and UIR will decrease monotonically, as illustrated in Figure 3.7 for DLR_{EF5}. This is because tornadoes are localized hazards when compared to other natural hazards such as hurricanes or earthquakes. The impact of an EF5 tornado on a small-area community can be much more overwhelming than its impact on a large community. This correlation

between DLR (or UIR) and A_C suggests that the cluster goal (G) expressed in term of DLR (or UIR) should be a function of A_C, as shown in the solid lines. The effect of community size A_C on the de-aggregated minimum building performance objectives will be further discussed in the case study in Section 3.5.5.

Table 3.5: UIR and DLR estimated for four 20-mile by 20-mile hypothetical building clusters consisting of well-performed building archetypes and proposed building cluster goals

Building Cluster Metrics (M)	**Hazard Intensity Levels (H)**	**Building Archetypes Included in Each Hypothetical Cluster** (No. of story/No. of dwelling unit) (Amini & van de Lindt, 2013)				**Proposed Goals (G)**		
		T1 (1/1)	T2 (1/1)	T3 (2/4)	T4 (2/2)	Code Level 1 (Baseline)	Code Level 2 (Enhanced)	Code Level 3 (Cont'd Use)
DLR	**EF2**	0.23%	0.42%	0.41%	0.37%	0.18%	0.10%	0.08%
	EF5	2.64%	2.99%	0.99%	2.87%	2.50%	1.80%	1.50%
UIR	**EF2**	0.22%	0.40%	0.44%	0.36%	0.18%	0.10%	0.08%
	EF5	2.64%	2.98%	3.08%	2.84%	2.50%	1.80%	1.50%

- T1 - Single family dwelling w/o basement; T2 - Single family dwelling; T3 - Multifamily dwelling; T4 - Multifamily dwelling.
- Code Level 1 – Baseline Code; Code Level 2 – Enhanced Code; Code Level 3 – Continued Use

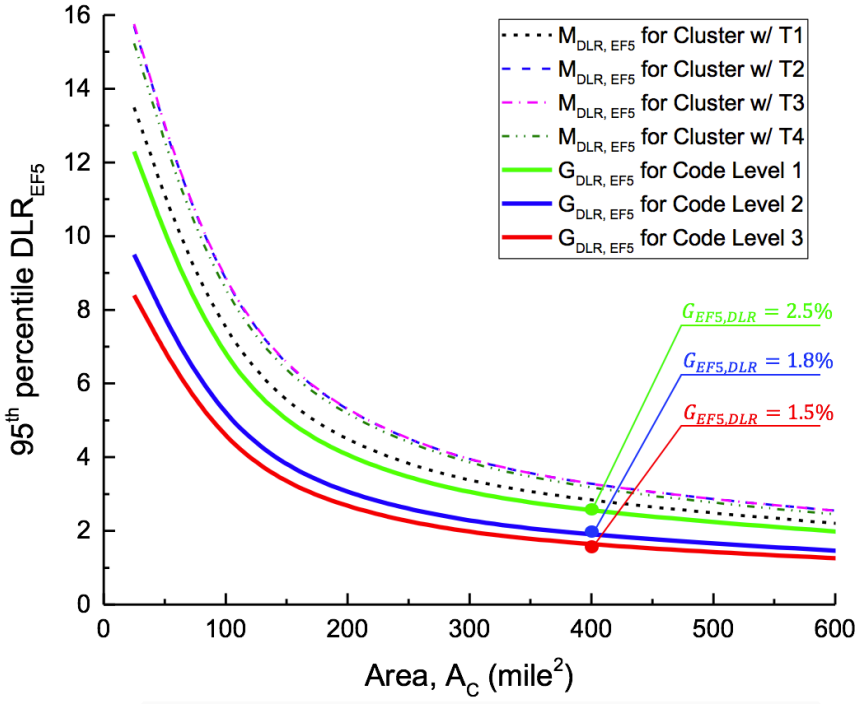

Figure 3.7: 95th percentile of $M_{UIR,EF5}$ as a function of community area (AC)

3.5.4 Formulation

De-aggregating resilience goals to obtain the strength criteria for individual buildings and engineered facilities is an inverse process of the resilience metric evaluation procedure presented in Section 3.4. The de-aggregation starts with a set of prescribed cluster resilience goals (Section 3.5.3) and determines the theoretical minimum individual building performance criteria enabling the cluster resilience goals to be achieved. The premise is that the de-aggregation should be independent of the current condition of a building cluster. The cluster resilience goal is a long-term target for a community to strive for; and it is this long-term target (i.e. what to achieve) that governs the de-aggregation, not

the existing situations (i.e. where we are). In other words, de-aggregation answers the question: what is the minimum building performance criteria necessary for a cluster of buildings to achieve the prescribed cluster resilience goals?

Accordingly, the de-aggregation problem is formulated as an inverse optimization problem, where the decision variables are building performance criteria expressed probabilistically in terms of lognormal fragility functions (Rosowsky & Ellingwood, 2002):

$$Fr_{ds}(x) = P(DS \geq ds|x) = \Phi\left[\frac{\ln(x) - \lambda_{R,ds}}{\varepsilon_{R,ds}}\right] \tag{3.5}$$

where x denotes the hazard demand; DS denotes the random variable of damage state; $ds \in (1,2,3,4)$ denotes the realization of DS; $\lambda_{R,ds}$ denotes the logarithmic median (or log-median) capacity, i.e., the median capacity equals $e^{\lambda_{ds}}$ for each damage state ds; $\varepsilon_{R,ds}$ denotes the logarithmic standard deviation for damage state ds. The analysis of typical, IRC-complied (IRC, 2015) wood residential buildings presented in the literature (Rosowsky & Ellingwood, 2002; Amini & van de Lindt, 2013) indicates that the $\varepsilon_{R,ds}$ is usually in the range of 0.10 – 0.17 under wind load. The source of this uncertainty includes component strength, connection details, modes of failure, construction quality, etc., which are less controllable in design than $\lambda_{R,ds}$. Accordingly, it is conservatively assumed that $\varepsilon_{R,ds}$ is consistently 0.17 for all four damage states to focus the de-aggregation process on determining the target for $\lambda_{R,ds}$.

De-aggregation is formulated as a multi-objective optimization problem (MOOP) in which the minimum building strength parameter, $\boldsymbol{\lambda_R^T} = [\lambda_{R1}^T, \lambda_{R2}^T, \lambda_{R3}^T, \lambda_{R4}^T]$ is to be sought, as illustrated in Figure 3.5, that enables a residential cluster to achieve its resilience goals expressed in Eq. (3.4). The MOOP formulation is summarized in Table 3.6. Eq. (3.6) defines the decision variables. Eq. (3.7) defines the objectives of the de-aggregation, i.e. searching for the minimum $\boldsymbol{\lambda_R}$ that enables the set of four cluster resilience goals expressed in Eq. (3.8) to be satisfied simultaneously. The values of $G_{q,h}$ are given in Table 3.5 for the three considered code levels, respectively. Eq. (3.9) is a local constraint, which ensures consistency between the relative magnitudes of the four elements in vector $\boldsymbol{\lambda_R}$ and the characteristics of the four damage states presented in Table 3.3 (Maloney et al., 2018). This constraint reduces the number of decision variables from four to two.

Table 3.6 De-aggregation Formulation under Tornadoes

Item	Expression	Eq. #
Decision Variables:	$\boldsymbol{\lambda_R} = [\lambda_{R1}, \lambda_{R2}, \lambda_{R3}, \lambda_{R4}]$	Eq. (3.6)
Objectives	$min\ \boldsymbol{\lambda_R} = \min([\lambda_{R1}, \lambda_{R2}, \lambda_{R3}, \lambda_{R4}])$	Eq. (3.7)
Constraints	$P(M_{q,h} < G_{q,h} \mid h) = a\%;$	Eq. (3.8)
	$q \in (UIR, DLR); h \in (EF2, EF5)$	
	$\lambda_{R,ds} = a + b * \ln(ds)$	Eq. (3.9)

The Multi-objective Particle Swarm Optimization (MOPSO) method is employed to find the optimal $\boldsymbol{\lambda_R}$. Particle Swarm Optimization (PSO) is easy to apply and converges rapidly when applied to MOOPs (Kennedy & Eberhart, 1995). The PSO starts with a

group of randomly generated population dubbed particles and the movement of particles is determined by three factors: Inertia (*I*), Cognitive influence (*C*) and Social influences (*S*), which are presented mathematically by the three terms in Eq. (3.10), respectively (Kennedy & Eberhart, 1995):

$$V_q^{t+1} = I + C + S = W_I \cdot V_q^t + \varphi_1 \cdot r_1 \cdot \left(P_q - X_q^t\right) + \varphi_2 \cdot r_2 \cdot \left(P_g - X_q^t\right) \quad (3.10)$$

where $V_q^{t+1} = \left(v_{q1}^{t+1}, v_{q2}^{t+1}, \dots, v_{qD}^{t+1}\right), q = 1,2, \dots, Q$ is the velocity of particle q at time $t+1$; Q is the size of the swarm population; D is the dimension of decision variables (which is 4 in the above multi-objective optimization problem); $X_q^t = \left(x_{q1}^t, x_{q2}^t, \dots, x_{qD}^t\right)$, $q = 1,2, \dots, Q$ is the position of particle q at t. $P_q = \left(p_{q1}, p_{q1}, \dots, p_{qD}\right) \in \mathbb{R}^D$ is the individual history best position of particle q and $P_g \in \mathbb{R}^D$ is the swarm's global best position; r_1, r_2 are random numbers which follow uniform distribution $U(0,1)$; φ_1 and φ_2 are acceleration constants; W_I denotes the "inertia weight" of the particle. Then the position of the particle at time $t+1$ is updated by:

$$X_q^{t+1} = X_q^t + V_q^{t+1} \quad (3.11)$$

To convert the original single-objective PSO into MOPSO, the approach proposed by Reddy and Kumar (2007) is employed. In their approach, a Pareto dominance criterion is employed for selecting non-dominated solutions, a crowing distance operator is used for ranking and creating elective pressure among the particles, and an elitist-mutation (EM) strategy is used

to introduce randomness to escape from locally optimal solutions. A flowchart of the MOPSO algorithm to solve the de-aggregation problem formulated in Table 3.6 is presented in Figure 3.8.

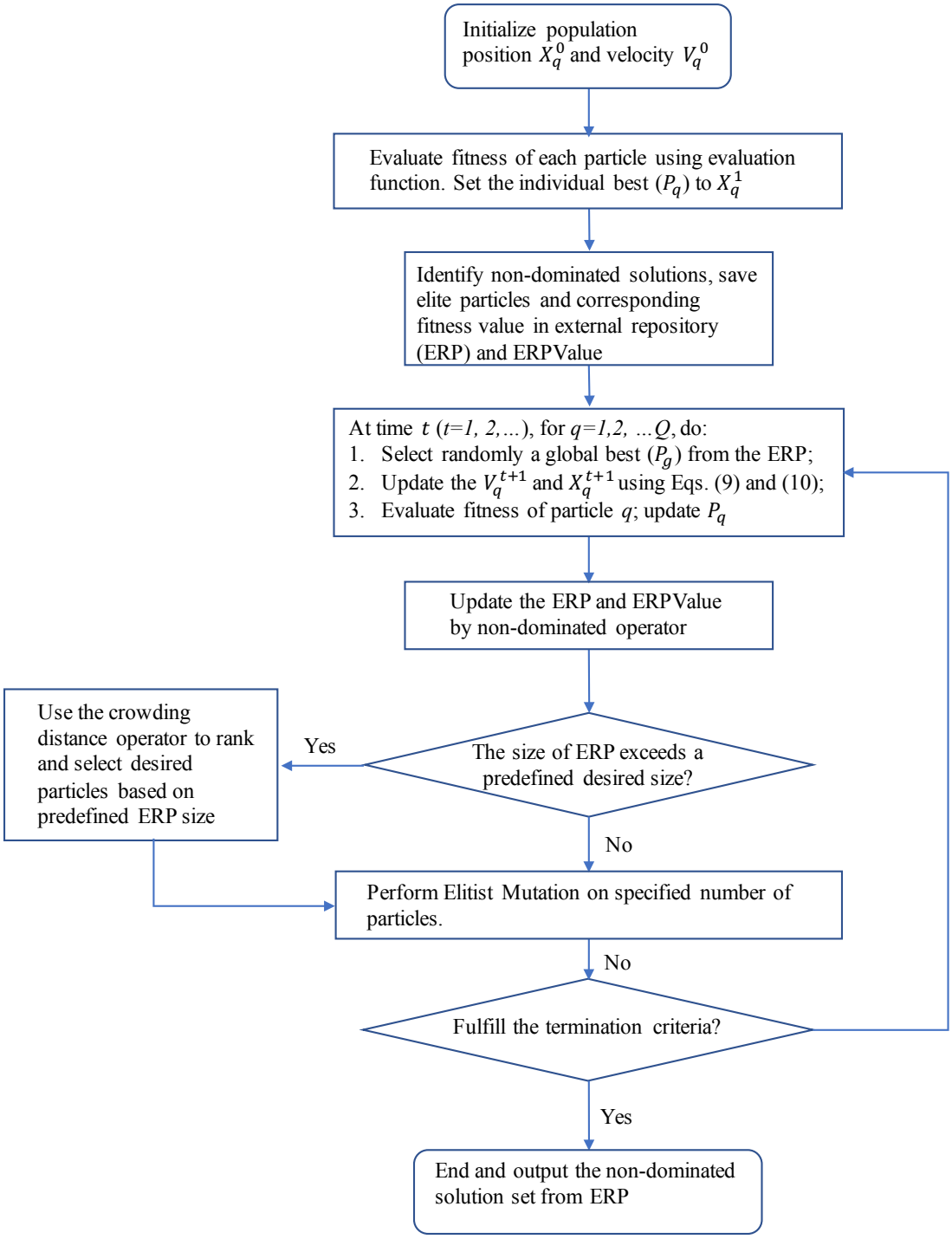

Figure 3.8 Flowchart of the MOPSO

3.5.5 Illustration

MOPSO is employed to de-aggregate the cluster resilience goals presented in the last three columns of Table 3.5, resulting in the minimum performance criteria for residential buildings expressed in terms of optimal $\boldsymbol{\lambda_R}$ for each of code levels. Figure 8 presents the Pareto Front from the MOPSO for the Code Level 3 – *Continued use*, showing the trade-off between the λ_{R1} and $\Delta\lambda_R$ (i.e. $\lambda_{R4} - \lambda_{R1}$). It is observed that $G_{DLR,EF5}$ governs the lower right portion of the Pareto Front where the optimal $\boldsymbol{\lambda_R}$ set is relatively narrowly spaced with a comparatively larger λ_{R1}; $G_{UIR,EF5}$ dominates the upper left portion of the Pareto Front where there is larger spacing between individual fragility functions of the optimal set starting with a comparatively smaller λ_{R1} ; and in between, $G_{DLR,EF2}$ determines the Pareto Front boundaries. This observation can be explained by the fact that all four damage states contribute to DLR while only DS_3 and DS_4 contribute to UIR (c.f. Table 3.4); thus UIR-related goals require larger values of λ_{R3} and λ_{R4} (corresponding to smaller λ_{R1} and larger $\Delta\lambda_{R1}$) and DLR goals require larger values of λ_{R1}.

Further, to select a target $\boldsymbol{\lambda_R^T}$ set from the Pareto Front, the typical value of $\Delta\lambda_R$ for existing well-built, IRC-complied wood residential building archetypes is considered, as listed Table 3.5. The gray-shaded horizontal band in Figure 3.9 shows the typical range of $\Delta\lambda_R$ of these archetypes being 0.26 ~ 0.39. This range is determined by the underlying structural mechanics of different failure modes (or damage states), which will remain unchanged as long as the damage state definition in Table 3.3 remains the same. Therefore

the optimal $\boldsymbol{\lambda_R}$ set within that band on the Pareto Front associated with the *smallest* λ_{R1}, i.e. red-highlighted $\boldsymbol{\lambda_R}$ set on Figure 3.9, is selected as the target $\boldsymbol{\lambda_R^T}$ for building design, since the *minimum* performance objectives is to be sought. As shown in Figure 3.9, the target λ_{R1}^T falls to the right side of the vertical dash-line bounded area, which is the typical range of λ_{R1} for the wood residential building archetypes listed in Table 3.5, suggesting that the cluster resilience goals associated with Code-Level 3, do impose more strict requirement on building performance than those in the current building practice only aimed at ensuring life safety. The $\boldsymbol{\lambda_R^T}$ for Code Level 1 (*Baseline*) and Code Level 2 (*Enhanced*) are derived similarly. The target $\boldsymbol{\lambda_R^T}$ sets for all three code levels are tabulated in Table 3.7, corresponding to the three sets of target fragility functions in Figure 3.10.

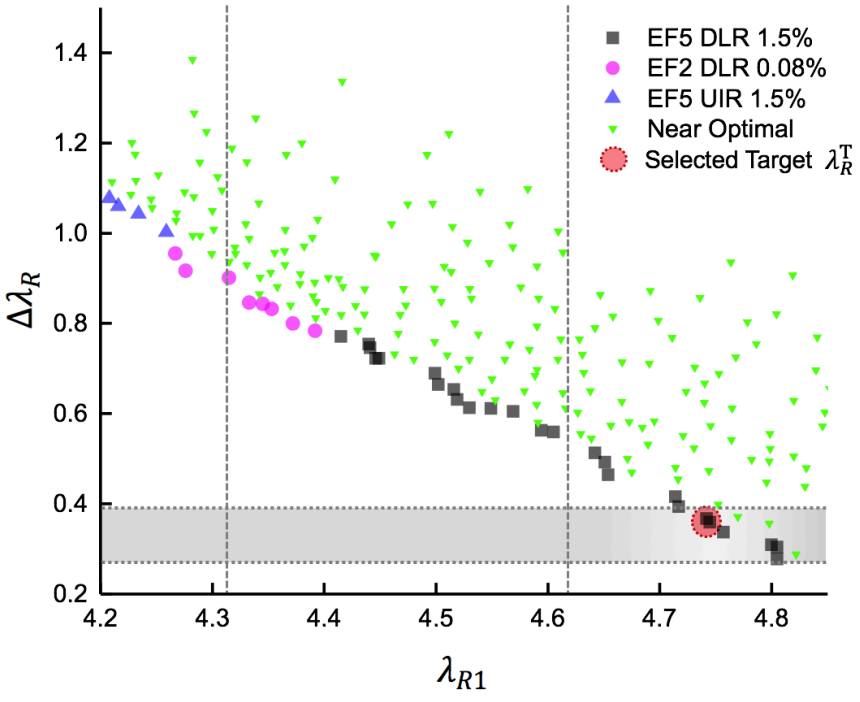

Figure 3.9: The trade-off between $\boldsymbol{\lambda_{R1}}$ and $\boldsymbol{\Delta\lambda_R}$ for Code level 3 – Continued Use

Table 3.7: Minimum performance objectives (Target λ_R^T)for individual residential buildings for the three code levels

Code Levels	**Performance Objective**	λ_{R1}^T	λ_{R2}^T	λ_{R3}^T	λ_{R4}^T
Baseline Code (BC)	$\lambda_R^{T,BC}$	4.53	4.72	4.82	4.90
Enhanced Code (EC)	$\lambda_R^{T,EC}$	4.67	4.86	4.97	5.05
Continued Use (CU)	$\lambda_R^{T,CU}$	4.74	4.93	5.01	5.11

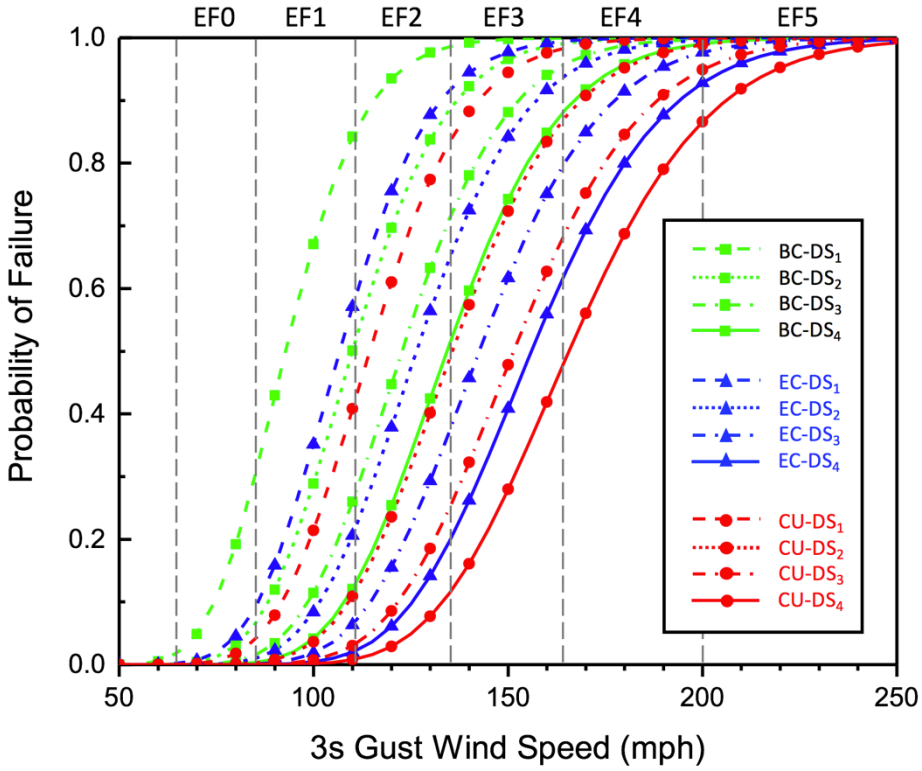

Figure 3.10: Target fragility functions for the three code levels

The sensitivity of the target $\boldsymbol{\lambda_R^T}$ to (a) the sample size of MCS of tornado scenarios (N_{MCS}), (b) the number of buildings in a cluster (N_b), and (c) the logarithmic standard deviation of the target fragility functions (ε_R) are further investigated. Figure 3.11 shows the sensitivity analysis results of $\boldsymbol{\lambda_R^T}$ for Code-Level 1 (*Baseline*). Figure 3.11(a) and (b) indicate that the MCS sample size and the number of buildings have little impact on the target $\boldsymbol{\lambda_R^T}$, especially when $N_{MCS} > 1000$ and $N_b > 2500$ (which are the cases for most typical size communities in the U.S.). Figure 3.11(c) shows that $\boldsymbol{\lambda_R^T}$, i.e. the logarithmic median of the target fragility function set, is not affected by the logarithmic deviation, ε_R, assumed in the de-aggregation. This is because the dominant source of uncertainty in the cluster resilience metrics is in the tornado hazards (i.e. path length and width, approaching angle, wind gradient and velocity); the impact of uncertainties in structural capacities of the buildings is secondary in importance. Finally, communities of different area (A_C) should stipulate different cluster resilience goals (G), as illustrated earlier in Table 3.7. Once the area of a community is reflected in its stipulation of G, as shown in Figure 3.12, the resulting target $\boldsymbol{\lambda_R^T}$ is invariant across communities of different areas.

The target $\boldsymbol{\lambda_R^T}$, calibrated as such, can be used as the minimum performance objectives in performance-based design and retrofit of individual buildings. In a concurrent study by Maloney et al. (2018), practical retrofit design of three residential building archetypes with typical construction in Norman, OK, are devised to realize the specified target fragilities derived herein.

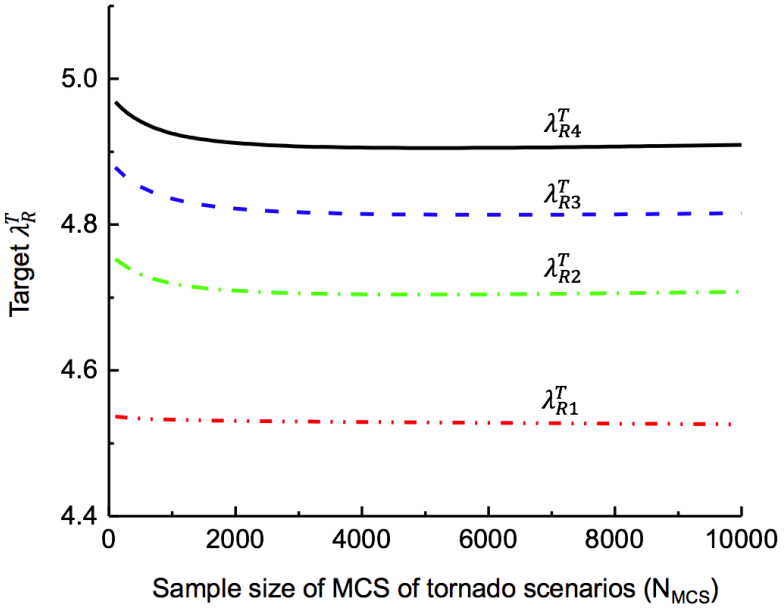
5.0
4.8
4.6
4.4
Target λ_R^T
λ_{R4}^T
λ_{R3}^T
λ_{R2}^T
λ_{R1}^T
0
2000
4000
6000
8000
10000
Sample size of MCS of tornado scenarios (N_{MCS})

(a)

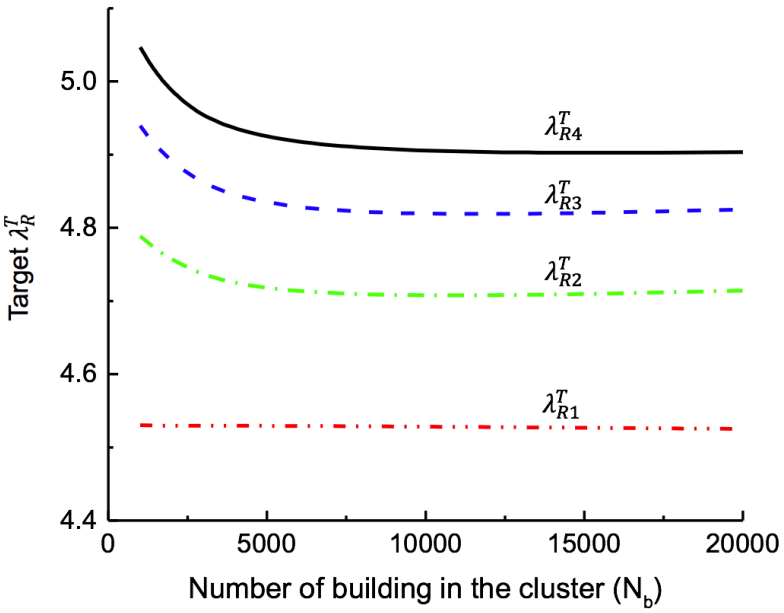
5.0
4.8
4.6
4.4
Target λ_R^T
λ_{R4}^T
λ_{R3}^T
λ_{R2}^T
λ_{R1}^T
0
5000
10000
15000
20000
Number of building in the cluster (N_b)

(b)

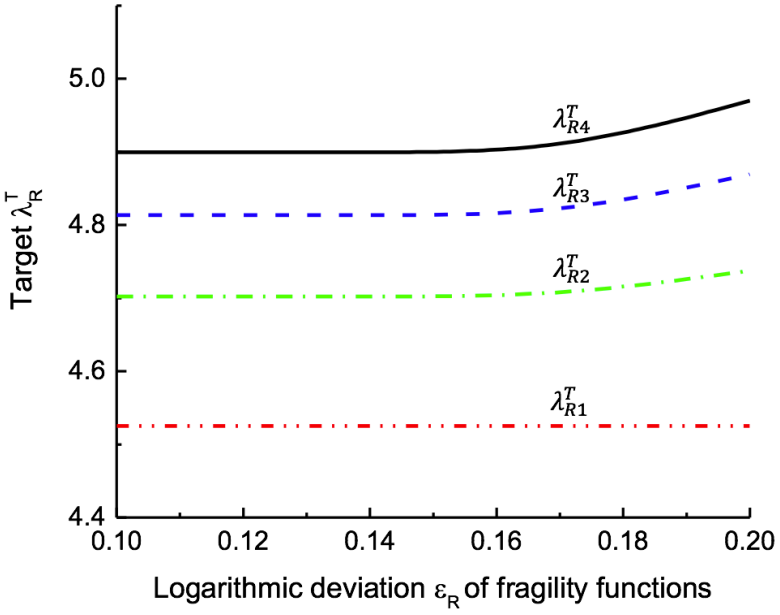

(c)

Figure 3.11: Target $\boldsymbol{\lambda_R^T}$ vs (a) sample size of MCS of tornado scenarios (N_{MCS}); (b) No. of buildings in the cluster (N_b); and (c) logarithmic deviation $\boldsymbol{\varepsilon_R}$ of fragility functions (illustrated for Code Level 1).

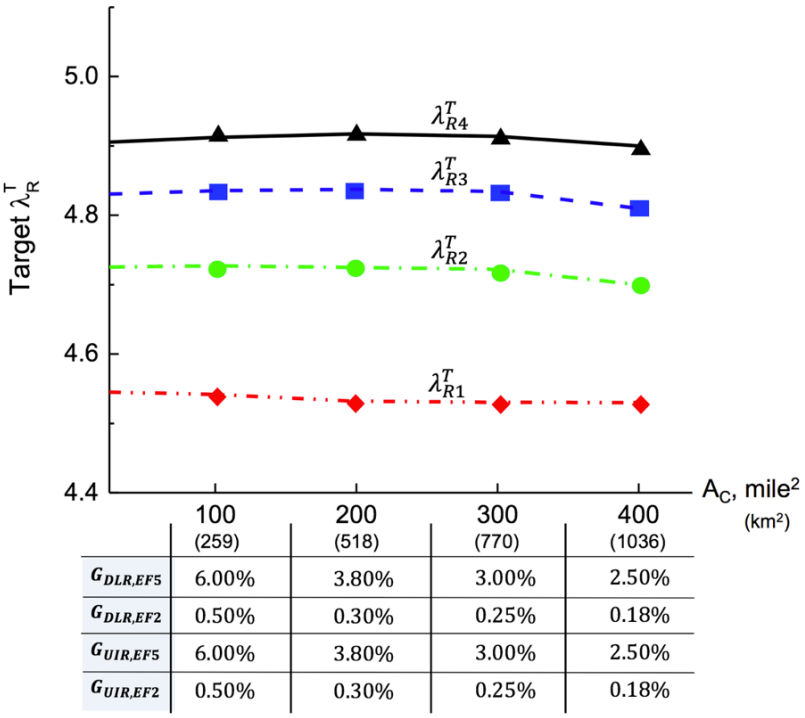

$G_{DLR,EF5}$	6.00%	3.80%	3.00%	2.50%
$G_{DLR,EF2}$	0.50%	0.30%	0.25%	0.18%
$G_{UIR,EF5}$	6.00%	3.80%	3.00%	2.50%
$G_{UIR,EF2}$	0.50%	0.30%	0.25%	0.18%

Figure 3.12: Target $\boldsymbol{\lambda_R^T}$ as a function of the cluster (or community) area, AC (illustrated for Code Level 1).

3.6 Risk De-aggregation Under Seismic Hazard

In this section, the performance of the portfolio under the design earthquake events is of interest, thus it will first give the definition and formulation of design earthquake for a portfolio. Then, Immediate-occupancy Ratio (IOR) is introduced as the primary performance metric for a building portfolio. The portfolio resilience goal is then defined probabilistically. Similar to Section 3.5, the risk de-aggregation under seismic hazard is formulated as an inverse optimization problem. The methodology is illustrated in a hypothetical homogeneous community.

3.6.1 Hazard Characterization

Definition of Portfolio Design Earthquake

The intensity of natural hazards (e.g. earthquake, hurricane) is traditionally represented in return period (e.g. 1000 year) for the hazard themselves as well as for specific sites. For civil engineering structures subjected to seismic hazard, ASCE-7 (ASCE, 2016) defines design earthquake intensity (in terms of spectrum acceleration, S_a, with a return period of about 475 years) as 2/3 of the intensity of risk-targeted maximum considered earthquake (MCE_R, with a return period of about 2475 years). Such definition of design earthquake intensity is tailored for designing individual buildings (or other engineered facilities) to achieve uniform failure probability associated with collapse and fatality. Neither portfolio-level resilience performance nor community scale hazard characterization is considered.

Generally, during an earthquake, ground motion intensities in various sites are different due to different site-to-epicenter distance, site soil amplification, and aleatory uncertainties, and are correlated due to location closeness. Here, it is proposed that the Portfolio Design Earthquakes (PDEs) is defined as the earthquake events of which the arithmetic mean PSA value within a portfolio has a return period of approximately 475 years. The ground motion realizations with mean ground motion metric closely matched with the target ground motion level are selected as the PDEs that have uniform exceedance probability consistent with the pre-defined probability level.

Formulation of Portfolio Design Earthquake

All possible seismic Faults (F), magnitudes (M) and epicenter locations (L) are considered to derive the portfolio design earthquake (PDE). From each scenario $S = (M, L)$, an attenuation model is employed to predict the median of intensity measure, $\boldsymbol{IM}$ as well as inter and intra-residual in each site. The joint CDF of $\boldsymbol{IM}$ can be written as

$$F_{\boldsymbol{IM}}(\boldsymbol{x}) = P(\boldsymbol{IM} \leq \boldsymbol{x}) = p_{NE} + \sum_{1}^{F_N} p_F(f) \cdot \iint_{\boldsymbol{M} \leq \boldsymbol{x}} f_{\boldsymbol{IM}|\boldsymbol{S}}(\boldsymbol{x}|\boldsymbol{s}) \cdot f_{\boldsymbol{S}|F}(\boldsymbol{s}|f) d\boldsymbol{x} ds \quad (3.12)$$

in which, $p_F(f)$ denotes the probability mass function (PMF) of the earthquake occurrence rate of fault $f \in (1,2, \dots, F_N)$, i.e. annual occurrence rate of earthquake in that fault; F_N denotes the total number of faults; p_{NE} denotes the probability of no earthquake in any faults annually, i.e. $p_{NE} = 1 - \sum_1^{F_N} p_F(f)$; $f_{\boldsymbol{S}|F}(\boldsymbol{s}|f)$ denotes the PDF of scenario parameter $\boldsymbol{S} = \boldsymbol{s}$ conditioned on certain fault *f*; $f_{\boldsymbol{IM}|\boldsymbol{S}}(\boldsymbol{x}|\boldsymbol{s})$ denotes the PDF of $\boldsymbol{IM}$ conditioned on $\boldsymbol{S} = \boldsymbol{s}$ according to the ground motion attenuation model. The bold-faced notion in $\boldsymbol{IM}$ and $\boldsymbol{s}$ denotes vector-valued intensity measure and scenario parameter. Generally, the above equation cannot be solved in closed-form in most real applications. To evaluate the above multi-layer conditional probability problem, one may employ the multi-layered Monte Carlo Simulation (MCS). The joint CDF of IM conditioned on specific hazard level $H = h$ is denoted by $F_{\boldsymbol{IM}}(\boldsymbol{x}|h)$, which is obtained by letting $F_{\overline{IM}}(\bar{u}) = 1 - 1/T_R$, where $\overline{IM} =$

$\frac{1}{I}\sum_{i=1}^{I} IM_i$ denotes the random variable of mean ground motion field, $\bar{u} = \frac{1}{I}\sum_{i=1}^{I} u_i$ denotes the realization of $\overline{IM}$, T_R denotes the return period corresponding to hazard level $H = h$.

Specifically, for fault $f \in [1,2,\dots,F_N]$, the possible magnitude m between M5 and M8 is sampled evenly into M_N segments, with the annual rate of earthquake v_{fm},in which $m \in [1,2,\dots,M_N]$, is modeled by certain magnitude-frequency relationship (e.g. Gutenberg & Richter (1944)). It is assumed that v_{fm} at any location of the fault *f* is equal. The fault line is further divided into *G* segments evenly. For scenario *s*, the ground motion at site *i* is modeled as (Atkinson & Boore, 1995; Jayaram & Baker, 2010):

$$ln(S_{a_{s,i}}) = ln(\bar{S}_{a_{s,i}}) + \sigma_s \varepsilon_{s,i} + \tau_s \eta_s \tag{3.13}$$

where $S_{a_{s,i}}$ represents the spectral acceleration (at certain period) at site *i* during earthquake scenario *s*; $\bar{S}_{a_{s,i}}$ represents the median spectral acceleration predicted by ground motion attenuation model; $\varepsilon_{s,i}$ represents the normalized intra-event residual at site *i,* and η_s represents the normalized inter-event residual. Both $\varepsilon_{s,i}$ and η_s follow a 1-d standard normal distribution. σ_s and τ_s denote standard deviation terms, generally given in ground motion attenuation model. $\sigma_s \varepsilon_{s,i}$ denotes the intra-event residual, whose value varies for different sites; $\tau_s \eta_s$ denotes inter-event residual, which is a constant for a given scenario *s*. Due to geographic closeness, correlation is considered in $\varepsilon_{s,i}$ (Jayaram & Baker, 2010).

3.6.2 Resilience Metrics

Suppose an individual building fulfills ***Immediate Occupancy (IO)*** performance limit if it has up to minor damage in structural components and up to moderate damage in non-structural components as introduced in Lin and Wang (2017) (they defined it as Re-occupancy). The functionality mapping of individual buildings is shown in Figure 3.13. In individual building level, indicator $IO^i = 1$ or 0 denotes the IO is fulfilled or not in building i. For simplicity, ST^i, NA^i, and ND^i denote the damage state of structural components, non-structural components acceleration-sensitive, and non-structural components drift-sensitive of building i. The definition of damage states for each component are tabulated in Table 3.8.

Functionality States (ATC Placard)			Damage Condition	Utility Availability	Building Repair Classes (RC) & Specific Repair Items
5	FF	Fully Functionality (Green Placard)	None	All available	N/A
4	BF	Baseline Functionality (Green Placard)	Minor cosmetic structural and nonstructural damage	Critical ones available	Repair Class 4 (RC4): • Minor structural damage such as shear wall, link beams, reinforced wall; Minor nonstructural damage such as stairs, partition, tiles
3	RO	Re-Occupancy (Green Placard)	Minor Str. damage and moderate non-Str. damage	Unavailable	Repair Class 3 (RC3): • Minor structural damage; Minor to moderate nonstructural damage; Mechanical equipment, electrical systems, emergency backup
2	RU	Restricted Use (Yellow Placard)	Moderate structural or nonstructural damage that does not threaten life safety	N/A	Repair Class 2 (RC2): • Moderate to heavy nonstructural damage such as glazing, exterior partitions, elevator, pipes, fire sprinkler drops
1	RE	Restricted Entry (Red Placard)	Extensive structural or nonstructural damage that threatens life safety	N/A	Repair Class 1 (RC1): • Heavy structural damage; Heavy nonstructural damage that threatens life safety

Figure 3.13 Functionality state mapping of individual buildings (Lin & Wang, 2017)

Table 3.8 Definition of damage state of each component under seismic hazard (FEMA/NIBS, 2003)

Item	Description
Slight Structural Damage $SD^i = 1$	Small plaster or gypsum-board cracks at corner of door and window openings and wall-ceiling intersections; small cracks in masonry chimneys and masonry veneer.
Moderate damage on non-structural draft-sensitive components $ND^i = 2$	**Partition walls**: larger and more extensive cracks requiring repair and repainting; some partitions may require replacement of gypsum board or other finishes **Exterior wall panels**: the movements are more extensive; connections of panels to structural frame are damaged requiring further inspection and repairs; some window frames may need realignment **Piping, Ducts**: piping leaks at few locations
Moderate damage on non-structural acceleration-sensitive components $NA^i = 2$	**Electrical-Mechanical Equipment:** Movements are larger, and damage is more extensive

Thus, the probability of IO of building *i* at ground motion level $IM = x, p_{IO}^i$ can be obtained by

$$p_{IO}^i(x) = P\left(IO^i = 1 | IM = x\right) = P\left(\left(ST^i \le 1\right) \cap \left(NA^i \le 2\right) \cap \left(ND^i \le 2\right) | IM = x\right)$$

$$= P\left(ST^i \le 1 | IM = x\right) \cdot P\left(NA^i \le 2 | IM = x\right) \cdot P\left(ND^i \le 2 | IM = x\right)$$

$$= \left(1 - P\left(ST^i \ge 2 | IM = x\right)\right) \cdot \left(1 - P\left(NA^i \ge 3 | IM = x\right)\right) \cdot \left(1 - P\left(ND^i \ge 3 | IM = x\right)\right)$$

$$= \left(1 - Fr_{ST|IM}^i(2|x)\right) \cdot \left(1 - Fr_{NA|IM}^i(3|x)\right) \cdot \left(1 - Fr_{ND|IM}^i(3|x)\right) \quad (3.14)$$

where $P\left(ST^i \leq ds|IM = x\right)$ denotes the probability of structural component, ST being not exceeding *ds* damage state, $ds \in [1,2,3,4]$, given the ground motion level $IM = x$, similar definition could be given for $P\left(NA^i \leq ds|IM = x\right)$ and $P\left(ND^i \leq ds|IM = x\right)$; $Fr^i_{ST|IM}(ds|x)$ denotes the CDF of structural component, ST being exceeding damage state ds or higher, given the ground motion $IM = x$, i.e. the fragility function of ST, similar definition could be given for $Fr^i_{NA|IM}(ds|x)$ and $Fr^i_{ND|IM}(ds|x)$. Eq. (3.14) implies that the failure probability of ST, NA, and ND components are independent. It is recognized by the authors that the performance of these components is indeed correlated, further study is needed to assess its effect on individual building IO performance and risk de-aggregation. The probability of un-occupancy (UO) of building *i* is defined by $p^i_{UO} = 1 - p^i_{IO}$, of which the mean value is denoted by $\bar{p}_{UO}$.

Further, the conditional joint probability of all component of all buildings $\boldsymbol{BDS} = \left(BDS_1, BDS_2, \dots, BDS_i, \dots, BDS_{I_N}\right), BDS_i = (ST_i, NA_i, ND_i)$ being in or exceeding damage state vector $\boldsymbol{ds} = [ds]_{\boldsymbol{I_N \times 3}}, ds \in (0,1,2,3,4)$ for the portfolio under the hazard level $H = h$ is obtained by

$$P(\boldsymbol{BDS} \geq \boldsymbol{ds}|h) = \int Fr_{\boldsymbol{DS|IM}}(\boldsymbol{ds}|\boldsymbol{x}) f_{\boldsymbol{IM}|H}(\boldsymbol{x}|h) d\boldsymbol{x} \tag{3.15}$$

where the bold-faced notations denote vector-valued variables. In Eq.(3.15), $Fr_{\boldsymbol{DS|IM}}(\boldsymbol{ds}|\boldsymbol{x})$ is the joint CDF of damage state $\boldsymbol{DS}$ being in or exceeding $\boldsymbol{ds}$ given intensity measure $\boldsymbol{x}$ (e.g. spectrum acceleration S_a), i.e. fragility function.

3.6.3 Resilience Goals

According to Eq. (3.1), when IOR performance is of interest, the resilience goals for a portfolio subjected to seismic hazards can be expressed as

$$R_{IOR} = P(M_{IOR} \geq G_{IOR}) = P\left(\sum_{i=1}^{I_N} IO^i \geq G_{IOR}\right)$$

$$= \sum_{\substack{All\ possible\ IO\ states \\ for\ all\ buildings}} \left[\prod_{i=1}^{I_N} P(IO^i) \cdot \left(\frac{\sum_{i=1}^{I_N} IO^i}{I_N} \geq G_{IOR}\right)\right] = a\% \qquad (3.15)$$

where $[T]$ is the Iverson bracket, which returns 1 if it is true, and 0 otherwise; M_{IOR} represents a ratio of building in the portfolio fulfill IO under design earthquake DE, DE is dropped in M_{IOR} for simplicity; G_{IOR} denotes the prescribed resilience goal corresponding to M_{IOR}, and the $R_{IOR} = a\%$ is a prescribed confidence level (reliability goal). For instance, $P(M_{IOR} \geq 80\%|DE) = 90\%$ means "Not less than 80% of the residential buildings are reached the IO performance limit under any design earthquake events with 90% probability". The selection of target resilience goals will be discussed in Section 3.6.5.

3.6.4 Formulation

The de-aggregation problem is treated as an inverse optimization problem such that the decision variables are the building performance criteria in the form of fragility parameters (Wang et al., 2018). In Section 3.5.4, formulation of fragility function has been given in Eq. (3.5), here modification is needed, as ST, NA, and ND components are considered. For instance, the fragility function for structural components ST can be formulated as

$$Fr_{ST,ds}(x) = P(ST \geq ds|x) = \Phi\left[\frac{\ln(x) - \lambda_{ST,ds}}{\varepsilon_{ST,ds}}\right] \tag{3.16}$$

where $\lambda_{ST,ds}$ denotes the logarithmic median capacity for ST at damage state $ds \in (1,2,3,4)$; $\varepsilon_{ST,ds}$ denotes the logarithmic standard deviation for ST at damage state ds. For simplicity, the subscript R is dropped in $\lambda_{ST,ds}$ and $\varepsilon_{ST,ds}$. Everything else is the same as Eq. (3.5). As in Eq. (3.5), $\boldsymbol{\varepsilon_R} = [\varepsilon_{Item,ds}]$, $Item \in (ST, NA, ND), ds \in (1,2,3,4)$ is treated as a constant and convert the problem into one that solves the value of $\boldsymbol{\lambda_R} = [\lambda_{Item,ds}]$. However, the number of decision variables are still large, i.e. 12.

More constraints are desirable to facilitate optimization. Firstly, from the examining of the existing wood-frame building in HAZUS, it is found that $\boldsymbol{\lambda_R}$ can be well expressed in terms of DS as in Section 3.5.4, due to the definition of fragility function and physical damage mechanism. That gives the second constraint of Eq. (3.20) in Table 3.9.

For given ds, parameter $a_{ST}, b_{ST}, and\ c_{ST}$ collectively define $\lambda_{ST,ds}$. Further, as the IO state of individual building are collectively defined by its SD, NA, and ND (c.f. Eq. (3.14)), it is proposed that optimal performance of individual building is achieved when the mean failure probability of SD, NA, and ND of all buildings within the portfolio under all selected portfolio design earthquake (PDE) scenarios s' (total number N_s) are identical, which gives the third constraint of Eq. (3.21) in Table 3.9.

Table 3.9 Formulation of risk de-aggregation as an inverse optimization under seismic hazard

Item	Expression	Eq. #
Decision Variables	$\boldsymbol{\lambda_R} = [\lambda_{Item,ds}], Item \in (SD, NA, ND), ds \in (1,2,3,4)$	(3.17)
Objectives	$\min \boldsymbol{\lambda_R} = \min([\lambda_{Item,ds}])$	(3.18)
Constraints	$R_{IOR} = P(M_{IOR} \geq G_{IOR} \mid DE) = a\%$	(3.19)
	$\lambda_{Item,ds} = a_{Item} + b_{Item} \cdot (ds)^{c_{Item}}$	(3.20)
	$\sum_{\substack{All\ PDE \\ Scenarios\ s'}}^{N_s} \sum_{i=1}^{I_N} P(SD^i \leq 1) = \sum_{\substack{All\ PDE \\ Scenarios\ s'}}^{N_s} \sum_{i=1}^{I_N} P(NA^i \leq 2) = \sum_{\substack{All\ PDE \\ Scenarios\ s'}}^{N_s} \sum_{i=1}^{I_N} P(ND^i \leq 1)$	(3.21)

3.6.5 Illustration

In this part, the risk de-aggregation framework is applied to a hypothetical community with homogeneous building portfolio under seismic hazard to illustrate the methodology and examine key factors that may affect the results of risk de-aggregation. By

default, the community is a 20km * 20km square located in Middle and East U.S. (MEUS). Suppose there is only one fault lies on the left side of the community with a length of 100 km. The distance *d* from the center of the community to the fault is 50 km. The layout of the community and the location of the fault line is illustrated in Figure 3.14. In this case study, uniform design objectives are considered throughout the portfolio, i.e. all buildings within the portfolio are associated with the same $\boldsymbol{\lambda_R}$.

To model the uncertainties within the fault rupture location, 30 possible epicenter locations are considered evenly distributed on the fault line. The magnitude, m ranging from 5.0 to 8.0 is partitioned into 15 discrete intervals. Stratified sampling is applied to increase the samples on large magnitudes. From tentative simulations, 500 MCS is employed for each (M, L) pair to generate random fields from ground motion attenuation model (Atkinson & Boore, 1995).

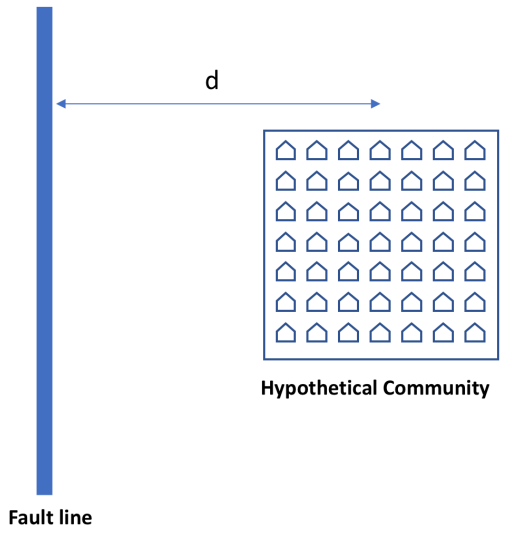

Figure 3.14 A hypothetical community with homogeneous portfolio and the seismic fault line

Firstly, the relation between the system reliability of the portfolio IO performance, R_{IOR} and mean individual building probability of un-occupancy, $\bar{p}_{UO}$ under different resilience goals, G_{IOR}, is investigated, as illustrated in Figure 3.15. For given G_{IOR}, when $\bar{p}_{UO}$ decreases, R_{IOR} increase monotonically. For fixed $\bar{p}_{UO}$, higher G_{IOR} corresponds to lower R_{IOR}. In addition, it is obtained the $\bar{p}_{UO} = 0.16$ for a homogeneous portfolio with W1 type (high code in HAZUS), and if $G_{IOR} = 0.8$, then $R_{IOR} = 0.65$ (65% confidence that 80% percent of the buildings within the portfolio will be in Immediate Occupancy or above under design earthquakes). The Target performance level for individual buildings is further defined as $\bar{p}_{UO} = 0.0928$, which corresponding to $R_{IOR} = 0.8$ given $G_{IOR} = 0.8$. Table 3.10 list the fragility parameters from Default (W1 in HAZUS) and Target performance. In the rest of this section, unless otherwise indicated, the combination of system reliability of the portfolio IO performance $R_{IOR} = 0.8$ and resilience goal $G_{IOR} = 0.8$ is selected as the Target.

Next, the relation between R_{IOR} and $\boldsymbol{\lambda}$ is examined. As illustrated in Figure 3.16, the value of $\boldsymbol{\lambda_R}$ for all of three components (ST, NA, and ND) increase non-linearly when R_{IOR} increases, given $G_{IOR} = 0.8$.

Table 3.10 The comparison of fragility parameters between Default (W1 high code in HAZUS) and Target performance

	Structural (ST)				**Non-structural Drift-sensitive (ND)**				**Non-structural Acceleration-sensitive (NA)**			
	DS_1	**DS_2**	**DS_3**	**DS_4**	**DS_1**	**DS_2**	**DS_3**	**DS_4**	**DS_1**	**DS_2**	**DS_3**	**DS_4**
Default	0.51	1.84	5.45	12.48	0.50	1.20	3.10	6.80	0.31	0.61	1.29	2.46
Target	0.72	3.51	11.08	25.82	0.61	2.04	5.94	13.53	0.30	0.58	1.18	2.22

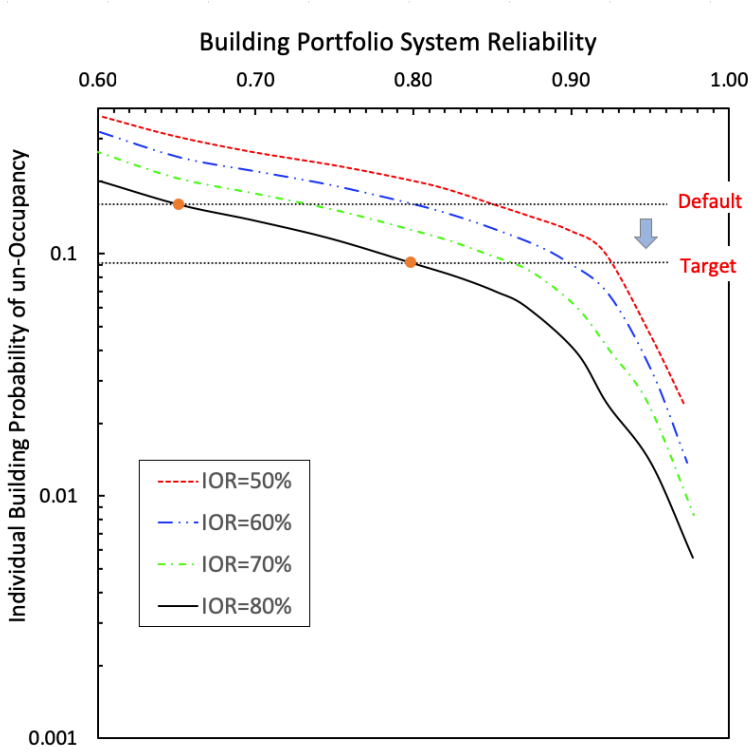

Figure 3.15 the relation between individual building probability of un-occupancy the system reliability of the portfolio IO performance, R_{IOR}, given different resilience goals, G_{IOR}

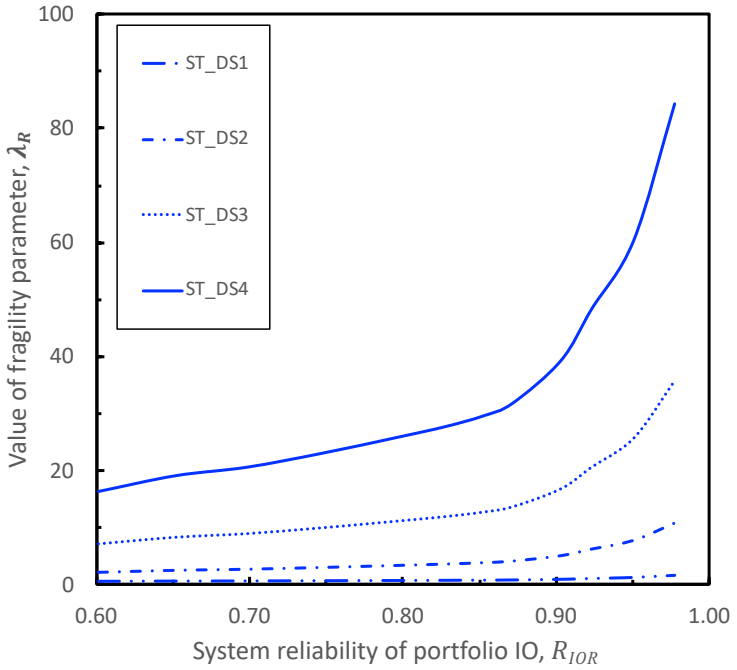
100
80
60
40
20
0
ST_DS1
ST_DS2
ST_DS3
ST_DS4
Value of fragility parameter, λ_R
0.60
0.70
0.80
0.90
1.00
System reliability of portfolio IO, R_{IOR}

(a)

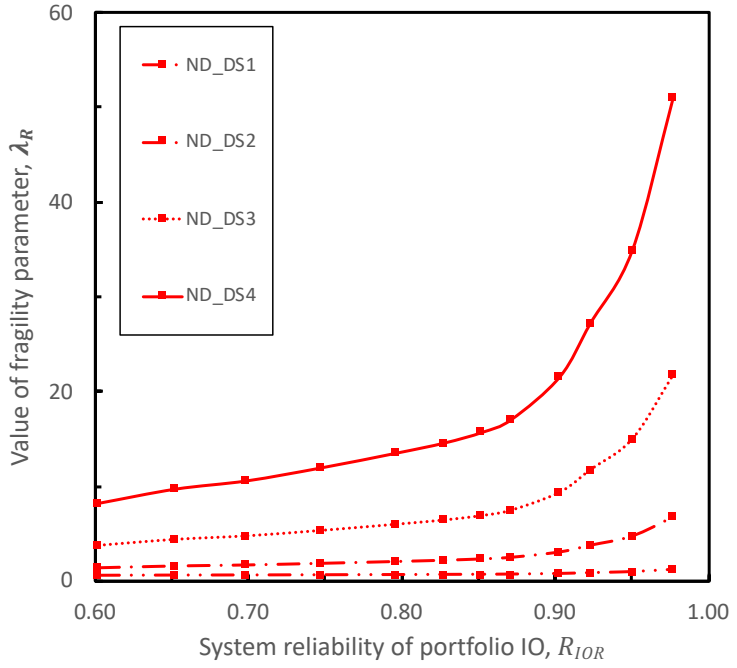
60
40
20
0
ND_DS1
ND_DS2
ND_DS3
ND_DS4
Value of fragility parameter, λ_R
0.60
0.70
0.80
0.90
1.00
System reliability of portfolio IO, R_{IOR}

(b)

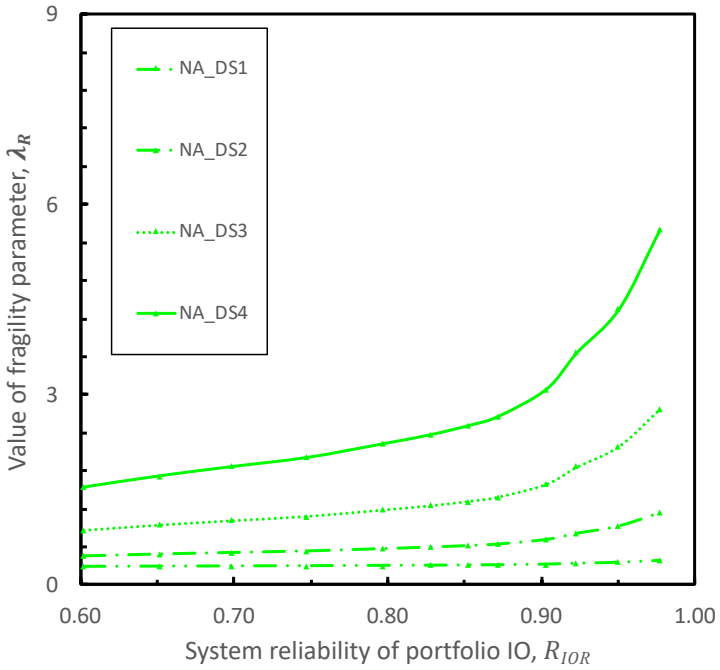

(c)

Figure 3.16 The relation between individual building probability of IO and fragility parameter, $\boldsymbol{\lambda_R}$ for (a)ST, (b) ND, and (c) NA components and the system reliability of the portfolio IO performance, R_{IOR}, given the resilience goal, $G_{IOR} = 0.8$

Some key parameters that may affect the result of de-aggregation are examined. Firstly, the effect of portfolio sample size (number of buildings sampled in the portfolio) is examined. As illustrated in Figure 3.17, the portfolio sample size has little effects on the value of fragility parameter, $\boldsymbol{\lambda_R}$.

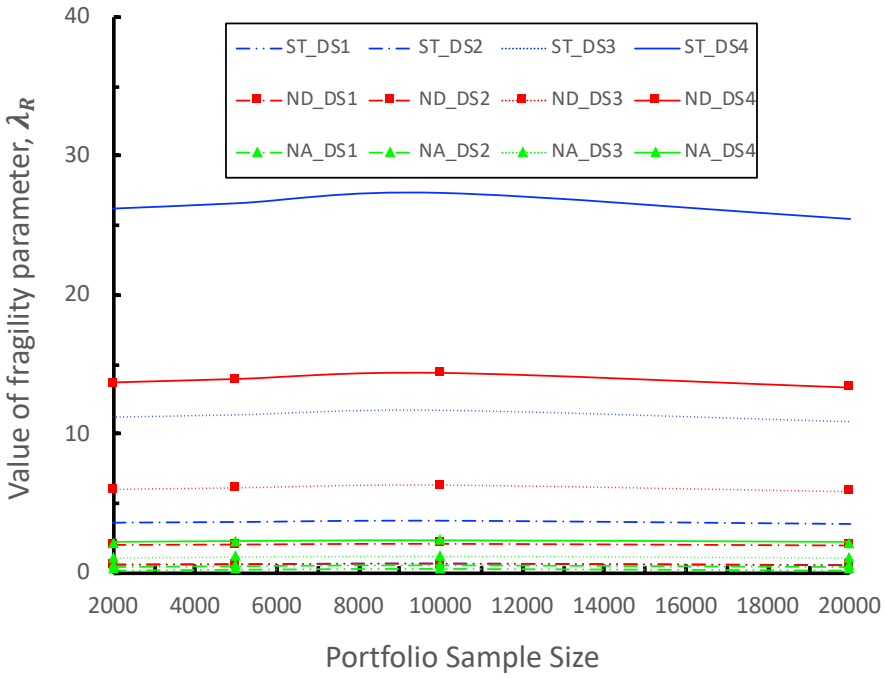

Figure 3.17 The effects of portfolio size (No. of buildings within portfolio): the value of fragility parameters, λ_R. associated with different portfolio sample size given building portfolio system reliability, $R_{IOR} = 0.8$ and resilience goal, $G_{IOR} = 0.8$.

Next, the effect of community expansion (e.g. due to economic and population growth) on risk de-aggregation is assessed. Here, two types of expansion pattern P1 and P2 are investigated, as illustrated in Figure 3.18(a) and (b) respectively. In Figure 3.19, for both P1 and P2, the expansion of the community tend to require lower fragility parameter, given the same building portfolio system reliability. Alternatively, if the fragility parameters keep the same (same individual building probability of un-occupancy), expansion of community will increase the building portfolio system reliability.

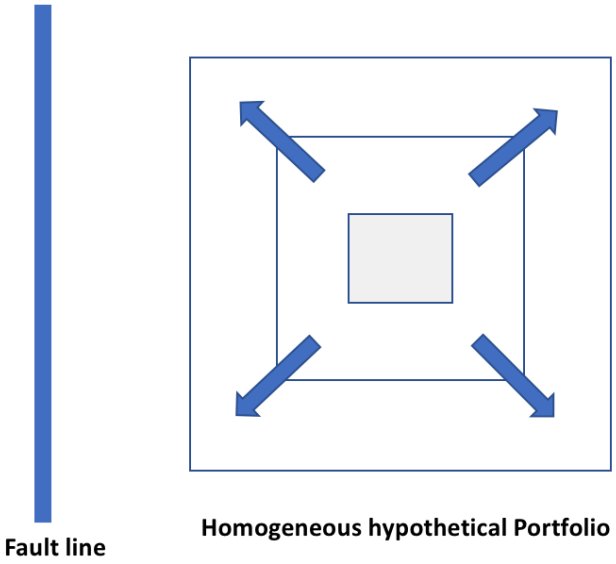

(a)

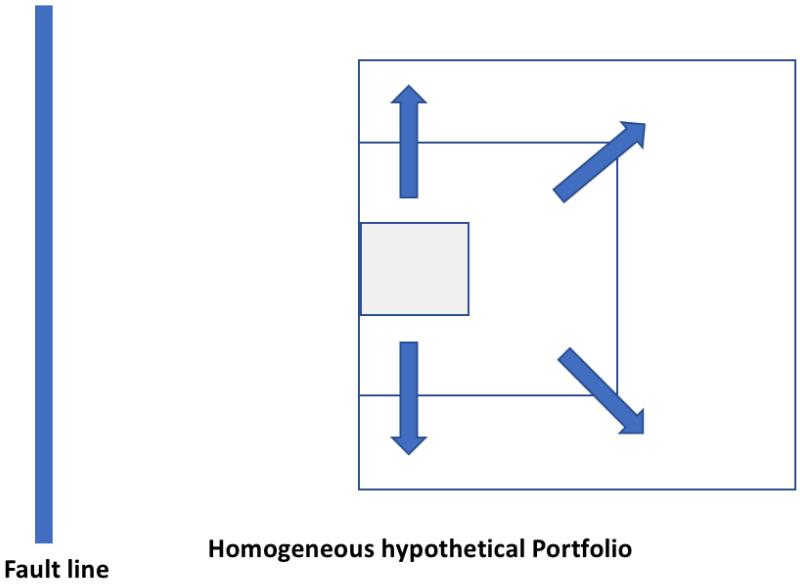

(b)

Figure 3.18 Portfolio expansion in (a) Pattern 1 (P1) and (b) Pattern 2 (P2)

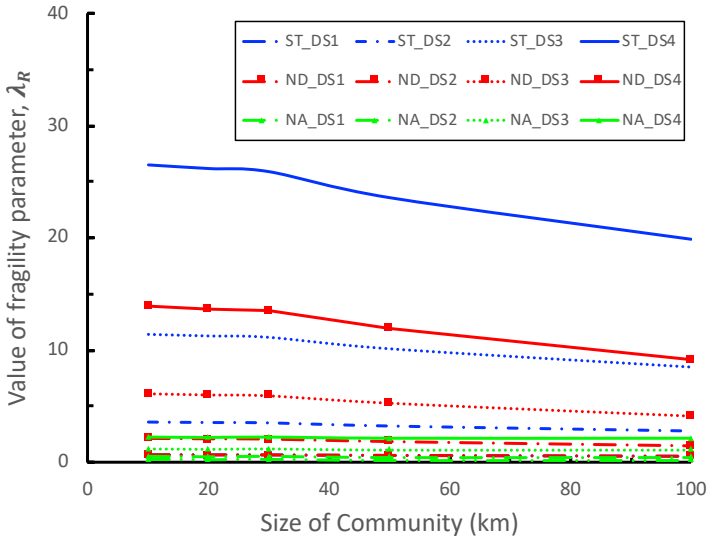

(a)

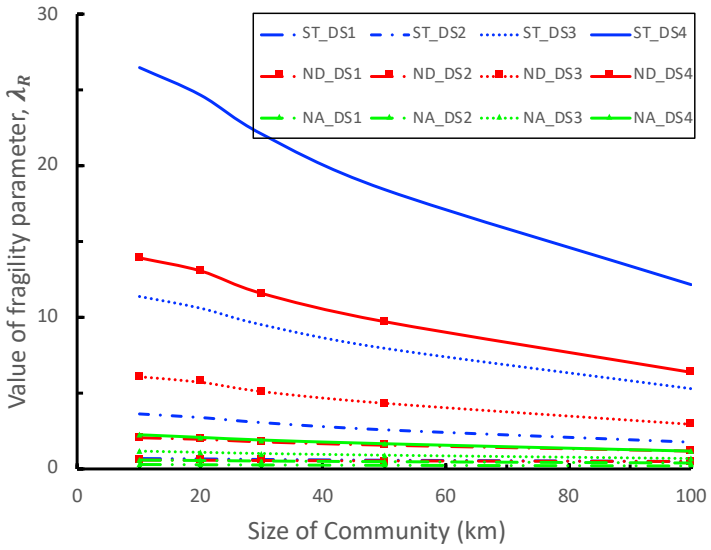

(b)

Figure 3.19 The effects of size of community for P1 ((a)) and P2 ((b)). (a) and (b) show the relation between value of fragility parameters, $\boldsymbol{\lambda_R}$ and size of community, given building portfolio system reliability, $R_{IOR} = 0.8$ and resilience goal, $G_{IOR} = 0.8$ for Pattern 1 and Pattern 2, respectively.

Lastly, the effects of the portfolio to fault distance is investigated. In Figure 3.20, the fragility parameters, $\boldsymbol{\lambda_R}$ decrease monotonically when the distance increases. Further, when the distance is not greater than 40 km, the value of $\boldsymbol{\lambda_R}$ become not sensitive to distance.

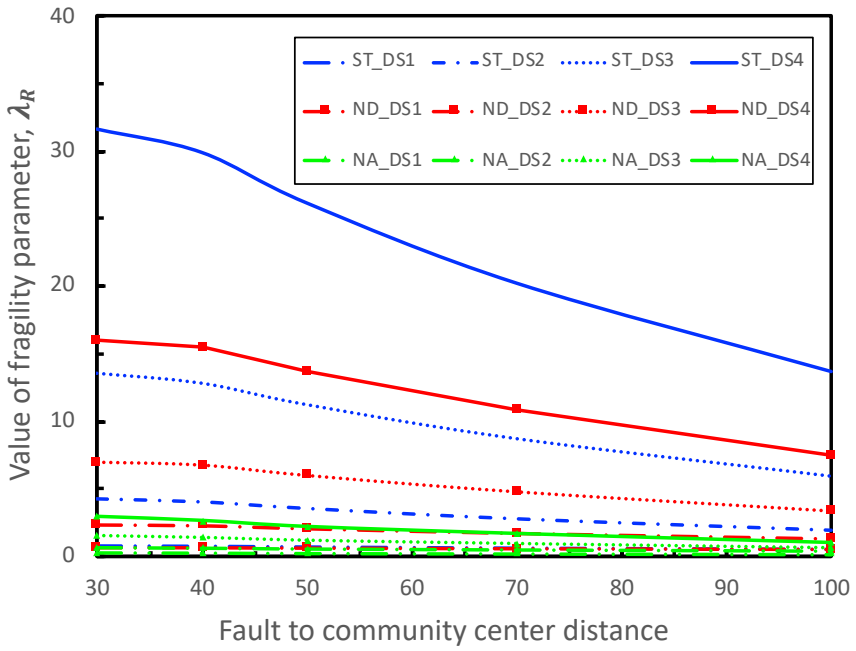

Figure 3.20 The effects of portfolio to fault distance on the fragility parameter b, given building portfolio system reliability, $R_{IOR} = 0.8$ and resilience goal, $G_{IOR} = 0.8$.

3.7 Closure

This section has proposed the concept of resilience-based design and tentatively established the link between the overarching community resilience goals and the minimum performance criteria of individual buildings for performance-based design, through a multi-layered, cascading de-aggregation framework. Resilience-based design emphasizes the design criteria of sub-systems and individual components should be linked to the requirement from global social and economic related community resilience goals. An essential part of the resilience-based design, de-aggregation consists of two parts: upper-level de-aggregation (relates sub-systems' performance goals to community's performance goals) and lower-level de-aggregation (relates individual components' minimum performance criteria to sub-systems' performance goals). It has been suggested that the performance criteria of buildings should be derived directly from the robustness portion of the community (or cluster) resilience goals, while de-aggregating the recovery portion of the resilience goals could yield organizational and preparedness guidelines for community resilience planning. This study has focused on the robustness and building performance criteria aspects. The feasibility of the de-aggregation framework has been verified by the residential building cluster exposed to tornadoes and earthquakes. Due to the distinct hazard characteristics and damage state definitions, different methodologies have been developed for portfolios under tornadoes and earthquake. The final outcome of the decision framework is a group of minimum fragility parameters that are ready to be applied to the development of new prototypes of residential buildings and form the basis for a new generation of design codes.

Chapter 4 Pre-hazard Retrofit Strategy

Chapter 3 has developed minimum performance criteria for designing of new residential buildings under natural hazards; however, existing buildings present even higher vulnerability as many of them are constructed in early times, when the design codes for residential buildings either did not exist or required lower performance levels than present ones. Traditionally, retrofit activities were limited in individual level and various guidelines have been published (e.g. FEMA 273 (FEMA, 1997) and FEMA 547 (FEMA, 2006)). It has been a great challenge for communities in hazard-prone regions to investigate the vulnerability of existing buildings and develop effective pre-hazard mitigation policies/incentives to enhance the performance of communities to avoid undesired outcomes such as economic recession and population outmigration in future hazards.

Aiming to minimize the gap between the "anticipated" and "desired" resilience performance for building portfolios, this chapter will develop a pre-hazard retrofit decision framework for existing building portfolios subjected to tornadoes. Retrofit is referred to as a pre-hazard mitigation strategy to enhance the robustness performance of individual components, which further contributes to a higher performance level in subsystems and communities as a whole. Retrofitting does not directly address the post-hazard recovery promptness, however, by eliminating the functionality drop and economic loss immediately after extreme hazards, communities can recover its functionality more quickly due to higher initiation point and more available resource. The minimum building

performance objectives derived from cluster resilience goals in Section 3.5 will be utilized to formulate the building cluster retrofit scheme. Two socioeconomic objectives: direct loss ratio (DLR) and un-inhabitable dwelling ratio (UIR) will be selected as the performance metrics. The task will result in a set of retrofitting recommendations and discuss how the preference of decision-makers and characteristics of buildings and their spatial distribution would affect the retrofitting strategies.

4.1 Decision Framework for Building Portfolio Retrofit

Led by proactive communities in California and Florida, there has been a growing trend of implementing large-scale, building cluster retrofit programs to enhance the resilience of under-performed community building clusters, however, to which extent such retrofit plan could close the gap between the anticipated resilience performance and desired performance goal is unknown. Limited studies have been done to investigate the optimal pre-hazard retrofit strategies for infrastructures in the context of community resilience. Cimellaro et al. (2010) compared four retrofit strategies for a hospital network consists of 6 hospitals in terms of the total cost (retrofit cost and expected earthquake loss), recovery time, and resilience value. Four strategies are considered for each structural type: (1) no action; (2) retrofit to life safety level (moderate code level in HAZUS); (3) retrofit to immediate occupancy level (high code level in HAZUS); (4) construction of a new building (a special high code level). In their assessment, the total cost is essentially a life-cycle loss. The expected earthquake loss in their study is obtained from loss-hazard curves with a control period (life-cycle) of 30 years. Jennings et al. (2015) proposed a seismic

retrofit optimization framework by considering four engineering and socioeconomic variables: morbidity rates, repair costs, relocation costs, and repair times. Pareto-optimal set of retrofit solutions are derived in a way that all metrics are first weight-summed to a single metric and minimized by genetic algorithm (GA). Zhang and Nicholson (2016) developed optimal retrofit strategies for a community with residential and commercial portfolios under a limited budget. The retrofit problem is formulated as a multi-objective linear programming (LP) mathematical model with two objectives: direct economic loss and population dislocation. However, their optimal strategies are conditioned on a pre-selected earthquake scenario, the effectiveness of such strategies for other scenarios is unclear. A decision framework for portfolio level retrofitting is needed that can incorporate the real hazard risk as well as target building performance criteria that fulfill community-level resilience goals.

This study, from a holistic perspective embodied in community resilience concept, develops a decision framework for building portfolio retrofit with the ultimate goal of enabling communities to achieve their resilience objectives under hazards. The decision framework includes three major steps, as illustrated in Figure 4.1: i) define community-level resilience goal(s), ii) de-aggregate the community-level goal to obtain individual building performance criteria as the building-level retrofit target, and iii) develop optimal retrofit strategies for existing building portfolios that minimize the gap between anticipated performance and the community-level resilience goals under specific hazard level.

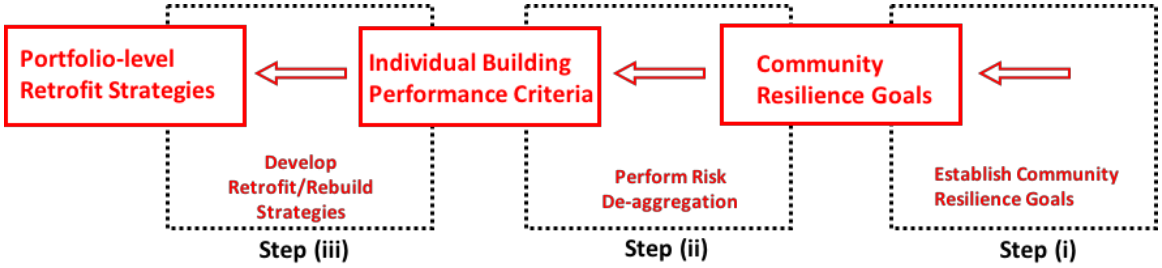

Figure 4.1: Flowchart of the decision framework for designing building portfolio retrofit strategies

In Step (i), community resilience goals with respect to building performance are defined by communities' stakeholders based on their risk perceptions, existing community infrastructure and available resources. Resilience goals "help a diverse set of stakeholders develop strategies for achieving the stated goals and prioritize supporting administrative and construction solutions, and guide the setting of specific goals for the desired performance of building and infrastructure systems" (NIST, 2015b). Three key components are needed in establishing the community resilience goals: a) appropriate resilience metrics (M), b) hazard levels and characterization (H), and c) acceptable risk threshold (G).

In Step (ii), with the resilience goals defined in (i), the individual building-level performance target (e.g. in terms of fragility parameters) is determined for retrofit constructions. A multi-layered risk de-aggregation algorithm could be developed to first de-couple the over resilience objectives to minimum performance requirements for each key functionality cluster, which further link to the minimum performance requirement of individual buildings that can facilitate these goals.

In Sept (iii), based on the building-level performance target derived in Step (ii), the optimal retrofit strategies for existing building portfolios are developed. Typically, it is desired more than one community-level performance goals (e.g. economic loss and population dislocation) could be achieved, thus the pre-hazard retrofit planning can be modeled as a multi-objective optimization problem (MOOP) under limited resources (e.g. budget). This decision step yields a set of recommended retrofit strategies that will enable the community to minimize the gap between its current resilience performance and its prescribed resilience goals (determined in Step (i)) under resource constraints.

This multi-step decision framework can facilitate communities' resilience planning over a long-time horizon through systemically designed, portfolio-level retrofit activities, and assist public decision makers (e.g., government agencies, building authorities, etc.) in creating policy incentives that can lead building owners towards decisions that collectively enhance community's resilience. As Chapter 3 has given a thorough discussion on Step (i) and (ii), the rest of this chapter will focus on Step (iii). For illustration purpose, the retrofit decision framework is implemented in residential building portfolio under tornado hazards. By employing the de-aggregated building performance criteria in Section 3.5 as the target for building retrofit construction, optimal retrofit strategies for building portfolios under limited resource (e.g. budget) are explored. Assessment of resilience metrics regarding different retrofit strategies forms the basis for optimization. Probabilistic assessment of community resilience metrics in Section 3.4 will be employed to evaluate and compare candidate retrofit strategies.

4.2 Resilience Metric

To be consistent with Chapter 3, two portfolio-level performance metrics - direct loss ratio (DLR) and un-inhabitable dwelling ratio (UIR) - are selected to represent the desire of communities to eliminate the adverse impact of extreme hazards on the economic development, social wellbeing, and long-term prosperity.

4.3 Retrofit Cost

A major challenge in the pre-hazard retrofit is to reasonably determine the retrofit cost, which can greatly determine the optimal retrofit strategies. Generally, the retrofit cost of the Type k building (C_k^{Ret}) depends on an array of factors: the original building resistance (R_k^0), the target resistance (R_k^T), building characteristics (e.g. roof type), local labor cost, availability of material, etc. Various studies have been done to estimate the retrofit cost. For instance, Stewart and Li (2010) assumed the retrofit cost to be 1% -50% for retrofit of buildings under cyclone hazard in Australia. FEMA P804 (FEMA, 2010) gave the retrofit cost ratio to be 1%-16%. Regarding the seismic hazard, Galanis et al. (2018) employed the retrofit cost to be varied from 5% to 30%. Kanda and Ellingwood (1991) suggested the retrofit cost for buildings might be approximated by a linear function of the difference between the target resistance and current resistance. Based on their work, in this study, the following formulation is proposed to model the retrofit cost:

$$C_k^{Ret} = C \cdot A_k \cdot (e^{\bar{\lambda}_k^T} - e^{\bar{\lambda}_k^0}) \tag{4.1}$$

$$\bar{\lambda}_k^T = \frac{1}{4}\sum_{ds=1}^{4} \lambda_{k,ds}^T \tag{4.2}$$

$$\bar{\lambda}_k^0 = \frac{1}{4}\sum_{ds=1}^{4} \lambda_{k,ds}^0 \tag{4.3}$$

where $\bar{\lambda}_k^0$ and $\bar{\lambda}_k^T$ are the mean of the logarithmic mean of capacity with respect to the four damage states for the *Type k* building of existing and target state, respectively; $\lambda_{k,ds}^0$ and $\lambda_{k,ds}^T$ are the logarithmic mean capacity of the logarithmic mean of capacity with respect to damage state ds for the *Type k* building of existing and target state, respectively. $\lambda_{k,ds}^T$ has been derived in Section 3.5. C is a constant associated with other characteristics of Type *k* building; A_k is the square footage of the Type *k* building.

4.4 Formulation

Generally, for existing building portfolios, communities seek to enhance their performance under future extreme hazard event by designing incentives to encourage individual building owners to implement pre-hazard mitigation activities. Thus, community decision-makers usually face the problem of allocating limited resources to support such mitigation activities to best close the gap between the target resilience goals and anticipated resilience performance under specific hazard intensity. This study will provide the basis for designing the incentives by determining the number of buildings to be retrofitted in each type in each zone.

Accordingly, the planning of retrofit strategies is formulated as an optimization problem to minimize DLR and UIR simultaneously under the limited financial budget subjected to EF5 tornadoes; The decision variables are the number of each type of building in each zone to be retrofitted to the performance level determined by risk de-aggregation. This optimization problem will be treated as a multi-objective integer programming problem (MOIPP) since all the decision variables are integers. Laskari (2002) compared the performance of particle swarm optimization (PSO) with branch and bound (BB) and found PSO to be an efficient optimization technique for solving integer programming problem even for a problem with high dimension cases. In most cases, PSO outperforms the BB approach and is not likely to suffer from search stagnation. Thus, the multi-objective particle swarm optimization (MOPSO) introduced in Section 3.5.4 is employed here with minor modification.

As tabulated in Table 4.1, Eq. (4.4) defines decision variables $\boldsymbol{x} = [x_{j,k}]$, where $x_{j,k} \in \mathbb{Z}$ is the number of Type k buildings in Zone j to retrofit, in integer; $N_{j,k}$ denotes the total number of Type k buildings in Zone j. Eq.(4.5) and Eq. (4.6) define the two objectives for the cluster retrofit strategy, i.e. minimizing 95 percentiles of DLR and UIR, respectively, under EF5 tornadoes. The calculation of $M_{DLR,EF5}$ and $M_{UIR,EF5}$ can be referred to Section 3.5.2. Eq. (4.7) defines the constraint that the total retrofit cost (C_T^{Ret}) should be not greater than the given budget B. Eq. (4.8) defines the constraint that the number of buildings to be retrofitted in Type k located in Zone j should not be greater than $N_{j,k}$.

The outcome of this task will be a Pareto-front curve that will give the trade-off between DLR and UIR performance conditioned on a specific financial budget.

Table 4.1 Decision variables, objectives and constraints of pre-event retrofit

Item	Equation	Equation No.
Decision Variables	$\boldsymbol{x} = [x_{j,k}], \quad x_{j,k} \in \mathbb{Z}$	Eq. (4.4)
Objectives	$\min.(M_{DLR,EF5})$	Eq. (4.5)
	$\min.(M_{UIR,EF5})$	Eq. (4.6)
Constraints	$C_T^{Ret} = \sum_j \sum_k x_{j,k} \cdot C_k^{Ret} \leq \mathrm{B}$	Eq. (4.7)
	$x_{j,k} \leq N_{j,k}$	Eq. (4.8)

4.5 Illustration

The cluster retrofit planning concept is illustrated by a hypothetical residential cluster with existing buildings distributed over 20 miles by 20 miles area and located in mid-west U.S., which consists of two residential zones (Z1 and Z2) and filled with two types of buildings: single-family houses (E1) and multi-family apartments (E2, with 4 dwelling units). Detailed attributes and spatial distributions of E1 and E2 are summarized in Table 4.2 (FEMA/NIBS, 2003; Amini & van de Lindt, 2013). The target performance for building retrofit construction is the Code Level 3 obtained in Section 3.5.5, i.e. $\boldsymbol{\lambda_R^T} = \boldsymbol{\lambda_R^{CU}}$, for this illustration.

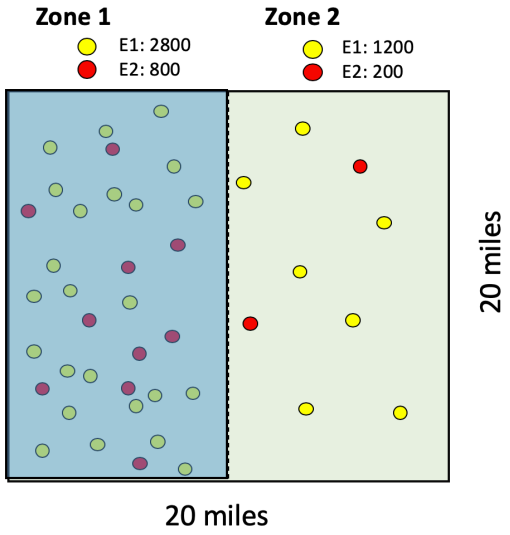

Figure 4.2 Illustration of a hypothetical community with two types of buildings in two zones

Table 4.2 Attributes of Existing Buildings

Type	Sq. Ft.	Roof type	Total Assessed Value (TAV_k) (USD)	λ_R^0	ε_R^0	C_k^{Ret} (USD)	Number of buildings		
							Zone 1	Zone 2	Total
1	1,253	Gable	$203,223	[4.52,4.70,4.77,4.81]	0.12	$3,600	2,800	1,200	4,000
2	3,180	Hip	$308,317	[4.42,4.51,4.60,4.69]	0.12	$13,800	800	200	1,000

Figure 4.3 presents the tradeoffs between the two optimization objectives and Prato-front of the "optimal" retrofit schemes (RS) under the budget limit of U.S. $12.0 Million (M). In all optimal schemes on the Prato-front, the absolute number and percentage of buildings to retrofit in Z1 (with higher building density) is much larger than that of Z2 (with lower building density). The relative proportion of retrofitted buildings

between E1 and E2 varies among the optimal schemes. For example, in the DLR-driven RS1, detailed in the upper left subplot, the majority of buildings to retrofit are of Type E1 located in Z1, while in the UIR-driven RS3, most retrofit activities are allocated to Type E2 buildings in Z1.

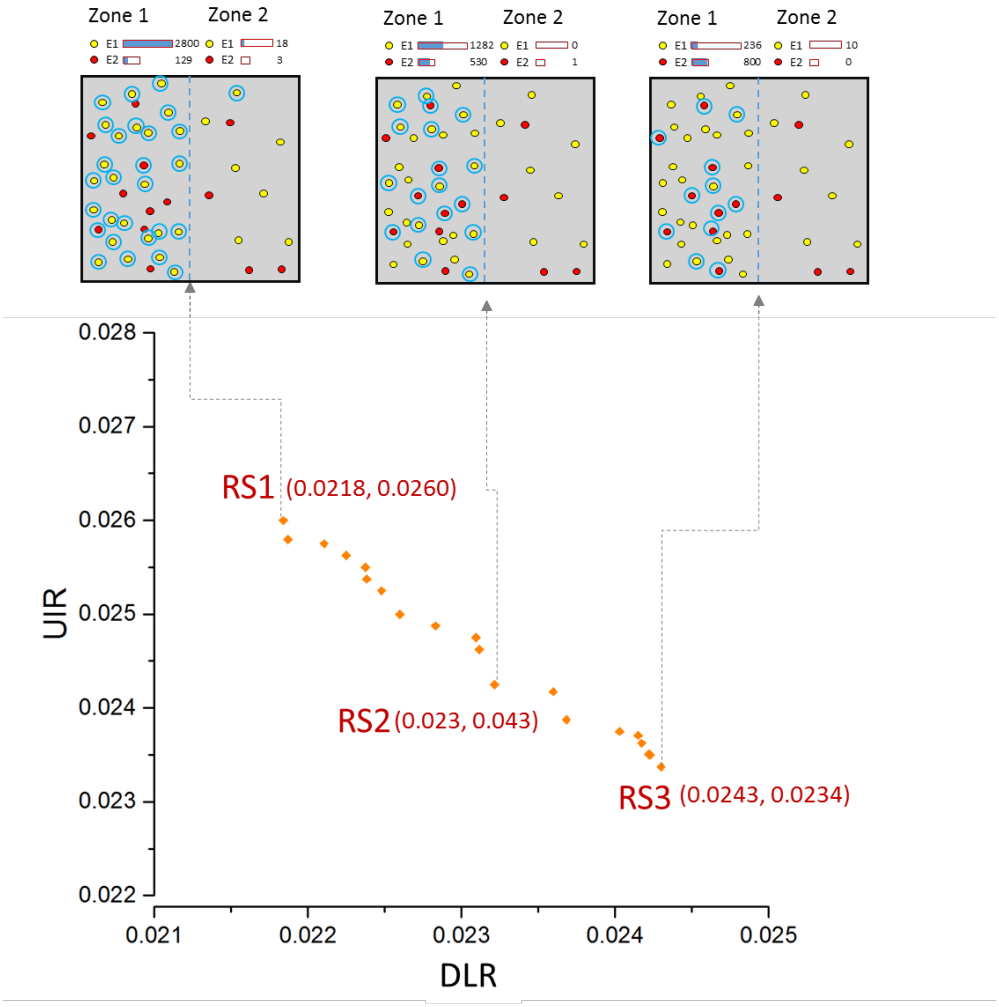

Figure 4.3 The trade-off between DLR and UIR in optimal retrofit scheme with $12 Million budget limit and distribution of retrofitted buildings in each zone and type from three typical locations of the curve.

Figure 4.4 shows the optimal retrofit scheme for a range of budget from U.S. $4M to $28.3M (full retrofit, i.e. all buildings in the portfolio can be retrofitted). Naturally, both DLR and UIR decrease monotonically when the available retrofit budget increases. When the budget is very low (e.g. $4M) or very high (e.g. $28.3M), the range of trade-off between the DLR and UIR is very limited with less-varying optimal strategies. On the contrary, a mid-range budget (e.g. $12M, about 42.4% of full retrofit budget) offers more alternative retrofit schemes with a wide range of relative preference between the two objectives. The proportion of buildings (in average for multiple retrofit schemes) recommended for retrofit between the two zones and two building types are summarized in Figure 4.5, indicating when the budget is in low to moderate range(i.e. $4M - $16M), almost all of the retrofit budget is allocated in Z1, and as the budget increases to over $20M, one start to observe a portion of buildings in Z2, mostly type E1, being recommended for retrofit. Regardless of the zones, type E1 buildings are the majority to be retrofitted for all the budgets investigated here.

Although these results are specific to the characteristics of the hypothetical community and the assumed retrofit cost estimation method, such methodology can provide a rich array of information to support community's hazard mitigation and policy design activities toward a hazard-resilient built environment that fully considers the uncertainties in future hazard.

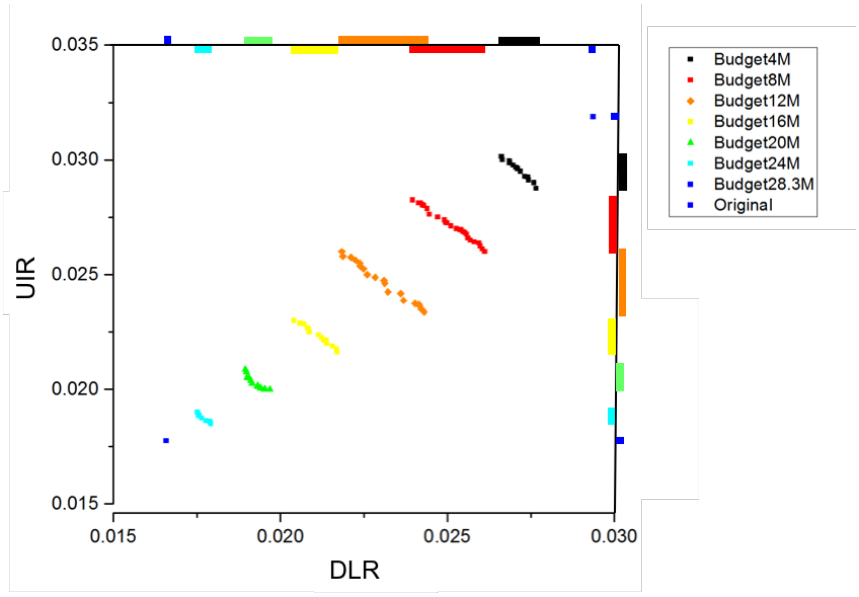

Figure 4.4 Trade-off between DLR and UIR in optimal retrofit schemes under different budget limit

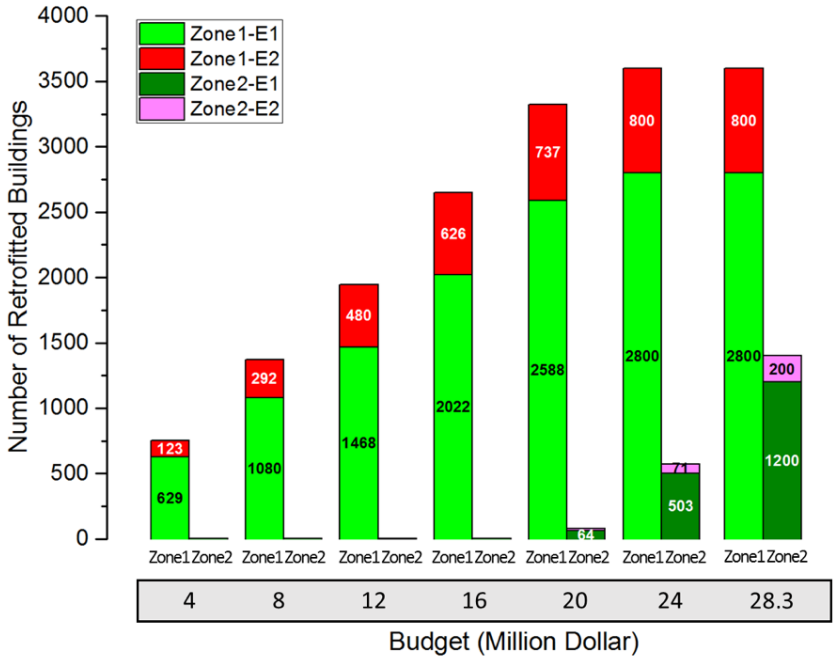

Figure 4.5 Average retrofitted buildings for each building type in each zone under different budgets

4.6 Closure

This chapter has proposed a decision framework for designing large-scale building portfolio retrofit strategies with an ultimate goal of achieving community resilience objectives under high uncertainties of future extreme hazard events. As an illustration, tornado hazards, specifically EF5 tornadoes, are selected to estimate the resilience performance and guide the retrofit strategies. Two performance metrics - direct loss ratio and un-inhabitable dwelling ratio - have been utilized to illustrate the condition when more than one performance metrics are selected by a group of stakeholders. The retrofit problem has been formulated as a multi-objective integer programming problem under a limited financial budget, solved by the algorithm of multi-objective particle swarm optimization. The outcome of this framework is a set of near-optimal retrofit strategies regarding the number of buildings to be retrofitted for each type in each zone. These retrofit schemes can facilitate communities' resilience planning over a long-time horizon through systemically designed, portfolio-level retrofit activities, and assist public decision-makers (e.g., government agencies, building authorities, etc.) in creating policy incentives which can lead building owners towards decisions that collectively enhance community's resilience.

Chapter 5 Post-hazard Reconstruction Strategy

For building portfolios just experienced catastrophic damage from severe natural hazards, it is imperative to implement post-hazard reconstructions. In addition, a given building portfolio would experience multiple hazard events over a long-time horizon. It is desirable to incorporate the hazard mitigation plan into the reconstruction decisions. The fact of future hazard exposure and considerable investment involved in implementing reconstruction suggest that the reconstruction of damaged building portfolios could be framed under the umbrella of life-cycle analysis (LCA). However, currently, the reconstruction of building portfolios after hazards tends to simply reconstruct the damaged buildings as before by individual owners. Further, no quantitative decision-making model has been developed to adequately address the difficulties in defining the optimal reconstruction levels as well as the resource allocation over a long-time horizon.

This task will scale the life-cycle analysis (LCA) from individual buildings to building portfolios and propose a framework that could support communities' building-back-better (BBB) decisions after major hazard events. It will first propose a post-hazard reconstruction decision framework followed by the development of building portfolio LCA (BPLCA) measured by expected building portfolio life-cycle cost (EBPLCC) and cumulative prospect value (EBPCPV) with two key ingredients: building portfolio life-cycle (BPLC) and renewal rate (BPRR). It will then discuss how to apply the BPLCA in seismic hazard considering the temporal characteristics of earthquakes. Further, the decision-making for reconstructions is modeled as an optimization problem by minimizing

the EBPLCC or maximizing the EBPCPV. It will discuss how the BPLC, risk averseness, and hazard characteristics would affect the BPLCA results and optimal reconstructions.

5.1 The Post-hazard Reconstruction Decision Framework

This section will propose a risk-informed decision framework that could enable a community to rebuild its damaged building portfolio to achieve pre-defined resilience and/or sustainability goals in the future in a most efficient way.

Firstly, it is proposed that BBB should be defined by the efficiency in the post hazard reconstruction process. Post-hazard reconstruction process is a large-scale investment issued by government agencies or private owners, in either way, decision-makers seek to find the strategy that minimizes overall monetary cost or maximizes value depending on their risk-attitude. Due to long time-horizon of future lifetime, life-cycle assessment (LCA) that scales to portfolio level (building portfolio LCA, BPLCA) will be employed to evaluate the total impact from the reconstruction, natural renewal, and future hazard exposure. The optimal post-hazard reconstruction strategy is the one that minimizes the expected building portfolio life-cycle cost (EBPLCC) or maximizes the expected building portfolio cumulative prospect value (EBPCPV).

Secondly, the optimal reconstruction strategy should also fulfill the performance requirement on resilience and/or sustainability. Resilience requirement ensures that the functionality loss and economic cost immediately after extreme hazard events are under control (Robustness) and the recovery process is in a prompt manner (Rapidity) to reduce indirect social-economic impact and avoid the grave result of population permanent

outmigration. Similarly, sustainability requirement ensures that the reconstruction strategy does not enforce excessive environmental pressure and financial burden on future generations. In this study, both resilience and sustainability are considered. It should be noted that the resilience and sustainability aspects of a certain strategy are evaluated in different time-frame. For the resilience assessment, only extreme events (e.g. M7 - M8 earthquakes) are considered and there is no "time" involved or limited to post-hazard recovery time. On the other hand, LCA is generally required in sustainability assessment and some resilience assessment, thus the BPLCA are needed for the portfolio level assessment.

Figure 5.1 illustrates the workflow of the post-hazard reconstruction decision framework. The framework begins with the given post-hazard damage state of each building in the portfolio as well as the hazard model of the geological location. Then, a reconstruction strategy (can be arbitrary at first) is generated, i.e. the reconstruction action for a certain type of building in certain damage state. After that, the feasibility of the strategy is checked in resilience aspect. For feasible strategies, BPLCA is conducted over the BPLC. The framework stops when the optimal reconstruction strategy is found with minimum EBPLCC or maximum EBPCPV, otherwise, a new strategy is generated by some algorithm (e.g. Genetic Algorithm).

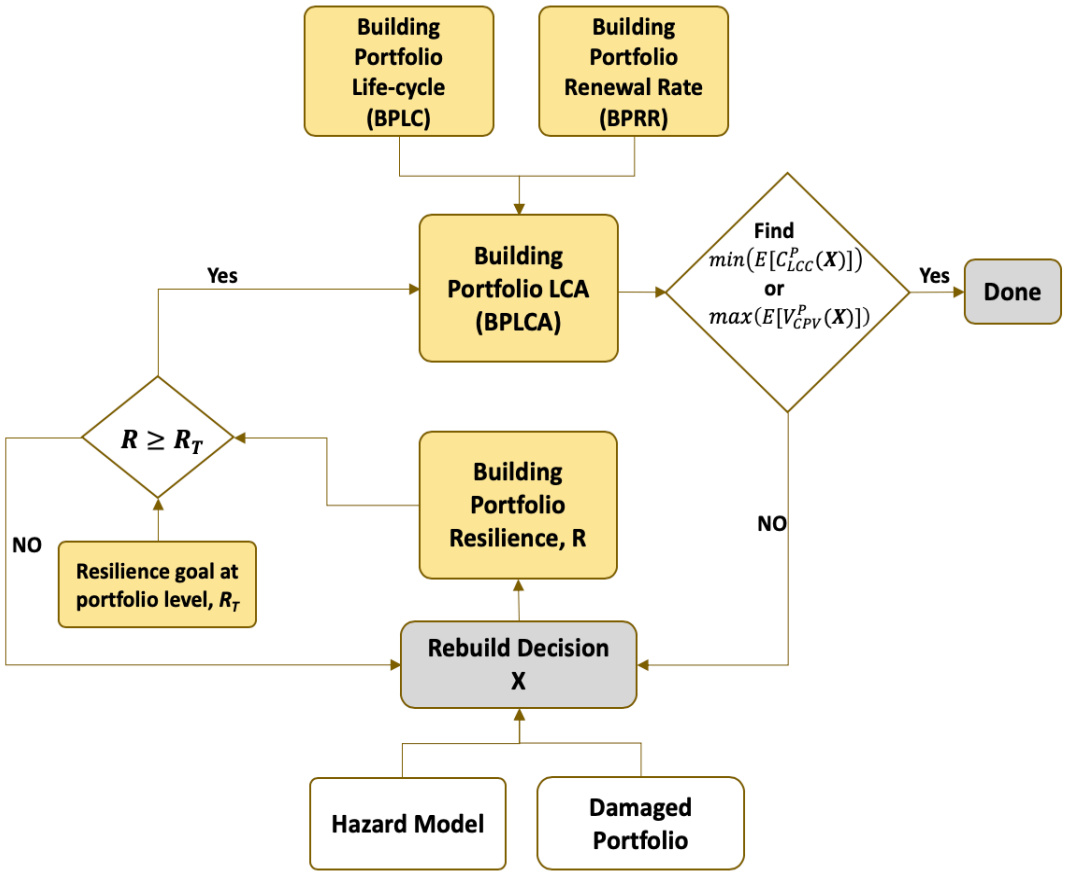

Figure 5.1: Illustration of the BBB decision framework

5.2 The Life-cycle of a Building Portfolio

Buildings in a community are continuously experiencing a dynamic renewal process and amending the existing building portfolio, i.e. constantly being constructed, maintained, repaired, retrofitted, damaged, demolished and rebuilt, as illustrated in Figure 5.2. A natural disaster is a temporary detour in this long-term process - to an extent, it accelerates the renewal of building portfolios, and well-designed building-back strategies could even help enhance future hazard preparedness of portfolios. This section will derive

two key ingredients for the BPLCA framework: 1) the "life-cycle" of a building portfolio (BPLC) and 2) its renewal rate (BPRR).

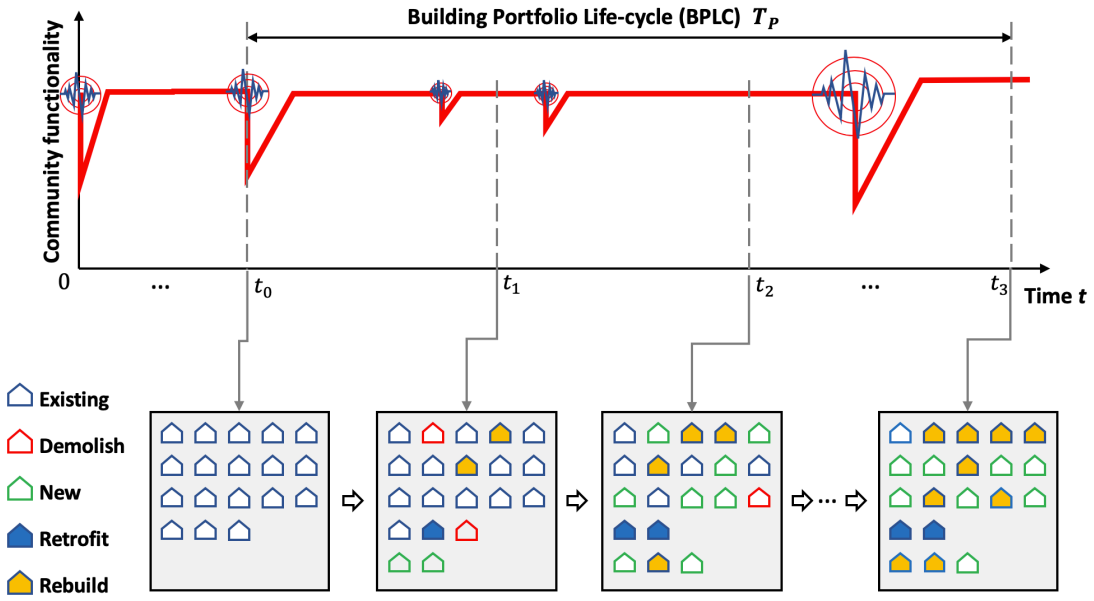

Figure 5.2 Illustration of portfolio renewal under natural hazard events over a long-time horizon

5.2.1 Life-cycle Length of Building Portfolios

Conceptually, the BPLC is defined as the time-span during which a building portfolio has been renewed completely, as shown in Figure 5.2, due to natural turnover and rebuilding, unrelated to hazard exposure. The renewal process is stochastic and affected by many variables, including the life-cycle of individual buildings (BLC), community's economic development, socio-demographics, etc.

Now it is assumed that the life-cycle of building portfolio (BPLC), T_P is only a function of the BLC, T_l , $l \in (1, 2, \dots, L)$, and L is the number of buildings in (or the size of) the portfolio. Further, let $T_{P,r}$ denote the time in which r% of buildings being replaced (e.g. the time takes for 90% of the portfolio being renewed is $T_{P,90}$). The PDF of $T_{P,r}$, $f_{T_{P,r}}(t)$ for a portfolio containing buildings, each with identical BLC, is (Larsen & Marx, 2011):

$$f_{T_{P,r}}(t) = L\binom{L-1}{rL-1} f_1(t)[F_1(t)]^{rL-1}[1 - F_1(t)]^{L-rL} \tag{5.1}$$

in which, $r \cdot L$ denotes the number of buildings that are replaced; $F_1(t)$ and $f_1(t)$ are the CDF and PDF of BLC, respectively. Eq. (5.1) can be extended to portfolios containing buildings with different BLCs. For realistic communities with a complex mix of buildings with different BLCs and built years, Monte Carlo Simulation (MCS) is generally needed to obtain the BPLC. Define $t^c_{p,r} = E[T_{P,r}]$ as the *characteristic* BPLC.

For example, consider a portfolio with 2 types of BLCs (BLC1 and BLC2, tabulated in **Error! Reference source not found.**) in which the ratio of the two types is $n1/n_2$ = 2.0. MCS is employed to obtain $t^c_{p,r}$ and its sensitivity to different portfolio sizes. Figure 5.3 shows the mean and c.o.v. of the BPLC $t^c_{p,r}$ from MCS. As the portfolio size increases, the mean of $t^c_{p,r}$ is quite stable while the c.o.v. of decreases monotonically. Thus, the $t^c_{p,90}$ obtained from a small building portfolio size is also applicable to large

portfolio size if n_1/n_2 is kept the same. By the end of BPLC, many buildings may already have been reconstructed for two times or more, since the mean BLC are much shorter than the BPLC as given in Eq. (5.1). For simplicity, T_P is defined as the BPLC and subscript r is dropped in the rest of this study.

Table 5.1 The statistics of two BLC types

BLC type	Mean BLC
BLC1	50
BLC2	30

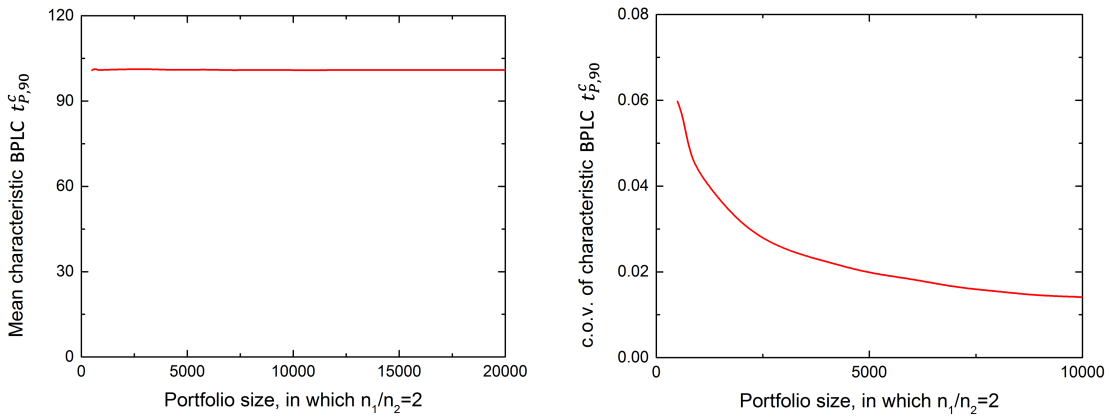

(a) (b)

Figure 5.3 The (a) mean and (b) c.o.v. of BPLC $t^c_{p,r}$ with different portfolio size

5.2.2 Renewal Rate of Building Portfolios (BPRR)

Let $N(t)$ = the number of building in the portfolio at time t, $\dot{N}(t)$ = growth rate of $N(t)$ at time t, $\dot{N}_N(t)$ and $\dot{N}_D(t)$ as the rate of new construction (renewal rate) and

demolition, respectively, within the portfolio. The equilibrium of portfolio renewal is written as

$$\dot{N}(t) = \frac{N(t+\Delta t) - N(t)}{\Delta t} = \dot{N}_N(t) \ - \dot{N}_D(t) \tag{5.2}$$

If the population of the community remains relatively stable, the size of the portfolio within a stable community is nearly constant over time, which implies $\dot{N}(t) = 0$ and $\dot{N}_N(t) = \dot{N}_D(t)$. The renewal rate $\dot{N}_N^i(t)$ of buildings of Type *i* BLC is:

$$\dot{N}_N^i(t) = n_i \cdot \int_0^\infty h_i(t,\tau) f_a^i(t,\tau) d\tau \tag{5.3}$$

where $h_i(t,\tau) = f_i(t,\tau)/\big(1 - F_i(t,\tau)\big)$ is the probability of demolition (due to natural replacement) of buildings with Type *i* BLC at time t (at age of τ) conditioned on no demolition prior to time t , where $f_i(t,\tau)$ and $F_i(t,\tau)$ are the PDF and CDF of Type *i* BLC evaluated in time t with an age of τ; $f_a^i(t,\tau)$ is the PDF of age τ for Type *i* BLC in time t; and n_i is the number of buildings with Type *i* BLC in the portfolio. For a portfolio with *I* types of BLC, the total renewal rate of the portfolio (BRR) is:

$$\dot{N}_N(t) = \sum_{i=1}^{I} \dot{N}_N^i(t) \tag{5.4}$$

To illustrate the proposed approach, it is assumed that the renewal process of individual buildings is a Poisson process. Thus, the Type *i* BLC follows the exponential distribution with $h_i(t,\tau) = 1/\lambda_i$, here λ_i is the mean value of BLC of Type *i*. Eq. (5.4) now becomes $\dot{N}_N^i(t) = n_i \cdot (1/\lambda_i) \cdot \int_0^\infty f_a^i(t,\tau)d\tau = n_i/\lambda_i$ if $f_a^i(t,\tau)$ is independent of time (i.e. $f_i(t,\tau) = f_i(\tau)$).

5.3 Building Portfolio Life-cycle Analysis

Building portfolio life-cycle analysis (BPLCA) is defined as a technique to analyze the impact of specific metric (e.g. monetary cost) associated with all stages of a building portfolio, which is extended from the concept of life-cycle assessment (LCA) for individual buildings (Simonen, 2014). BPLCA may include not only the direct economic impact from post-hazard reconstruction and repair, but also indirect impact from the loss of building functionality, fatality, population dislocation, and reduced economic activities etc. (NIST, 2015b). In the following, a BPLCA formulation is introduced with the objective of facilitating decision-making in post-event reconstruction.

5.3.1 Expected Building Portfolio Life-cycle Cost

The building portfolio LCC (BPLCC) may be expressed as a function of reconstruction actions $\boldsymbol{X}$:

$$C_{LCC}^{P}(\boldsymbol{X}) = C_{Re}(\boldsymbol{X}) + C_{New}^{C}(\boldsymbol{X}) + C_{Dam}^{C}(\boldsymbol{X}) + C_{Cas}^{C}(\boldsymbol{X}) + C_{Ind}^{C}(\boldsymbol{X}) \quad (5.5)$$

in which $C_{Re}(\boldsymbol{X})$ denotes the cost of reconstruction and repair of the damaged portfolio at t_0 (immediately following the hazard event); $t = 0$ is the time of last characteristic earthquake event (c.f. Figure 5.2). $C_{Re}(\boldsymbol{X})$ depends on the number of each building type (defined by structural system, occupancy type and number of stories) in each of damage state, DS (total of four damage states: minor ($DS = 1$), moderate ($DS = 2$), extensive ($DS = 3$), complete ($DS = 4$)) following the disruptive event. The superscript *C* on the rest of the terms represents that the corresponding cost is accumulated throughout the entire BPLC, T_P. Specifically, $C_{New}^{C}(\boldsymbol{X})$ is the cumulative construction cost of new buildings due to natural renewal; $C_{Dam}^{C}(\boldsymbol{X})$ and $C_{Cas}^{C}(\boldsymbol{X})$ are the cumulative costs of building damages and casualty due to future hazard exposure, respectively; $C_{Ind}^{C}(\boldsymbol{X})$ is the cumulative indirect loss due to disruptions of local economy and social well-being caused by functionality loss of buildings following future disasters. All items in Eq. (5.5) depend on the reconstruction action $\boldsymbol{X}$ at t_0. The expected BPLCC (EBPLCC) is:

$$E[C_{LCC}^{P}(\boldsymbol{X})] = E[C_{Re}(\boldsymbol{X})] + E[C_{New}^{C}(\boldsymbol{X})] + (\omega + 1) \cdot E[C_{Dam}^{C}(\boldsymbol{X})] + E[C_{Cas}^{C}(\boldsymbol{X})] \quad (5.6)$$

in which $E[C_{Ind}^{C}(\boldsymbol{X})]$ is assumed to equal ω times $E[C_{Dam}^{C}(\boldsymbol{X})]$ (Crowther & Haimes, 2005); $E[C_{Re}(\boldsymbol{X})]$ can be expressed as:

$$E[C_{Re}(\boldsymbol{X})] = \sum_{i=1}^{I}\sum_{j=1}^{4} n_{i,j,x} \cdot C_{Re}^{i,j}(x) \tag{5.7}$$

in which $n_{i,j,x}$ denotes the number of Type *i* buildings in *j-th* damage state at t_0 with rebuilt action x ; $C_{Re}^{i,j}(x)$ denotes the reconstruction (or structural repair) cost of the $n_{i,j,x}$ buildings. $E[C_{New}^{C}(\boldsymbol{X})]$ in Eq (5.6) is expressed by:

$$E[C_{New}^{C}(\boldsymbol{X})] = \int_{t_0}^{t_0+T_P} \sum_{i=1}^{I} e^{-r_d(t-t_0)} \cdot C_{Con}^{i}(x) \cdot n_{i,x} \cdot \dot{N}_N^i(t)\, dt = \sum_{i=1}^{I} \frac{C_{Con}^{i}(x) \cdot n_{i,x}}{\lambda_i \cdot r_d}\left(1 - e^{-r_d \cdot T_P}\right) \tag{5.8}$$

in which $C_{Con}^{i}(x)$ denotes the construction cost of Type *i* building with action x ; $n_{i,x}$ denotes the number of Type *i* buildings in the portfolio with rebuilt action x; $\dot{N}_N^i(t)$ denotes the renewal rate of Type i building at time t (derived in Section 5.2.2); r_d denotes the discounting rate; and $e^{-r_d(t-t_0)}$ denotes the discounting of all future new construction cost to the current cost at t_0 (which is the time of current earthquake, as shown in Figure 5.2).

The last two terms in Eq. (5.6), C_{Dam}^{C} and C_{Cas}^{C}, depend on the future hazard exposure of the community. This hazard is modeled by discretizing the mean annual frequency vs intensity into *K* frequencies and intensity levels, with each level $k \in (1,2,\dots,K)$ represented by the median value of the interval. Accordingly, $E[C_{Dam}^{C}(\boldsymbol{X})]$-can

be obtained by calculating the discounted annual building damage cost over the BPLC, T_P (derived in Section 5.2.1). Alternatively, $E[C_{Dam}^{C}(\boldsymbol{X})]$-can be expressed as:

$$E[C_{Dam}^{C}(\boldsymbol{X})] = \sum_{k=1}^{K} E[C_{Dam}(k,\boldsymbol{X})] \cdot \int_{t_0}^{t_0+T_P} \sum_{i=1}^{I} e^{-r_d(t-t_0)} \cdot v_k^H(t)\, dt$$

$$= \sum_{k=1}^{K} E[C_{Dam}(k,\boldsymbol{X})] \cdot E[N_H(k)] = \sum_{k=1}^{K} E[C_{Dam}^{C}(k,\boldsymbol{X})] \qquad (5.9)$$

where $C_{Dam}(k,\boldsymbol{X})$ denotes the building damage due to hazard level k with rebuilt action $\boldsymbol{X}$; $v_k^H(t)$ denotes the occurrence rate of hazard level k at time t. Eq. (5.9) implies that the $C_{Dam}(k,\boldsymbol{X})$ is time-independent (assume complete repair after damage). For $C_{Cas}^{C}(\boldsymbol{X})$ in Eq. (5.6), calculations are similar. The cost from demolition has not been considered due to lack of available data, but such cost can be added to the framework easily when data becomes available.

5.3.2 Expected Building Portfolio Cumulative Prospect Value

The key assumptions underlying minimum expected life cycle cost analysis are that all risks can be monetized (e.g. Wen & Kang, 2001; Ellingwood & Wen, 2005), and that decision-makers are risk-neutral (Raiffa & Schlafer, 1961; Tversky & Kahneman,1992). However, decision-makers often value monetary consequences nonlinearly according to their risk tolerance; even large companies and governments exhibit this behavior when the consequence of damage is large relative to their wealth or available resources. In addition,

low-probability/high-consequence hazard events pose difficulties for decision-makers in reasonably assessing their risk and designing post-hazard reconstruction strategies because estimates of likelihood and consequences for low-probability, high-consequence events are biased. Cumulative Prospect Theory (CPT), which is based on cognitive research on real-world decision-making, converts objective consequences and probability into subjective ones (Tversky & Kahneman,1992) and addresses the difficulties in perception encountered when dealing with events for which there is little or no experience.

CPT was proposed by Tversky and Kahneman (1992) based on cognitive researches on real-world decision-making evidence. In CPT, firstly N_C consequences are ranked in ascending order (i.e. $y_1 < \cdots y_\xi \leq 0 \leq y_{\xi+1} < \cdots < y_{N_C}$). Then, the monetary cost y_i and probability p_i of i-th event are converted into value $v(y_i)$ and decision weight π_i, respectively (Eqs. (5.10) - (5.12)) to reflect the subjective utility and perception of probability of decision-makers. CPT is the generalized form of the expected LCC (ELCC) and expected utility theory (EUT) models (Von Neumann & Morgenstern, 1944). The *status quo* is commonly selected as the reference point (the point differentiates gain and lose), then the total value of N_C events (Goda & Hong, 2008) is

$$V = V^- + V^+ = \sum_{i=1}^{\xi} v(y_i) \cdot \pi_i^- + \sum_{i=\xi+1}^{N_C} v(y_i) \cdot \pi_i^+ \tag{5.10}$$

where $v(y_i)$ is the value of the consequence of i-th event. To reflect the loss-averse nature of the decision-maker, the value function $v(\cdot)$ (Eq. (5.11)) is different for gain ($y \geq 0$) and loss ($y < 0$), with parameter θ controlling the difference and α and β being exponent parameters.

$$v(y) = \begin{cases} y^{\alpha}, & if\ y \geq 0 \\ -\theta(-y)^{\beta}, & if\ y < 0 \end{cases} \tag{5.11}$$

The decision weight (subjective probability) of the i-th positive or negative event (π_i^+ or π_i^-) are calculated by Eq.(5.12a), where w^- and w^+ are nonlinear subjective probability functions for loss and gains (obtained from Eq.(5.12b) and Eq.(5.12c)). The parameters γ^-, γ^+, and φ control the shape of the curve mapping from real probability p to nonlinear subjective probability function w^- and w^+(Goda & Hong, 2008). The contribution of rare events to value function, adjusted by the subjective probability function, not only depends on the magnitude of the impact but also the occurrence probability. For typical risk-averse decision makers, an inverse-S shaped transformation function ($\gamma^+ = 1.0\ , \gamma^- = 1.0$, and $0 < \varphi < 1.0$, e.g. as shown in Figure 5.4; See Cha & Ellingwood (2012)) implies that the decision-maker subjectively elevates the importance of LPHC events, which is the case for decision-making under earthquake hazards (and many other extreme natural events).

$$\pi_i^- = w^-\left(\sum_{j=1}^{i} p_j\right) - w^-\left(\sum_{j=1}^{i-1} p_j\right) \quad \pi_i^+ = w^+\left(\sum_{j=i}^{N_C} p_j\right) - w^+\left(\sum_{j=i+1}^{N_C} p_j\right) \quad (5.12a)$$

$$w^-\left(\sum_{j=1}^{i} p_j\right) = exp\left[-\gamma^-\left(-ln\left(\sum_{j=1}^{i} p_j\right)\right)^{\varphi}\right] \quad (5.12b)$$

$$w^+\left(\sum_{j=i}^{N_C} p_j\right) = exp\left[-\gamma^+\left(-ln\left(\sum_{j=1}^{N_C} p_j\right)\right)^{\varphi}\right] \quad (5.12c)$$

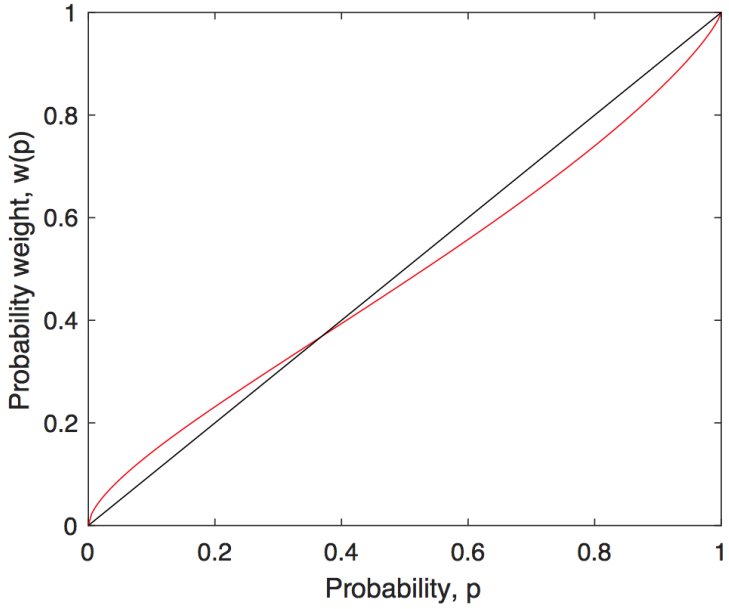

Figure 5.4 The decision weight of cumulative prospect theory (CPT) when $\gamma^- = 1.0$ and $\varphi = 0.8$.

In this study, the reference point of the value function is set equal to $V = 0$, and it is assumed the value function is linear, i.e. $v(y) = y$. Thus, the expected BPCPV (EBPCPV) under decision $\boldsymbol{X}$ is:

$$E[V_{CPV}^{P}(\boldsymbol{X})] = E[C_{Re}(\boldsymbol{X})] + E[C_{New}^{C}(\boldsymbol{X})] + (1+\omega)E[V_{Dam}^{C}(\boldsymbol{X})] + E[V_{Cas}^{C}(\boldsymbol{X})] \quad (5.13)$$

in Eq. (5.13), $E[C_{Re}(\boldsymbol{X})]$ and $E[C_{New}^{C}(\boldsymbol{X})]$ are taken as deterministic given the reconstruction and renewal are events with probability 1, thus $\pi_i^- = p_i = 1$ from Eq. (5.12). $V_{Dam}^{C}(\boldsymbol{X})$ and $V_{Cas}^{C}(\boldsymbol{X})$ denote EBPCPV of building damage and casualty, respectively. Only loss is considered in Eq. (5.13) (as by Cha & Ellingwood (2012)). For simplicity, the negative sign "−" in $E[V_{CPV}^{P}(x)]$ is neglected in this study. The EBPCPV of damage due to a future level k hazard, $E[V_{Dam}^{C}(k,\boldsymbol{X})]$, can be expressed as

$$\begin{aligned} E[V_{Dam}^{C}(k,\boldsymbol{X})] &= E[C_{Dam}(k,\boldsymbol{X})] \cdot \int_{t_0}^{t_0+T_P} e^{-r_d(t-t_0)} \cdot [\eta_k \cdot v_k^H(t)]\, dt \\ &= E[C_{Dam}(k,\boldsymbol{X})] \cdot \eta_k \cdot E[N_H(k)] \end{aligned} \quad (5.14)$$

where η_k is the probability adjustment factor for level k hazard. $E[V_{Cas}^{C}(k,\boldsymbol{X})]$ could be calculated similarly. Comparing Eq. (5.14) to Eq. (5.9), the original $v_k^H(t)$ and $E[N_H(k)]$

are replaced by $\eta_k \cdot v_k^H(t)$ and $\eta_k \cdot E[N_H(k)]$; everything else is the same. η_k can be obtained by

$$\begin{cases} \eta_k = \dfrac{\bar{\pi_k}}{p_k} \\ p_k = v_k^H(t) \end{cases} \tag{5.15}$$

where $\bar{\pi_k}$ is obtained by substituting the p_k in Eq. (5.15) into Eq. (5.12).

5.4 Building Portfolio Life-cycle Analysis Under Seismic Hazards

The BPLCA poses a new challenge in modeling the spatial and temporal characteristics of natural hazards. In this study, the BPLCA framework is illustrated under seismic hazards. Traditionally, the occurrence of seismic events has been modeled as a Poisson process, implying that the inter-arrival time can be described by an exponential distribution. However, analysis of historical records (Takahashi et al., 2004) suggests that the occurrence of earthquakes in a certain seismic source may be related to previous seismic history, and that the Poisson occurrence model may not be appropriate in such cases. The optimal post-hazard portfolio-level BBB decisions should be conditional on the characteristics of the event that as just occurred, which is the motivation for incorporating the more sophisticated non-Poisson occurrence model in the BPLCA.

This study adopts the methodology developed by Takahashi et al. (2004) with the modification that employs the log-normal distribution (an approximate model to BPT

model) to model the inter-arrival time for characteristic earthquakes (CE) (Nishenko & Buland, 1987; Jara & Rosenblueth, 1988). The comparison of the EBPLCA results and optimal BBB strategies from non-Poisson hazard model (NPHM) and Poisson hazard model (PHM) will be made in Section 5.7 and 5.8.

Consistent with Section 5.3, the magnitude of earthquakes M is discretized into K intervals, $k \in (1,2,\dots,K-1)$ for non-characteristic earthquake (NCE), and $k = K$ for characteristic earthquake (CE) (Takahashi et al., 2004). Eq. (5.9) is re-written as

$$E[C_{Dam}^{C}(\boldsymbol{X})] = \sum_{k=1}^{K} E[C_{Dam}(m_k,\boldsymbol{X})] \cdot \int_{t_0}^{t_0+T_P} \sum_{i=1}^{I} e^{-r_d(t-t_0)} \cdot v_K^E(t,t_0)\ dt$$

$$= \sum_{k=1}^{K} E[C_{Dam}(m_k,\boldsymbol{X})] \cdot E[N_E(m_k,t_0)] = \sum_{k=1}^{K} E[C_{Dam}^{C}(m_k,\boldsymbol{X})] \quad (5.16)$$

t_0 is considered in $N_E(m_k,t_0)$ to designate the time of current earthquake; When all seismic sources (faults or zones) are considered for each m_k, the $E[C_{Dam}^{C}(t_0,\mathbf{X})]$ becomes:

$$E[C_{Dam}^{C}(\mathbf{X})] = \sum_{all\ sources} \sum_{k=1}^{K} E[C_{Dam}^{C}(m_k,\boldsymbol{X})] \quad (5.17)$$

Let $T_q, q \in (1,2,\dots)$ be the inter-arrival time between the $(q-1)^{\text{th}}$ and q^{th} events of magnitude m_k, for simplicity, k is omitted. Thus $T_1,\ T_2, \dots, T_q, \dots$ are independent and identically distributed (i.i.d.) random variables. $W_q = \sum_1^q T_q$ is the waiting time to the q$^{\text{th}}$ earthquake. From Takahashi et al. (2004), $E[N_E(m_k)]$ is

$$E[N_E(m_k, t_0)] = \int_{t_0}^{t_0+T_P} \sum_{i=1}^{I} e^{-r_d(t-t_0)} \cdot v_K^E(t, t_0)\, dt$$

$$= \int_{t_0}^{t_0+T_P} e^{-r_d(t-t_0)} \cdot \sum_{q=1}^{\infty} f_{W_q}(t, m_k | W_1 > t_0)\, dt \qquad (5.18)$$

where $f_{W_q}(t, m_k | W_1 > t_0)$ denotes the PDF of W_q at time t given there is no CE between $t = 0$ and t_0. The summation of $f_{W_q}(t, m_k | W_1 > t_0)$ over all $q, q \in (1,2,\dots)$ yields $v_K^E(t, t_0)$.

For the CE m_K, according to Takahashi et al. (2004),

$$f_{W_q}(t, m_K | W_1 > t_0) = \int_{t_0}^{t} f_{T_2+\cdots+T_q}(t-\tau, m_K)\, f_{W_1}(\tau, m_K | W_1 > t_0) d\tau \qquad (5.19)$$

in which $T_q \sim LN\ (\lambda_K, \zeta_K)$, $q = 1,2,\dots$, where *LN* stands for the log-normal distribution. Eq. (5.19) becomes

$$f_{W_q}(t, m_K | W_1 > t_0)$$

$$= \frac{1}{1 - \Phi\left(\frac{\ln(t_0) - \lambda_K}{\zeta_K}\right)} \int_{t_0}^{t} \left[\frac{1}{\tau \cdot (t - \tau)}\right] \varphi\left(\frac{\ln(t - \tau) - \lambda_K^{q-1}}{\zeta_K^{q-1}}\right) \varphi\left(\frac{\ln(\tau) - \lambda_K}{\zeta_K}\right) d\tau \quad (5.20)$$

Figure 5.5(a) illustrates the $f_{W_q}(t, m_K | W_1 > t_0)$ for $q = 1, 2, and\ 3$ and $v_K^E(t, t_0)$ when the $t_0 = 1$. The mean and c.o.v. for inter-arrival time of CE are 500 years and 0.3, respectively. In the first 300 years, $v_K^E(t, t_0)$ is lower than the mean occurrence rate of 0.002 in the Poisson model; $v_K^E(t, t_0)$ reaches its highest value near $t = 500$ and reach second highest value near $t = 1000$. As t increases, $v_K^E(t, t_0)$ approaches the mean occurrence rate 0.002. Figure 5.5(b) shows $v_K^E(t, t_0)$ for CE when $t_0 = 1, 100, 300, and\ 500$. It is found that the t_0 value will greatly affect the $v_K^E(t, t_0)$ in the log-normal inter-arrival time model. For example, when $t_0 = 500$ and $500 \leq t \leq 700$, the $v_K^E(t, t_0)$ is higher than the mean occurrence rate.

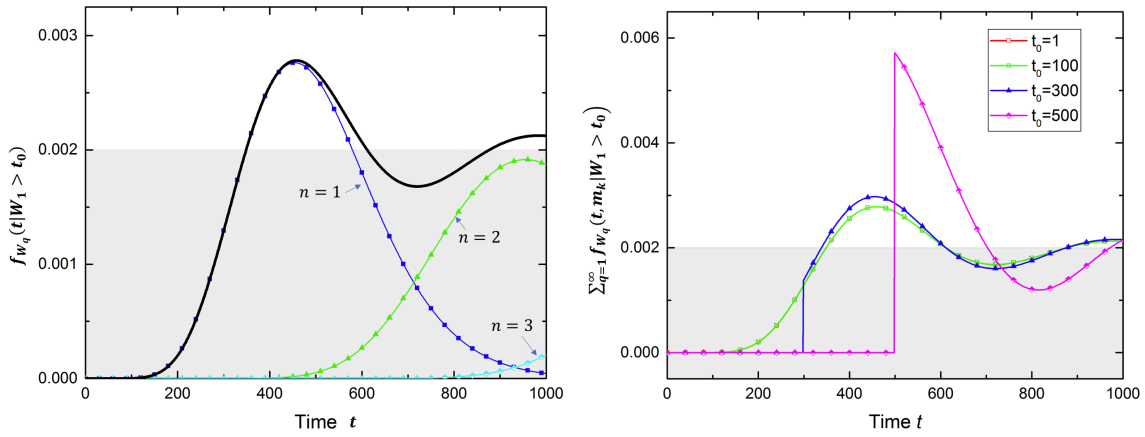

(a) (b)

Figure 5.5(a) Conditional PDF of waiting time to the q-th event of log-normal occurrence time model $f_{W_q}(t, m_K|W_1 > 1)$ and $v_K^E(t, 1)$(black line); (b) the sum of these PDF functions $v_K^E(t, t_0)$ when $t_0 =$ 1, 100, 300, and 500 for CE. The shadowed area marks the mean occurrence rate CE.

For the NCEs, $m_k, k = 1,2, \dots, K-1$ with exponential inter-arrival times, the term in Eq (5.18), $\sum_{q=1}^{\infty} f_{W_q}(t, m_k|W_1 > t_0) = v_k^E$ (Takahashi et al., 2004). Thus, Eq. (5.18) is simplified:

$$E[N_E(m_k)] = v_k^E \cdot \frac{1}{r_d}(1 - e^{-r_d \cdot T_P}) \tag{5.21}$$

To quantify $E[C_{Dam}(m_k, \boldsymbol{X})]$ in Eq. (5.16), one must consider uncertainties in magnitude *M*, the source to site distance *R*, ground motion attenuation, local soil condition, and building fragilities (related to $\boldsymbol{X}$). For each seismic fault, it is assumed that the

location of future earthquake epicenter is uniformly distributed over the fault. To reduce the sample points, Latin Hypercube Sampling (Stein, 1987) is employed with a sample size of 100 for *R*. Further, for each hazard scenario (in combination of M and R), 1000 simulations are employed to consider the uncertainty in ground motion attenuation at each building site (Campbell, 2003), considering the correlation between sites by an exponential function (Wang & Takada, 2005). The mean loss is calculated at a given hazard demand from a total of $K \times 100 \times 1000$ simulations.

The total damage cost $C_{Dam}(m_k, \boldsymbol{X}) = C_S(m_k, \boldsymbol{X}) + C_{NA}(m_k, \boldsymbol{X}) + C_{ND}(m_k, \boldsymbol{X}) + C_{CT}(m_k, \boldsymbol{X})$, where S, NA, ND, and CT denote structural, non-structural acceleration sensitive, non-structural drift sensitive component, and contents damage, respectively. $C_{Dam}(m_k, \boldsymbol{X})$ in *s*-th scenario can be calculated by

$$C_{Dam}(m_k, s, \boldsymbol{X}) = \sum_{item} \sum_{i=1}^{I} n_{i,x} \cdot \left(C_{Con}^{i}(x) \cdot \sum_{j=1}^{4} DV_{Item}^{i,j} \cdot p_{Item}^{i,j}(m_k, s, x) \right) \quad (5.22)$$

In Eq. (5.22), $p_{Item}^{i,j}(m_k, s, x)$ denotes the probability of the *j*-th damage state for component $item \in (S, NA, ND, CT)$ of Type i building under the $s\text{-}th$ scenario of magnitude m_k earthquake under decision x_{ij} (for simplicity, *i* and *j* are dropped in subscript of x); $DV_{Item}^{i,j}$ denotes the damage to Type i building with respect to

component *item* due to physical damage in *j*-th damage state (Lin & Wang, 2016; Wang et al., 2018).Similarly, for $C_{Cas}(m_k, s, \boldsymbol{X})$

$$C_{Cas}(m_k, s, \boldsymbol{X}) = \sum_{i=1}^{I} n_{i,x} \cdot \left(N_O^i \cdot \sum_{j=1}^{4} DV_{cas}^{i,j} \cdot p_{ST}^{i,j}(m_k, s, x) \right) \tag{5.23}$$

where $DV_{cas}^{i,j}$ denotes the casualty loss in Type *i* building due to physical damage in *j*-th damage state; N_O^i is the number of occupants in Type *i* building. Thus, the mean damage loss due to m_k earthquake is

$$E\left[C_{Dam}(m_k, \boldsymbol{X})\right] = \frac{1}{N_S} \sum_{s=1}^{N_s} C_{Dam}(m_k, s, \boldsymbol{X}) \tag{5.24}$$

in which N_S denotes the total number of MCS for each magnitude m_k. The mean casualty loss due to m_k earthquake, $E\left[C_{Cas}(m_k, \boldsymbol{X})\right]$ can obtained similarly.

As introduced in Section 5.2.2, the only difficulty in EBPCPV-based methodology lies in the quantification of η_k, which relates to $v_k^E(t)$. For CE m_K, $v_K^E(t, t_0)$ is time-dependent, which causes difficulties in defining η_k. In this study, we employ the mean

occurrence rate v_k^E for both NCE and CE, $k = 1,2,\dots,K$, i.e. $v_k^H(t) = v_k = p_k$, when quantifying η_k. Then η_k can be obtained by Eq. (5.15).

5.5 Building Portfolio Resilience Goal

To avoid tremendous socio-economic consequences in communities exposed to natural hazards, reconstructing portfolio to achieve certain resilience goal is desirable. The probabilistic form of resilience goal statement has been given in Section 3.3. This chapter employs the Direct Loss Ratio (DLR), i.e. the ratio of direct economic loss of portfolio due to hazard damage to total portfolio replacement cost as the resilience metric. Under earthquake magnitude m_k, the DLR can be represented as

$$M_{DLR,k} = \frac{C_{Dam}(m_k, \boldsymbol{X})}{\sum_{i=1}^{I} n_i \cdot C_{Con}^i}, \qquad k \in (1,2,\dots,K) \tag{5.25}$$

in which $C_{Dam}(m_k, \boldsymbol{X})$ = damage loss due to earthquake m_k under decision, $\boldsymbol{X}$ (Eq (5.9)); n_i = number of buildings of Type i; and C_{Con}^i = replacement cost of each building in Type i. $M_{DLR,k}$ must be calculated by MCS (c.f. Section 4.1 of Wang et al. (2018)). Thus, Eq. (3.1) is re-written as

$$P\left(M_{DLR,m_k} < G_{DLR,m_k} \middle| m_k\right) = a\% \tag{5.26}$$

where M_{DLR,m_k} denotes the resilience metric of DLR conditioned on hazard level m_k; G_{DLR,m_k} denotes the prescribed resilience goal corresponding to M_{DLR,m_k}; and the $a\%$ is a prescribed confidence level. An example of Eq. (5.26) is $P\left(M_{DLR,m_3} < 20\% \,\middle|\, m_3 = 7.5\right) = 95\%$, meaning "with 95% probability, the direct loss in the residential buildings are less than 20% of the overall portfolio replacement cost, given the occurrence of any earthquake event with a magnitude M_w = 7.5. The presence of the $a\%$ in the goal statement acknowledges the uncertain nature associated with any community resilience assessment, reflects the risk level that a community is willing to tolerate, and should be aligned with a community's preferences.

5.6 Formulation

As formulated in Eqs. (6) and (13), the EBPLCC and EBPCPV is conditioned on portfolio level reconstruction decision **x.** An optimal reconstruction strategy for a building portfolio damaged by a major event should be determined such that the sum of reconstruction cost, nature renewal cost, and discounted future hazard loss during the BPLC is minimized in the EBPLCC framework (or the value is maximized in the EBPCPV framework).

Ideally, after a major earthquake event, there should be optimal reconstruction decision for each building *k.* To simplify the optimization problem and considering the situation in a real-world implementation, it is assumed that for each Type $i \in (1, \ldots, I)$

building under damage state $j \in (1,2,3,4)$, there is only one reconstruction decision $x_{ij} \in \{0,1,2\}$ (Eq. (27)). In other words, the reconstruction decision of specific building, x_{ij} is determined by its Type *i* and post-hazard damage state j. Three reconstruction levels are defined in the below

0: Rebuild as before (lower than any current code)

1: Rebuild to Enhanced Level 1 (E1) (current high design code)

2: Rebuild to Enhanced Level 2 (E2) (higher than any current code)

The decision matrix **X** define the post-hazard reconstruction strategy for each (building type, damage state) pair. The mathematical formulation of the optimization problem is tabulated in Table 5.2. The objective of the problem is to minimize EBPLCC,-$E[C_{LCC}^{P}(\boldsymbol{X})]$ (Eq. (5.28)) or maximize EBPCPV, $E[V_{CPV}^{P}(\boldsymbol{X})]$ (Eq. (5.29)) under the constraints of portfolio level resilience performance goals (formulated in Eq. (5.32)) given the formulation of $E[C_{LCC}^{P}(\boldsymbol{X})]$ (Eq. (5.30)) and $E[V_{CPV}^{P}(\boldsymbol{X})]$ (Eq. (5.31)).

Table 5.2 Post-hazard Reconstruction Problem Formulation

Item	Expression	Eq. #
Decision Variables:	**X**, element $x_{ij} \in \{0,1,2\};\ i \in (1,2,\dots,I),\ j \in (1,2,3,4)$	Eq. (5.27)
Objectives	min $E[C_{LCC}^{P}(\boldsymbol{X})]$) or	Eq. (5.28)
	max $E[V_{CPV}^{P}(\boldsymbol{X})]$	Eq. (5.29)
Constraints	$C_{LCC}^{P}(\boldsymbol{X}) = C_{Re}(\boldsymbol{X}) + C_{New}^{C}(\boldsymbol{X}) + (\omega+1)C_{Dam}^{C}(\boldsymbol{X}) + C_{Cas}^{C}(\boldsymbol{X})$	Eq. (5.30)
	$V_{CPV}^{P}(\boldsymbol{X}) = V_{Re}(\boldsymbol{X}) + V_{New}^{C}(\boldsymbol{X}) + (\omega+1)V_{Dam}^{C}(\boldsymbol{X}) + V_{Cas}^{C}(\boldsymbol{X})$	Eq. (5.31)
	$P\left(M_{DLR,k} < G_{DLR,k} \middle| m_k\right) = a\%$	Eq. (5.32)

The optimization problems in this study is formulated as a single-objective, integer programming problem, illustrated in Fig. 2, which can be solved using a Genetic Algorithm (GA) (Goldberg & Holland, 1988). The matrix **X** is converted into a one-dimensional array as the "gene". The GA based algorithm for searching the optimal reconstruction strategy is illustrated in Figure 5.6. As the iterative GA algorithm runs, better reconstruction strategies are found with lower $E[C_{LCC}^{P}(\boldsymbol{X})]$ or higher $E[V_{CPV}^{P}(\boldsymbol{X})]$. Here, it is prescribed that the algorithm stops when no better solution is found in 100 consecutive steps. The typical convergence of the algorithm is illustrated in Figure 5.7.

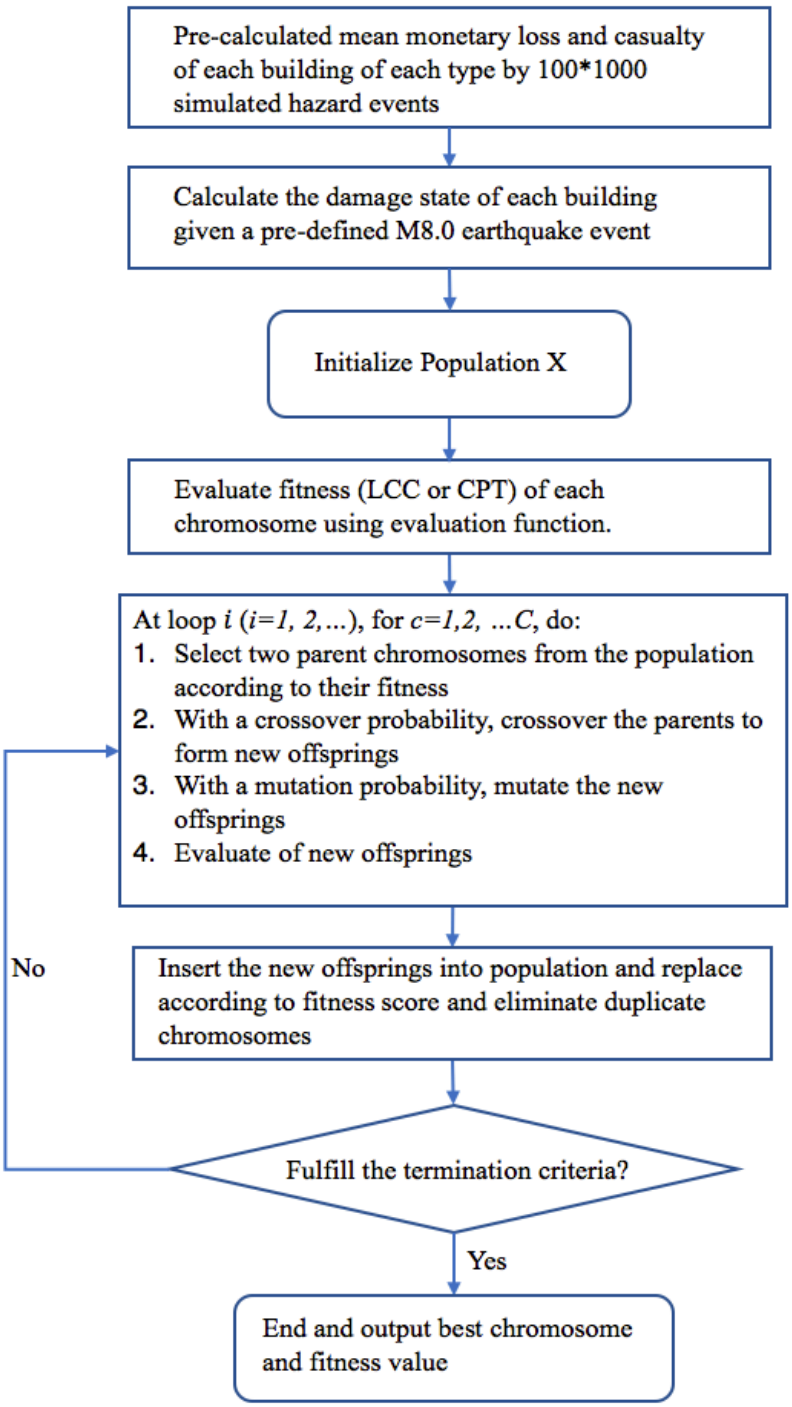

Figure 5.6 Flowchart of the GA-based optimization algorithm for BBB decision

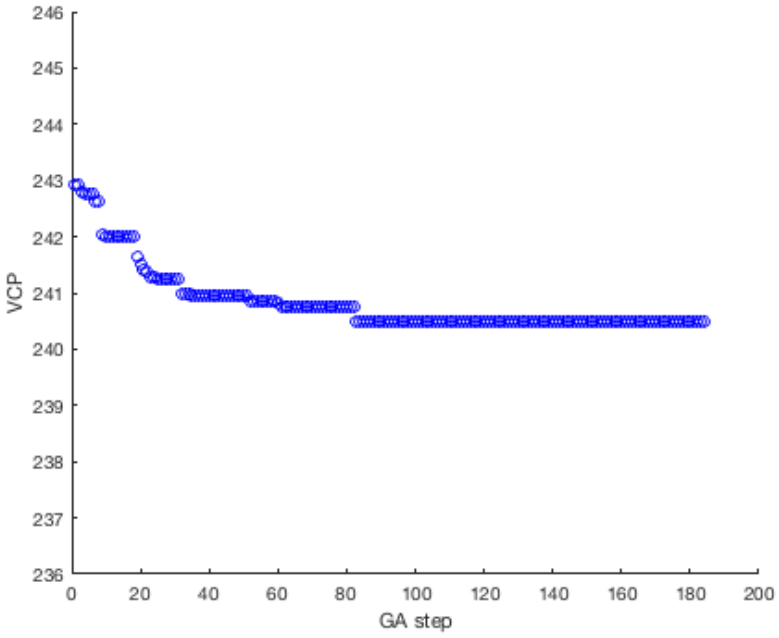

Figure 5.7 The typical convergence route of the optimization algorithm

5.7 Illustration 1– Centerville BPLCA

The community investigated in this study is Centerville, a hypothetical community for resilience-related analyses and decision-making of physical, social and economic infrastructure systems (Ellingwood et al., 2016; Lin & Wang, 2016). Centerville represents a community with moderate population (50000) and size (8 km by 13km), located in Midwest of the U.S. As shown in Figure 5.8, Centerville includes 7 residential zones (Z1-Z7) with approximately 13,500 single and multi-family residential units. Notably, Z1 is a high income/low density (HI/LD) area near the western hills, Z2-Z4 are zones with moderate income (MI), Z5-Z6 are low-income (LI) residential areas close to the

business/retail district, and Z7 is a mobile home zone abutting industrial facilities. All residential buildings in Centerville are light frame wood structures with different occupancy types, stories, and built year (denoted as W1 – W6 in Table 5.3). The fragility and capacity parameters of each types of buildings are given in Appendix A and B. To reduce computational time, 1,500 buildings are randomly sampled from the portfolio. The results in this case study are all based on this reduced sample.

Table 5.3 Building characteristics

Bld. ID	**Occup. class**	**# of occupants**	**Story**	**Year built**	**Area (ft^2)**	**Building value (2003 estimate)**	**# in Centerville**	**BLC, T_l**
W1	SF[1]	2	1	1945 – 1970	1,400	$139,426	6,190	50
W2	SF[1]	3	1	1985 – 2000	2,400	$239,016	4,000	50
W3	SF[1]	5	2	1985 – 2000	5,200	$318,816	50	50
W4	SF[1]	3	1	1970 – 1985	2,400	$239,016	3,196	50
W5	MF[2]	90	3	1985	36,000	$3,918,960	102	50
W6	MH[3]	2	1	NA	NA	$61,800	1,352	30

1. SF: Single-family dwelling
2. MF: Multi-family dwelling
3. MH: Mobile home
4. Assume content value is 50% of building value according to HAZUS (FEMA/NIBS, 2003)

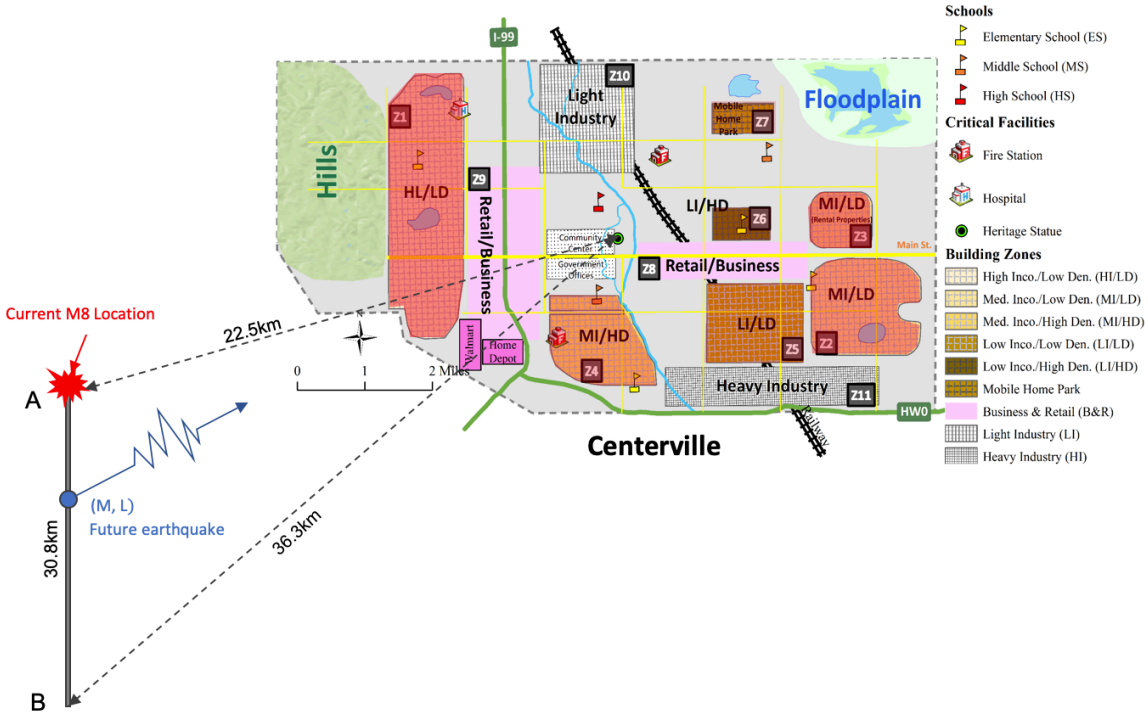

Figure 5.8 The location of Centerville, earthquake fault line and current earthquake location

The characteristic BPLC, $t_{p,90}^{c}$ is calculated first, assuming that the mean BLC of an individual building relates to the occupancy type. Single-family dwelling units (SF) and multi-family dwelling units (MF) are assumed to have the same mean BLC - $E[T_1] = 50$ years - while mobile homes (MH) have mean BLC $E[T_2] = 30$ years (tabulated in Table 5.3). $t_{p,r}^{c} = 115$ years is obtained by MCS. Notably, since the portfolio is dominated by SF and MF buildings, the portfolio lifetime is almost identical to the BPLC of a portfolio with one type of BLC (T_1). In rest of this study, $T_P = t_{p,r}^{c} = 115$ years is employed for BPLCA by default.

Suppose that the building portfolio is severely damaged by a destructive $M_w = 8$ earthquake with an epicenter (Point A in Figure 5.8) located southwest of Centerville with a distance of to 22.5 km to the centroid of Centerville. Assume that Centerville is situated on Site Class B soil (ASCE 7-16). A summary of the post-hazard damage states of buildings is shown in Table 5.4. Most of the residential buildings in Centerville are damaged to some extent and require either repair or reconstruction. The mean occurrence rate of future earthquakes is tabulated in Table 5.5. It is assumed that the c.o.v. in inter-arrival time = 0.3 for CE (Wesnousky et al., 1984; Takahashi et al., 2004). The low mean hazard occurrence rate is meant to represent the low probability/high consequence natural of earthquakes in mid-America (e.g. sites near the New Madrid Seismic Zone) (Toro & Silva, 2001). Since the optimal reconstruction decisions are unknown now, unless otherwise indicated, in this section, it is assumed that the decisions are rebuilding to current performance levels ($x_{ij} = 0$) regardless of their post-hazard damage states. More discussion on optimal decisions will be given extensively in illustration 2 in Section 5.8. The costs of reconstruction and casualties are tabulated in Table 5.6 and Table 5.7. In addition, $\omega = 1.0$ is employed as the default value for indirect loss in Eqs. (5.6) and (5.13).

Table 5.4 Number of building in each damage state after a M_w - 8 earthquake event

Bld. ID	DS_0	DS_1	DS_2	DS_3	DS_4	Total
W1	11	76	207	192	122	608
W2	9	80	166	133	40	428
W3	1	2	2	0	0	5
W4	8	49	109	93	55	314
W5	0	1	5	2	1	9
W6	0	6	35	56	39	136

Table 5.5 Mean annual occurrence rate of each magnitude representative v_k^E (Toro and Silva, 2001) and amplification factor η_k in BPCPV model

Item		$m_1 = 5.5$	$m_2 = 6.5$	$m_3 = 7.5$
v_k^E		0.033	0.0033	0.002
η_k	$\gamma^- = 1, \varphi = 0.9$	1.31	1.86	2.82
	$\gamma^- = 1, \varphi = 0.8$	1.60	2.98	6.70
	$\gamma^- = 1, \varphi = 0.7$	1.82	4.16	13.77
	$\gamma^- = 1, \varphi = 0.6$	1.93	5.14	25.08
	$\gamma^- = 1, \varphi = 0.5$	1.91	5.66	41.33

Table 5.6 Reconstruction cost (only structural part) of each building in each post-hazard damage state (based on 2003 estimate) (FEMA/NIBS, 2003)

Bld. ID	Post-hazard Damage State											
	DS_1^P			DS_2^P			DS_3^P			DS_4^P		
	Orig.	**E1**	**E2**	**Orig.**	**E1**	**E2**	**Orig.**	**E1**	**E2**	**Orig.**	**E1**	**E2**
W1	697	5,591	10,485	3,207	8,101	12,995	16,313	21,207	26,101	32,626	37,520	42,413
W2	1,195	9,585	17,974	5,497	13,887	22,276	27,965	36,354	44,744	55,930	64,319	72,709
W3	1,594	12,785	23,975	7,333	18,523	29,714	37,301	48,492	59,682	74,603	85,793	96,984
W4	1,195	9,585	17,974	5,497	13,887	22,276	27,965	36,354	44,744	55,930	64,319	72,709
W5	11,757	92,879	174,002	54,865	135,988	217,110	270,408	351,531	432,653	540,816	621,939	703,061
W6	247	2,509	4,771	1,483	3,745	6,007	4,511	6,773	9,035	15,079	17,341	19,603

1. Assume the reconstruction cost (structural part) of E1 is 15% higher than Orig. and E2 is 30% higher than Orig. structural cost
2. The actual reconstruction cost for building in specific damage state are calculated as a percentage of full reconstruction cost in the table
3. Assume the additional reconstruction cost to enhance the building from Orig. to E1 and E2 is same for post-state DS_j^P, $j \in (1,2,3,4)$.

Table 5.7 Monetary value of human casualty (FEMA/NIBS, 2003; FEMA,2015)

Severity Level	S1	S2	S3	S4
Cost	$1,000	$5,000	$100,000	$6,600,000

With $T_P = t^c_{p,90}$= 115 years and portfolio post-hazard damage state, the EBPLCA is conducted, i.e. $E[C^P_{LCC}(\boldsymbol{X})]$ and $E[V^P_{CPV}(\boldsymbol{X})]$ for different discount rates r_d of economic losses and keep 0.01 for the discount rate of casualties. A non-Poisson hazard model (NPHM) with $t_0 = 1$, and $x_{ij} = 0$ is employed as the default condition. Figure 5.9 shows the curves of $E[C^P_{LCC}(\boldsymbol{X})]$ and $E[V^P_{CPV}(\boldsymbol{X})]$ when the time increases from 0 to $T_P = 115$ years under different discount rates for economic losses. It is found that when time $t = 0$, $E[C^P_{LCC}(\boldsymbol{X})] = E[V^P_{CPV}(\boldsymbol{X})] = \$23.41M$, which is the reconstruction cost $C_{Reb}(\boldsymbol{X})$ (given in Table 5.8). The BPLCA curves diverge as time increases. In all cases, the curves from EBPCPV-based methodology incorporating risk aversion are greater than those from EBPLCC-based methodology due to η_k. When the discount rate is relatively high (e.g. 5%), the $E[C^P_{LCC}(\boldsymbol{X})]$ and $E[V^P_{CPV}(\boldsymbol{X})]$ become almost constant after $t = 60$ years while for low discount rates (e.g. 1% or less), the BPLCA results increase even after $T_P = 115$ years, indicating that more risk is being assumed by the present generation.

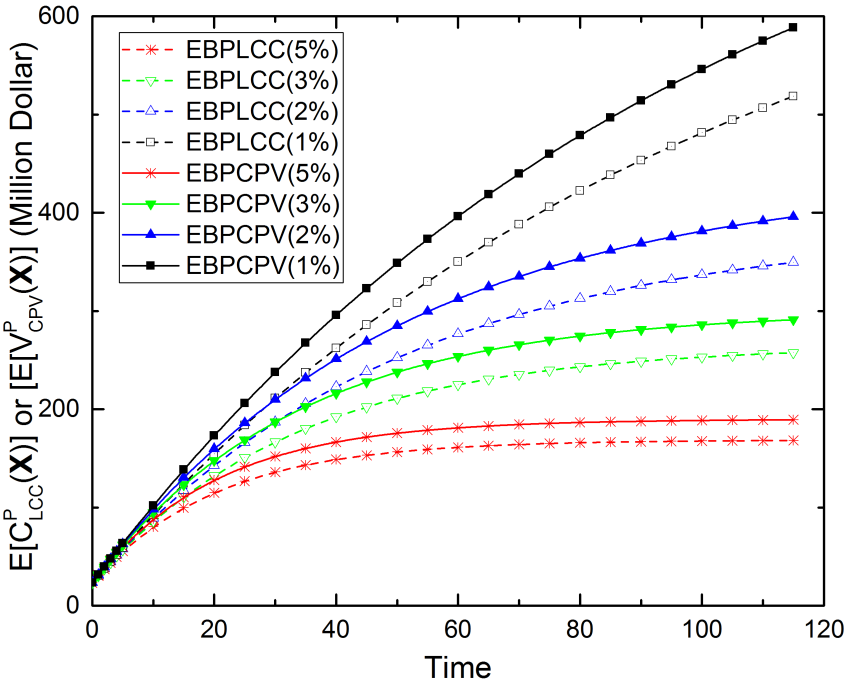

Figure 5.9 $E[C^P_{LCC}(t_0, \boldsymbol{X})]$ and $E[V^P_{CPT}(t_0, \boldsymbol{X})]$ grow with time under different discount rate for economic loss

Table 5.8 summarizes the BPLCA results from different hazard models and values of t_0 when the discount rate on economic losses and human casualties are 3% and 1%, respectively. The EBPLCA value and the contribution from each component are greatly affected by t_0 under NPHM for both methodologies. For instance, if $t_0 = 1$ (the current earthquake is a CE), the $E[C^C_{Dam}]$ from $m_3 = 7.5$ interval is zero, which can also be seen from the near-zero hazard rate ($v^E_K(t, t_0)$) of CE in Figure 5.5(a) within $t^c_{p,90}$. When the t_0 increases, the contribution of $m_3 = 7.5$ interval becomes higher. For instance, when $t_0 = 500$, for $E[C^C_{Dam}(\boldsymbol{X})]$ and $E[V^C_{Dam}(\boldsymbol{X})]$, the contributions from $m_3 = 7.5$ interval are 56.4% and 81.0% respectively; for $E[C^C_{Cas}(\boldsymbol{X})]$ and $\mathrm{E}[V^C_{Cas}(\boldsymbol{X})]$, the contribution from

$m_3 = 7.5$ interval are 82.7% and 92.52% respectively. The trend of the $E[C_{LCC}^{P}(\boldsymbol{X})]$ and $E[V_{CPV}^{P}(\boldsymbol{X})]$ with different t_0 and contribution of each component are illustrated in Figure 5.10, which shows that the contributions from $C_{Dam}^{C}(\boldsymbol{X})$, $C_{Cas}^{C}(\boldsymbol{X})$, and $C_{Ind}^{C}(\boldsymbol{X})$ in EBPLCC (or $V_{Dam}^{C}(\boldsymbol{X})$, $V_{Cas}^{C}(\boldsymbol{X})$, and $V_{Ind}^{C}(\boldsymbol{X})$ in EBPCPV) increase when t_0 increases. For rest of this section, unless otherwise indicated, the NPHM with $t_0 = 1$ as well as 3% and 1% discount rate on economic loss and human casualty, respectively.

Table 5.8 The BPLCA decomposition from different hazard models (when $x_{ij} = 0$, for $\forall\ i$ and j) in million dollars

Hazard Model		Metric	C_{Reb} or V_{Reb}	C^C_{Ini} or V^C_{Ini}	C^C_{Dam} or V^C_{Dam}				C^C_{Cas} or V^C_{Cas}				C^C_{Ind} or V^C_{Ind}	C^P_{LCC} or V^P_{CPV}
					$m_1 = 5.5$	$m_2 = 6.5$	$m_3 = 7.5$	Sum	$m_1 = 5.5$	$m_2 = 6.5$	$m_3 = 7.5$	Sum		
Poisson hazard model (PHM)		EBPLCC	23.41	202.04	10.84	4.92	7.61	23.38	0.19	0.43	1.16	1.78	23.38	273.98
		EBPCPV	23.41	202.04	17.39	14.66	7.61	39.65	0.31	1.27	1.16	2.73	39.65	307.49
Non-Poisson hazard model (NPHM)	$t_0 = 1$	BPLCC	23.41	202.04	10.84	4.92	0.00	15.77	0.19	0.43	0.00	0.62	15.77	257.60
		EBPCPV	23.41	202.04	17.39	14.66	0.00	32.04	0.31	1.27	0.00	1.57	32.04	291.11
	$t_0 = 300$	BPLCC	23.41	202.04	10.84	4.92	7.19	22.96	0.19	0.43	1.27	1.89	22.96	273.25
		EBPCPV	23.41	202.04	17.39	14.66	48.19	80.23	0.31	1.27	8.53	10.11	80.23	396.02
	$t_0 = 500$	BPLCC	23.41	202.04	10.84	4.92	20.41	36.18	0.19	0.43	2.92	3.53	36.18	301.34
		EBPCPV	23.41	202.04	17.39	14.66	136.77	168.81	0.31	1.27	19.54	21.12	168.81	584.19

- The values in the table are all expected values, due to lack of space, notation $E[\cdot]$ and $\boldsymbol{X}$ are omitted.

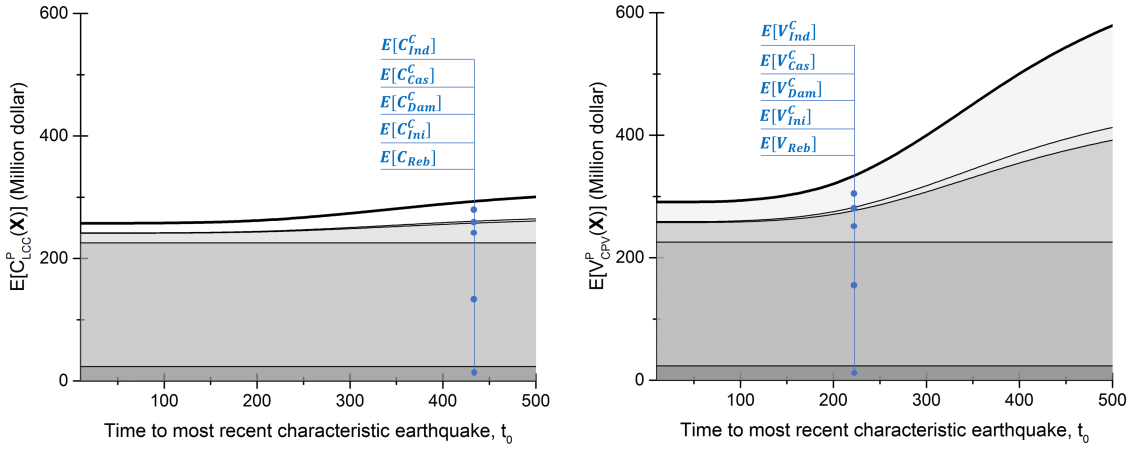

(a) (b)

Figure 5.10 (a) The de-composition of $E[C_{LCC}^{P}(X)]$and (b) $E[V_{CPV}^{P}(X)]$ under NPHM with different $\boldsymbol{t_0}$ (each shadowed area corresponding to a component of the BPLCA formulation)

Next, the effect of T_P on $E[C_{LCC}^{P}(\boldsymbol{X})]$ and $E[V_{CPV}^{P}(\boldsymbol{X})]$ is investigated. Since T_P depends on BLC T_i for Type I and the corresponding number, n_i, a group of mean BLC for SF and MF (T_1) is employed and fix the mean BLC of MH (T_2) as $E[T_2] = E[0.6T_1]$ to obtain an array of T_P. Table 5.9 illustrates the effect of T_P on the $E[C_{New}^{C}(\boldsymbol{X})]$ *and* $E[V_{New}^{C}(\boldsymbol{X})]$ under Poisson and non-Poisson hazard models (with different values of t_0), showing that $E[C_{LCC}^{P}(\boldsymbol{X})]$ and $E[V_{CPV}^{P}(\boldsymbol{X})]$ both decrease monotonically as T_P increases. While this behavior seems counter intuitive, it results from the cumulative new construction cost ($C_{New}^{C}(\boldsymbol{X})$ or $V_{New}^{C}(\boldsymbol{X})$), as the other components either remain the same ($C_{Reb}(\boldsymbol{X})$ *or* $V_{Reb}(\boldsymbol{X})$) or increase ($C_{Dam}^{C}(\boldsymbol{X})$ or $V_{Dam}^{C}(\boldsymbol{X})$, $C_{Cas}^{C}(\boldsymbol{X})$ or $V_{Cas}^{C}(\boldsymbol{X})$, and $C_{Ind}^{C}(\boldsymbol{X})$ or $V_{Ind}^{C}(\boldsymbol{X})$) when T_P increases. Eq. (5.8) shows that the $E[C_{New}^{C}(\boldsymbol{X})]$ (equal to $E[V_{New}^{C}(\boldsymbol{X})]$) is proportional to $1/\lambda_i$, where λ_i is the mean BLC of a Type *i* building; when mean BLC is short, the cumulative cost due

to natural updating within the T_P, $E[C_{Ini}^C(\boldsymbol{X})]$ is high since demolition and reconstruction occur in a short period with high discount factor (larger $e^{-r_d(t-t_0)}$), and vice versa. This supports the idea that individual buildings and portfolios with longer life-cycles will lead to lower LCA values and are considered as more *sustainable*. Figure 5.11 also illustrates the effect of T_P length on the $E[C_{New}^C(\boldsymbol{X})]$ and $E[V_{New}^C(\boldsymbol{X})]$ with Poisson hazard model (PHM) or non-Poisson hazard model (NPHM) (under different t_0). In Figure 5.11, LCC-P denotes the case for EBPLCC-based methodology in PHM, while CPV-NP-300 denotes the EBPCPV-based methodology in NPHM with $t_0 = 300$ years.

Table 5.9 The BPLCA de-composition with different BPLC

BLC $(E[T_1], E[T_2])$	BPLC T_P	Metric	$\boldsymbol{C_{Reb}}$ or $\boldsymbol{V_{Reb}}$	$\boldsymbol{C_{New}^C}$ or $\boldsymbol{V_{New}^C}$	$\boldsymbol{C_{Dam}^C}$ or $\boldsymbol{V_{Dam}^C}$	$\boldsymbol{C_{Cas}^C}$ or $\boldsymbol{V_{Cas}^C}$	$\boldsymbol{C_{Ind}^C}$ or $\boldsymbol{V_{Ind}^C}$	$\boldsymbol{C_{LCC}^P}$ or $\boldsymbol{V_{CPV}^P}$
(30,18)	69	EBPLCC	23.41	303.89	14.23	0.45	14.23	356.20
		EBPCPV	23.41	303.89	28.92	1.15	28.92	386.28
(50,30)	115	EBPLCC	23.41	202.04	15.77	0.62	15.77	257.60
		EBPCPV	23.41	202.04	32.04	1.57	32.04	291.11
(100,60)	230	EBPLCC	23.41	104.23	16.27	0.82	16.27	160.99
		EBPCPV	23.41	104.23	33.07	2.12	33.07	195.90
(150,90)	345	EBPLCC	23.41	69.55	16.29	0.93	16.29	126.47
		EBPCPV	23.41	69.55	33.12	2.64	33.12	161.84

- The values in the table are all expected values, due to lack of space, notation $E[\cdot]$, t_0, and $\boldsymbol{X}$ are omitted.

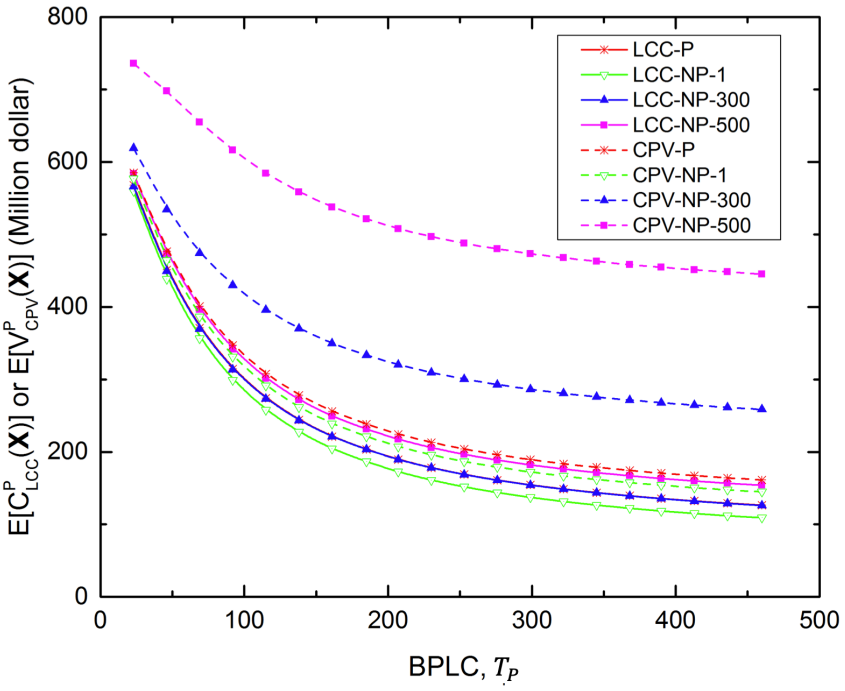

Figure 5.11 $E[C^P_{LCC}(X)]$ and $E[V^P_{CPV}(X)]$ under different T_P with different metrics and hazard models

Further, the sensitivity of $E[V^P_{CPV}(\boldsymbol{X})]$ on the CPT parameters is investigated. Specifically, the effect of different φ (0.5 to 1.0) is investigated with $\gamma^- = 1.0$. Figure 5.12 shows that lower φ value leads to higher $E[V^P_{CPV}(\boldsymbol{X})]$ because it implies that the decision-maker is overestimating the probability of an extreme event and is more risk-averse. Notably, the contribution of $E[V^C_{Dam}(m_k, \boldsymbol{X})]$ from the (CE) $(k = K)$ is more sensitive to the φ than that from the lower magnitude non-characteristic earthquake (NCE) $(k = 1, .., K-1)$. A comparison of Figure 5.12 (a) and (b) reveals that the which the effect of different φ on $E[V^C_{Dam}]$ also depends on t_0. Note that when $\varphi = 1$,

$E[V_{CPV}^{P}(\boldsymbol{X})] = E[C_{LCC}^{P}(\boldsymbol{X})]$ because of the assumption (Eq. (10)) that the value function is linear.

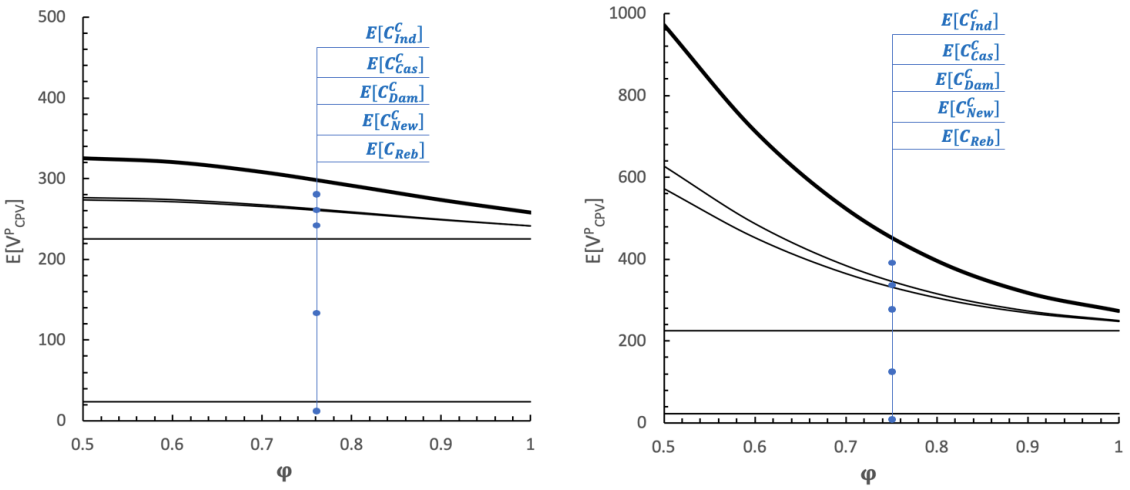

(a) (b)

Figure 5.12 $E[V_{CPV}^{P}(X)]$ under different φ by using non-Poisson hazard model with (a), $t_0 = 1$ and (b) $t_0 = 300$

Lastly, the impact of different reconstruction decisions on BPLCA values is explored. Since no decision tools have been developed in this study, the BPLCA from three decision matrix $\boldsymbol{X}$ - (a). all $x_{ij} = 0$, (b). all $x_{ij} = 1$, and (c). all $x_{ij} = 2$ - are compared under different hazard rate factors. The $E[C_{LCC}^{P}(\boldsymbol{X})]$ and $E[V_{CPV}^{P}(\boldsymbol{X})]$ under different $\boldsymbol{X}$ are illustrated in Figure 5.13(a) and (b), respectively. In both methodologies, decision $\boldsymbol{X} = [\boldsymbol{0}]$ has the lowest value in low hazard rate factor (e.g. 0.2) while decision $\boldsymbol{X} = [\boldsymbol{2}]$ has the lowest value in high hazard rate (e.g. 10). In addition, decisions $\boldsymbol{X}$ that

have the lowest BPLCA value in medium hazard rate factor (e.g.1 to 4) are different according to different methodologies. For instance, when the hazard rate factor is 4, $E[C_{LCC}^{P}(\boldsymbol{X})]$ is lowest at $\boldsymbol{X} = [\mathbf{1}]$ while $E[V_{CPV}^{P}(\boldsymbol{X})]$ is lowest at $\boldsymbol{X} = [\mathbf{2}]$. In other words, the EBPCPV-based methodology (in which risk aversion of decision-makers can be considered) tends to favor higher reconstruction levels. A more complete analysis of optimal reconstruction decision-making will be given in Section 5.8.

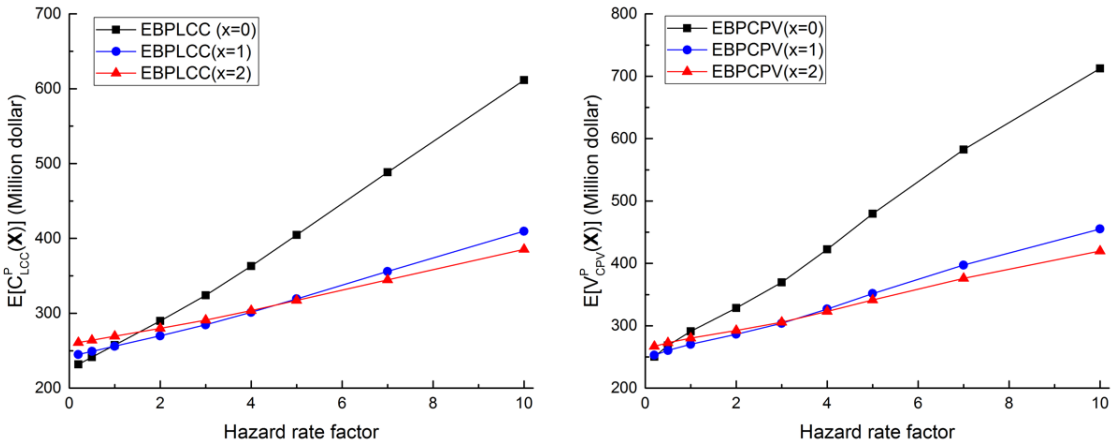

(a) (b)

Figure 5.13 (a) $E[C_{LCC}^{P}(X)]$ and (b) $E[V_{CPV}^{P}(X)]$ for different reconstruction decision X under different hazard rate factors

5.8 Illustration 2 – Centerville Reconstruction Decision-making

As illustration 1, Centerville is employed to exemplify the application of developed methodology. Suppose the residential building portfolio of Centerville is severely damaged in a destructive M_w = 8 earthquake with epicenter distance equal to 22.5 km. The spatial distribution of the post-hazard damage state of the portfolio is shown in Figure 5.14 and

summarized in Table 5.4. Most of the buildings are damaged needing either repair or reconstruction. For future earthquakes, the mean hazard occurrence rate is tabulated in Table 5.5. The low mean hazard occurrence rate is meant to represent the low-frequency, high consequence natural of earthquakes in mid-America (e.g. sites near the New Madrid Seismic Zone, NMSZ) (Toro, 2001). The cost of reconstruction and casualty are given in Table 5.6 and Table 5.7. The BPLC is obtained to be 115 years in Section 5.7. $\omega = 1.0$ is employed as the default value for indirect loss in Eq. (5.6) and Eq. (5.13).

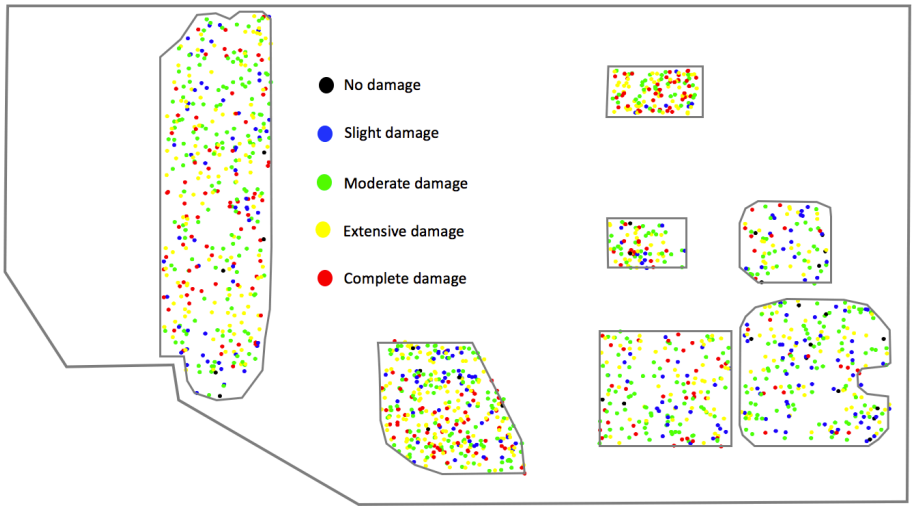

Figure 5.14 Damage state distribution of building portfolio after a M8 earthquake event

Firstly, the optimal post-hazard strategy is derived when EBPLCC is the only objective to minimize (Eqs. (5.27) and (5.29)), no resilience goal is considered. Different discount rates are employed for economic losses and human casualties, i.e. 3% and 1%, respectively by default (Lee & Ellingwood, 2015). The effect of Poisson hazard model (PHM) (Figure 5.15 (a)) and the non-Poisson hazard model (NPHM) (Figure 5.15(b) - (e))

on the optimal reconstruction strategy is investigated. For the latter case, the c.o.v. of the return period of m_3 = 7.5 representative earthquake is assumed to be 0.3. $t_0 = 1\ (and\ 100), 200, 300,$ and 500 is considered respectively in Figure 5.15(b) - (e) to investigate its effect. In Figure 5.15(b), $t_0 = 1$ (when last major earthquake occurs last year), NPHM relates to lower reconstruction level than the PHM does. Further, the optimal strategy for $t_0 = 1$ and $t_0 = 100$ is the same, due to the fact that the occurrence rate of next CH is very low when the time to last CH is short in the NPHM (see Figure 5.5). From Figure 5.15 (c) – (e), one finds that as the t_0 increases, the reconstruction level trends to be higher. However, no (building type, damage state) pair needs to rebuild to E2, implies that when minimizing EBPLCC is the only objective, rebuild to high-code level according to current seismic design code is sufficient. For rest of the case study, unless otherwise indicated, the NPHM with $t_0 = 1$ and original hazard rate is employed as the default.

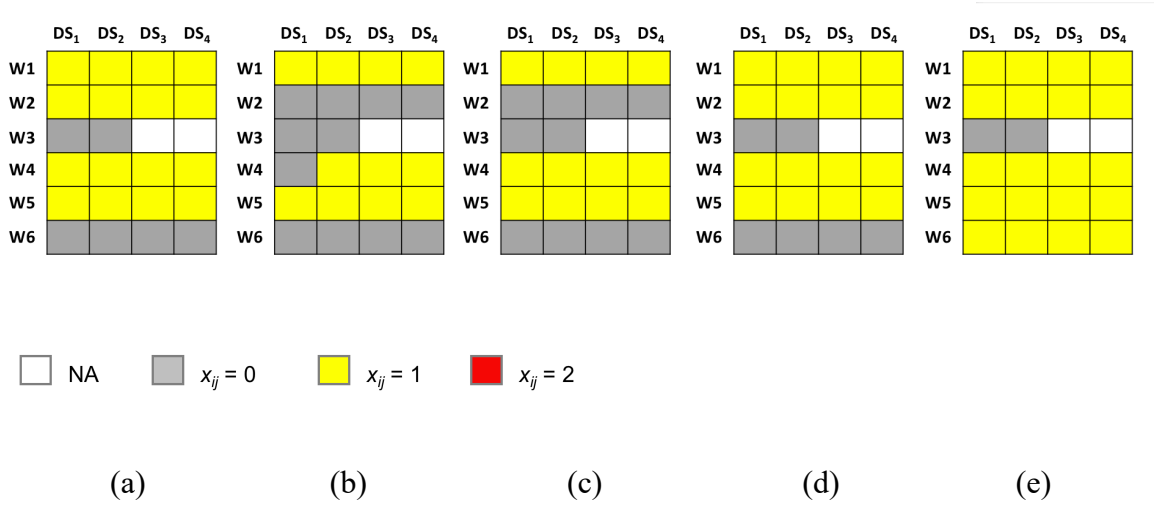

Figure 5.15 The optimal post-hazard reconstruction strategy based on EBPLCC when the hazard occurrence model is (a) Poisson model; non-Poisson model with (b) $t_0 = 1, 100$, (c) $t_0 = 200$, (d) $t_0 = 300$, and (e) $t_0 = 500$

Then, the effect of mean hazard occurrence rate on optimal reconstruction strategy is examined based on EBPLCC (shown in Figure 5.16). When the hazard rate is low (e.g. in Figure 5.16(a)), all optimal decisions are $x_{ij} = 0$ (rebuild as before), by contrast when the hazard rate is high (e.g. Figure 5.16(e)), most optimal decisions are $x_{ij} = 2$ (rebuild to E2). Figure 5.16 suggests that for regions with low annual hazard rate (e.g. (a) – (c)), current high design code (E1) is sufficient to ensure BBB when minimizing EBPLLC only.

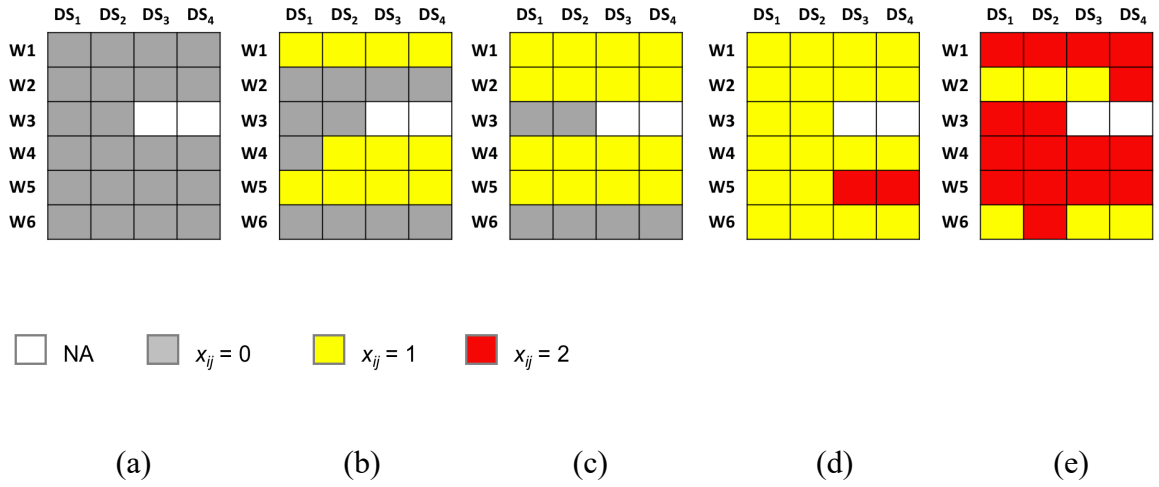

Figure 5.16 The optimal post-hazard reconstruction strategy based on EBPLCC when the mean hazard occurrence rate is (a) 0.5 time, (b)1 time, (c) 2 times, (d) 3 times, and (e) 5 times of the default value in Table 3.

Further, the resilience metric/goal introduced in Section 5.5 is incorporated into the optimization and its effect on optimal reconstruction strategy as well as the trade-off between reduced DLR and increased EBPLCC are investigated. Case a-1 is defined as all $x_{ij} = 0$, related to portfolio resilience performance metric $M_{DLR,m_3} = 249.57/460 = 54.3\%$; Case a-5 is defined as all $x_{ij} = 2$, $M_{DLR,m_3} = 110.83/460 = 24.1\%$. Thus, Case

a-2 is the optimal strategy with corresponding resilience $M_{DLR,m_3} = 179.5/460 = 39.0\%$. Case a-3 and a-4 have moderate resilience goal G_{DLR,m_3}. As the resilience goal becomes more and more strict, the optimal rebuild strategy yields more pairs with $x_{ij} = 1$ or 2 (rebuild to E1 or E2). Further, the EBPLCC and its decomposition is investigated under different cases. From Table 5.10, it is also found that $E[C_{New}^C(\boldsymbol{X})]$ constitutes 78.4% - 79.9% of $E[C_{LCC}^P(\boldsymbol{X})]$, $E[C_{Reb}(\boldsymbol{X})]$ is the second largest item, then followed by $E[C_{Dam}^C(\boldsymbol{X})]$ and $E[C_{Ind}^C(\boldsymbol{X})]$. $E[C_{Cas}^C(\boldsymbol{X})]$ are negligible in all cases. When the resilience goals decrease from 54.3% to 24.1%, the $E[C_{LCC}^P]$ increases insignificantly ($11.75M, 4.56%). In Table 5.10, the net cost is defined as the additional $E[C_{Reb}(\boldsymbol{X})]$ and $E[C_{New}^C(\boldsymbol{X})]$ while net benefit is defined as reduced $E[C_{Dam}^C(\boldsymbol{X})]$, $E[C_{Cas}^C(\boldsymbol{X})]$, and $E[C_{Ind}^C(\boldsymbol{X})]$, when compared to the baseline (Case a-1). Generally, a benefit-cost ratio greater than 1 is preferred in decision-makings. The cost-benefit suggests that strict resilience goals (e.g. $G_{DLR,m_3} = 130$ or lower) will lead to lower than 1 of the benefit-cost ratios in the EBPLCC-based methodology.

The optimal EBPCPV-based strategies with different resilience goals/performance levels are compared in Figure 5.17(b) and Table 5.11. Case b-1 and Case b-5 are minimum and maximum reconstruction level as before; in Case b-2, EBPCPV is the only objective to minimize for reconstruction strategy; In Case b-3 and b-4, different levels of resilience goals are considered. As a baseline, the parameter of the CPT model is $\alpha = 1, \varphi = 0.8$ corresponding to an inverse-s shaped probability transformation function (c.f. Eq. (5.12) and Figure 5.4). From the comparison of Case a-1-5 in Table 5.10 and Case b-1-5 in Table 5.11, it is found that the contribution of damage loss, casualty and indirect loss is amplified

in Table 5.11 due to the risk aversion reflected in the EBPCPV methodology. Further, the benefit-cost ratios for Case b-2 – b-5 in Table 5.11 are all greater than 1, suggesting that even though considering the resilience goals will associate with higher EBPCPV, it is worthwhile to do so. In other words, the EBPCPV-based methodology justifies higher level reconstruction strategies with higher resilience performance with rigor basis.

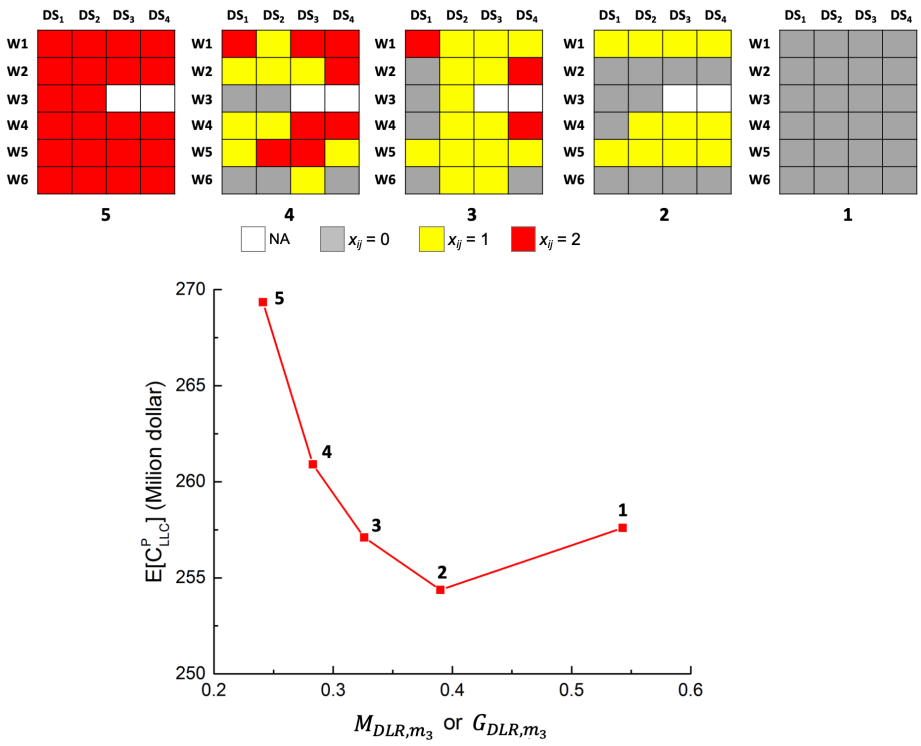

(a)

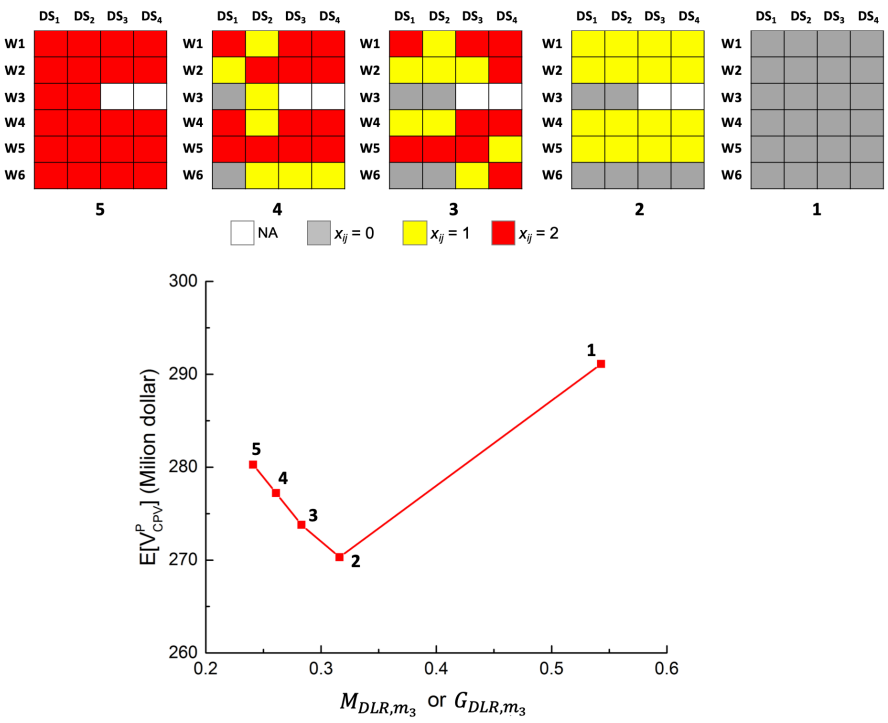

(b)

Figure 5.17 The optimal post-hazard reconstruction strategy under different resilience goals based on (a) EBPLCC, (b) EBPCPV ($\alpha = 1, \varphi = 0.8$)

Table 5.10 The EBPLCC decomposition and cost-benefit analysis under different resilience metrics/goals

Case	$G_{DLR,M7.5}/M_{DLR,M7.5}$	C^P_{LCC}	C_{Reb}	C^C_{New}	C^C_{Dam}	C^C_{Cas}	C^C_{Ind}	Net Benefit	Net Cost	Benefit-Cost Ratio
a-1	249.57/460 = 54.3%	257.60	23.41	202.04	15.77	0.62	15.77	N/A	N/A	N/A
a-2	179.50/460 = 39.0 %	254.37	29.22	205.79	9.58	0.22	9.58	12.78	9.56	1.34
a-3	150.00/460 = 32.6%	257.10	33.46	208.61	7.45	0.13	7.45	17.13	16.62	1.03
a-4	130.00/460 = 28.3%	260.90	37.32	211.07	6.21	0.09	6.21	19.65	22.94	0.86
a-5	110.83/460 = 24.1%	269.35	43.58	215.32	5.20	0.05	5.20	21.71	33.45	0.65

- The LCA results in the table are all expected values, due to lack of space, notation $E[\cdot]$ is omitted.

Table 5.11 The EBPCPV decomposition and cost-benefit analysis under different resilience metrics/goals

Case	$G_{DLR,M7.5}/M_{DLR,M7.5}$	V^P_{CPV}	V_{Reb}	V^C_{New}	V^C_{Dam}	V^C_{Cas}	V^C_{Ind}	Net Benefit	Net Cost	Benefit-Cost ratio
b-1	249.57/460 = 54.3%	291.11	23.41	202.04	32.04	1.57	32.04	N/A	N/A	N/A
b-2	145.13/460 = 31.6%	270.30	33.14	208.32	14.27	0.29	14.27	36.82	16.01	2.30
b-3	130.00/460 = 28.3%	273.79	37.24	211.10	12.62	0.21	12.62	40.20	22.89	1.76
b-4	120.00/460 = 26.1%	277.21	40.59	213.26	11.59	0.17	11.59	42.30	28.40	1.49
b-5	110.83/460 = 24.1%	280.27	43.58	215.32	10.62	0.12	10.62	44.29	33.45	1.32

- The LCA results in the table are all expected values, due to lack of space, notation $E[\cdot]$ is omitted.

Then, the impact of risk aversion (represented by φ and keeping $\gamma^- = 1$) on the EBPCPV of optimal reconstruction decisions is investigated. Resilience performance goal is not imposed, instead, the resilience performance M_{DLR,m_3} is estimated corresponding to each optimal strategy. The comparison of the optimal strategy from different φ under $t_0 = 1$ and $t_0 = 200$ are illustrated in Figure 5.18(a) and (b) respectively. In Figure 5.18(a), when $\varphi = 1.0$ (identical to EBPLCC-based methodology), $E[V_{CPV}^P(\boldsymbol{X})] = \$254.37\text{M}$ is the lowest while resilience performance M_{DLR,m_3}= 39.02% is the highest indicating great loss in extreme events. On the other hand, when $\varphi = 0.5$ (very conservative on LPHC events), the $E[V_{CPV}^P(\boldsymbol{X})] = \$284.93\text{M}$ is the highest while resilience performance M_{DLR,m_3} = 30.84% is the lowest. Also, it is found that for $\varphi = 0.9$ or smaller, the M_{DLR,m_3} is not sensitive to φ value. One observes similar trend in Figure 5.18(b), expect that the optimal strategies becomes higher in all cases and M_{DLR,m_3} is very sensitive to φ value. Thus, different risk preference of decision makers can lead to a spectrum of optimal reconstruction strategies corresponding to different resilience performance.

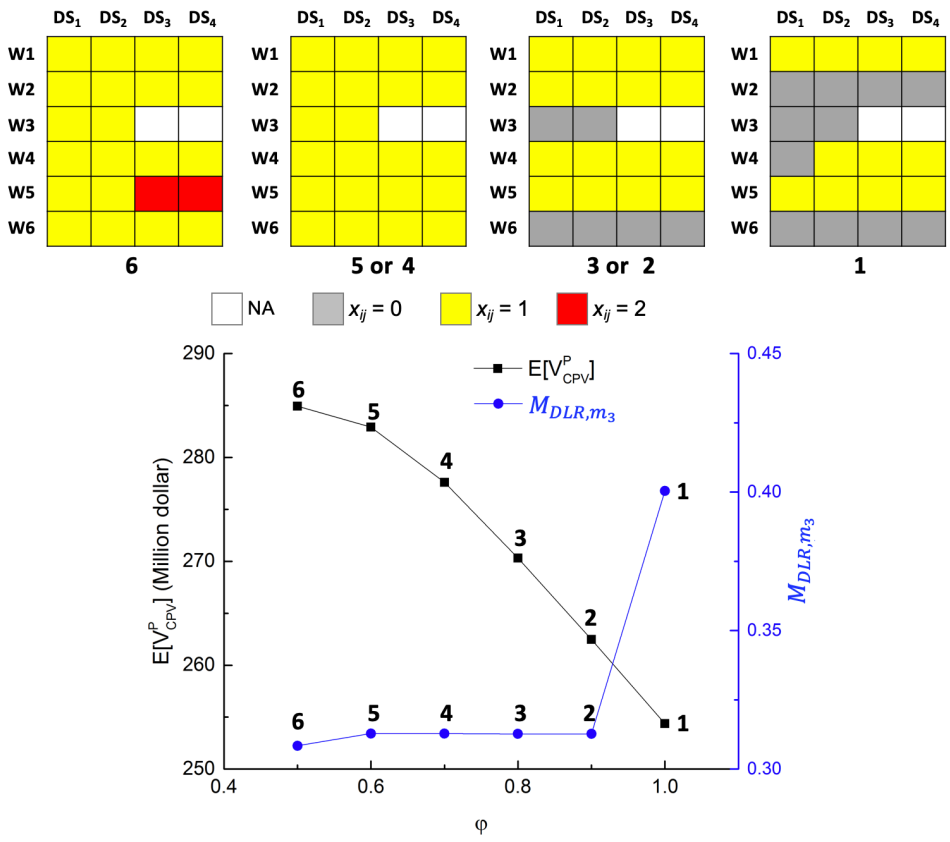
DS1 DS2 DS3 DS4
W1
W2
W3
W4
W5
W6
6
5 or 4
3 or 2
1
NA
x_{ij} = 0
x_{ij} = 1
x_{ij} = 2
E[V^P_{CPV}] (Million dollar)
M_{DLR,m_3}
φ

(a)

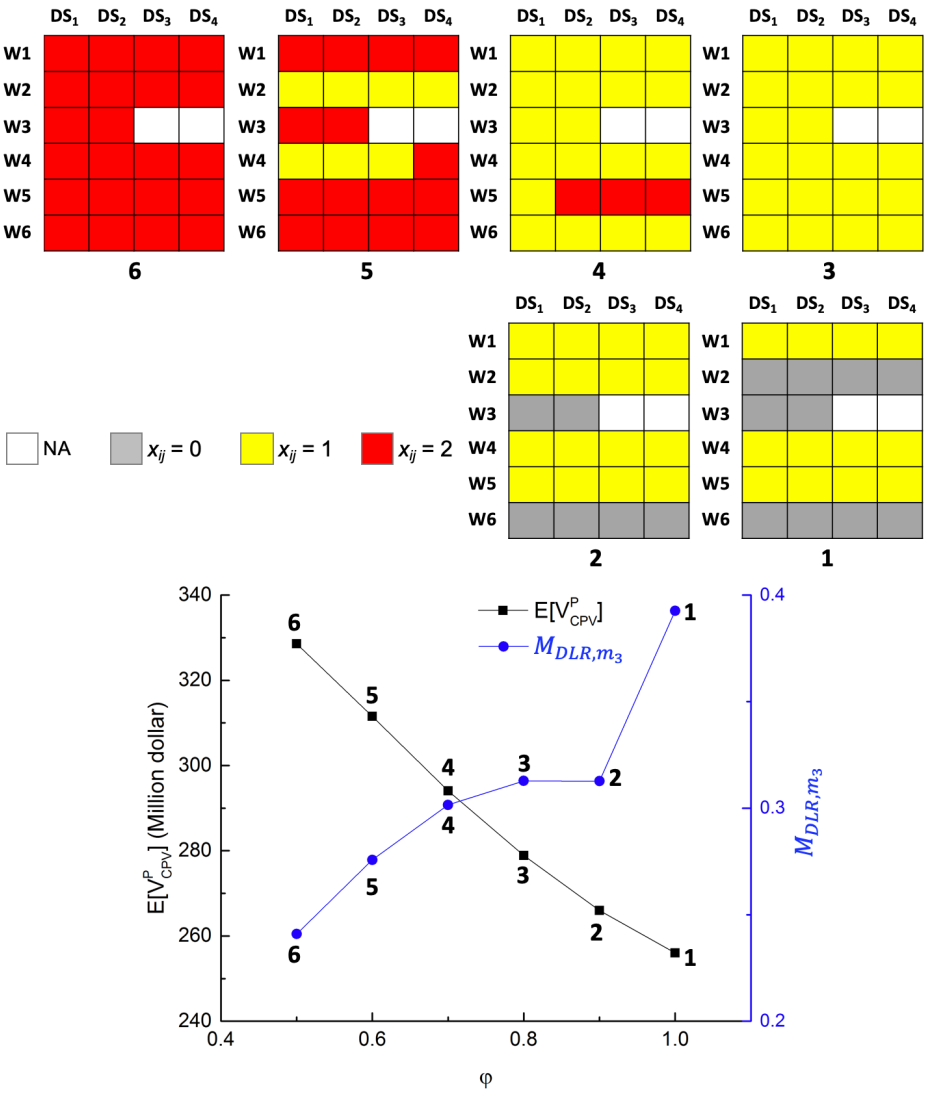

(b)

Figure 5.18 The optimal post-hazard reconstruction strategy given different φ (keep $\gamma^- = 1$) when (a) $t_0 = 1$ and (b) $t_0 = 200$

The effect of BPLC length on EBPCPV ($\alpha = 0.8$ and $\varphi = 1$) and optimal reconstruction strategy is examined under different hazard models: (a). PHM, and NPHM with (b) $t_0 = 1\ or\ 100$, (c) $t_0 = 200$, and (d) $t_0 = 300$, as illustrated in Figure 5.19. No

resilience goal is considered. One can find that the optimal strategy is sensitive to BPLC length in all cases, longer BPLC generally requires higher reconstruction level and verse versa. Further, the classical way of assuming infinite life-cycle length (e.g. Wen & Kang, 2001) and the optimal decision based on may be problematic and over-conservative. The cases with different discount rate for economic loss (e.g. 2% and 5%) are examined further, similar trends are observed. However, it is recognized that the conclusion may not be general and need more researches to be done.

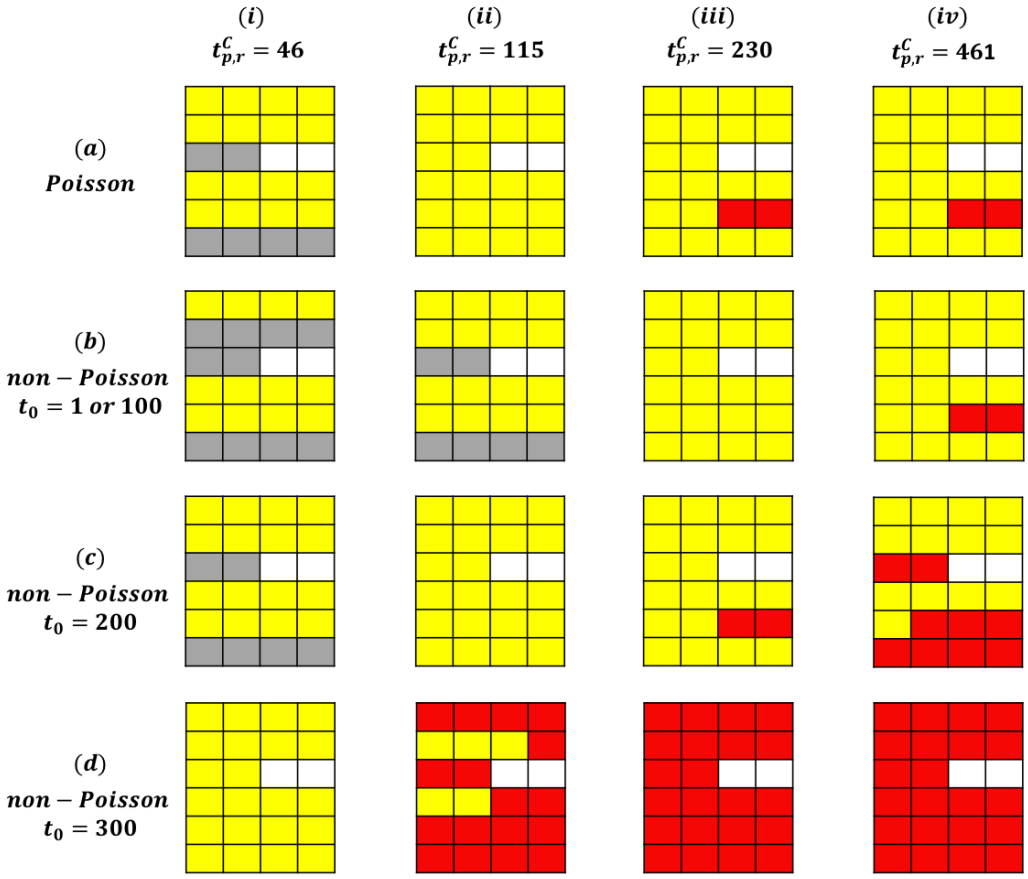

Figure 5.19 The optimal post-hazard reconstruction strategy for different hazard model and BPLC combinations based EBPCPV

Lastly, the optimal decisions for individuals and the portfolio are compared. For illustration purpose, W4 building with post-hazard $DS = 4$ (complete damage) is selected as an example. Figure 5.20 gives the Expected LCC (ELCC) value for two individual building in different zones under different hazard rate factor. In both Figure 5.20(a) and (b), the ELCC curve from $x = 0$ trends to have lower value at low hazard factor and grow quickly when hazard factor increases; by contrast, the ELCC curve from $x = 2$ trends to have higher value at low hazard factor and grow slowly when hazard factor increases; the ELCC curve from $x = 1$ lies between those from $x = 0$ and $x = 2$. In addition, the ELCC curves from Zone1, Building $ID = 4$ are higher than that from Zone3, Building $ID = 46$, due to that the former is closer to the seismic fault. In Figure 5.16 and Figure 5.20, it is found that from both individual buildings' and portfolio's perspective, the optimal decision is 0 (rebuild as before) when the hazard factor is low (e.g. equal to 0.5); while the optimal decision is 2 (rebuild to E2) when the hazard factor is high (eq. equal to 5). However, for the hazard factor between these two extremes, the portfolio decision and individual decisions (with lowest ELCC) could be different. For instance, when hazard factor equals to 2, for the portfolio, $x_{44} = 1$ is the optimal decision. In individual building level, the optimal decision is $x = 2$ for building ID = 4 at Zone 1 and $x = 1$ for building ID = 46 at Zone 3. Such difference of optimal decisions between portfolio and individual buildings could provide basis for communities designing reconstruction incentives to achieve its performance goals with the cooperation from building owners.

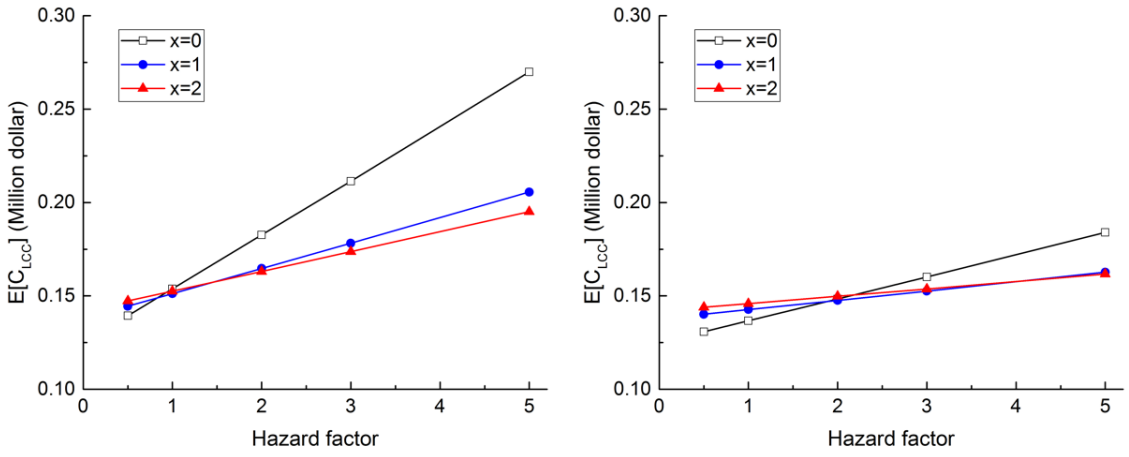

Figure 5.20 The ELCC corresponding to three different reconstruction strategies of W4 building with post-hazard DS = 4 (a)Zone 1, Building ID = 4; (b) Zone 3, Building ID = 46

5.9 Closure

Reconstruction of a community building portfolio after a major hazard event, in the light of similar impacts from future hazards, has motivated the development of optimal post-hazard reconstruction strategies based on building portfolio life cycle analysis in which costs from reconstruction, natural urban renewal, and future hazard exposure are considered. The concomitant needs for quick post-hazard recovery and recovery of functionality require the portfolio resilience goal to be satisfied. This chapter has developed a methodology for life-cycle analysis of a building portfolio and presented a framework that can support the post-hazard reconstruction process by establishing the optimal reconstruction strategies based on minimizing expected building portfolio life cycle costs or maximizing cumulative prospect values while fulfilling resilience goals. The

life-cycle analysis methodology and decision-framework developed in this chapter can be directly applied to post-hazard reconstruction of building portfolios by assisting communities in post-hazard planning and incentives/policies designing. The decision-framework could support building back better following earthquake (or other severe natural hazard events with minor modification) and guide a community toward achieving resilience goals in an efficient manner.

Chapter 6 Summary, Contributions, and Recommendations

6.1 Summary

Building portfolios form the physical basis and essential part of a community and their performance is critical to the resilience and sustainability of a community: reduction of socioeconomic loss, preservation of integrity, acceleration of functionality recovery under natural hazards, and relief of financial and environmental burden on future generations. However, currently, there is no explicit consideration on the performance requirement of individual buildings directly related the performance objectives on the community level. Rather, typically buildings are designed, retrofitted, and reconstructed individually according to codes/standards to ensure Life Safety under rare hazard events. In addition, community-level hazard prevention and mitigation strategies involve considerable financial and organizational resources, bear a long-term impact on the wellbeing of future generations, and could greatly affect the hazard performance and the prosperity of communities. Decision-making framework that can systematically support developing the hazard mitigation strategies to enhance the resilience and sustainability of communities in different stages of life-cycle does not exist.

This dissertation has proposed a risk-informed decision-making framework for building portfolios under natural hazards. It could help communities identify their resilience performance goals corresponding to the selected performance metrics, assess the performance of community in current condition, and develop disaster prevention and mitigation decisions in a most efficient and sustainable way. This study has explored three

categories of decision-making problems for residential buildings - new construction, pre-hazard retrofit, and post-hazard reconstruction decision - that can be directly utilized to help communities achieve their long-term resilience and sustainability goals.

The first element of the decision-making framework is the derivation of the minimum performance criteria of individual buildings, which will form the basis for new construction as well as for retrofitting and reconstruction. Currently, the aim of design codes/standards is to ensure Life Safety of occupants under rare hazards. The performance criteria for buildings implied in these codes were obtained by back-calibrating the performance of buildings designed by previous codes without rational justification on the permitted failure probability as well as relating to higher-level resilience performance goals expressed in socioeconomic metrics. Thus, current design codes/standards are not sufficient to protect communities from the natural hazards and avoid grave consequences (e.g. permanent population out-migration). This part of the study firstly proposed a resilience-based design philosophy, with key features including: 1) functionality and loss are considered as the major performance criteria defined at the community-level; 2) the minimum performance criteria of individual buildings are derived from a risk de-aggregation methodology, which consists of a lower level and a higher level de-aggregation and eventually links the performance criteria of individual buildings to the community-level resilience goals; and 3) explicit statement of the performance requirement for individual buildings, clusters, and the community. The probabilistic assessment of a building portfolio's performance under specific hazard level (e.g. design hazard) poses significant challenges in characterizing the spatial variation and correlation of hazard

fields. A simulation-based hybrid methodology has been proposed to generate a spectrum of hazard scenarios of specific hazard level to capture the uncertainties in hazard demand. The lower level de-aggregation has been formulated as an inverse optimization problem to derive the minimum performance criteria for individual buildings in terms of fragility function parameters. Owing to different hazard characterizations, damage state definitions, and performance preferences under tornadoes and earthquakes, risk de-aggregation methodologies have been developed for communities under tornadoes and earthquakes. These methodologies shows that it is possible to design individual buildings by performance-based design with performance criteria calibrated with the performance requirement of the community as a whole.

The second element of the decision-making framework is the pre-hazard retrofit strategy. Many communities in the U.S. have implemented or about to implement large-scale community-level pre-hazard retrofit plans, either mandatory or voluntary, hoping to significantly enhance the performance of vulnerable existing building portfolios, protect the properties and occupants, and prevent detrimental consequences in future extreme hazards. However, it is unclear to which extent such large-scale retrofit plan could close the gap between the anticipated performance and the desired performance objective under specific hazard level, and more importantly. Further, it is unclear on how to design the retrofit plan such that the performance gap could be mostly closed with limited resources (e.g. budget and work crew). The proposed pre-hazard retrofit framework includes three steps: (1) defining building cluster resilience goals; (2) implementing risk de-aggregation to obtain the target performance criteria for individual buildings; and (3) developing

retrofit strategies by modeling the retrofit planning as an optimization problem and solving it by optimization tools. As Chapter 3 had given a thorough discussion of steps (1) and 2), this task focused on step (3). The retrofit planning problem has been formulated as a multi-objective optimization problem, specifically, a multi-objective integer programming problem, as a community may interest in achieving more than one performance goal (e.g. economic loss and population dislocation). The final outcome is a group of optimal retrofit strategies defining the level of target performance for each building type in each zone.

The third element of the decision-making framework regards the post-hazard reconstruction strategies. Destructive hazard events provide valuable opportunities for communities to re-think the performance level of current infrastructure systems and rebuild in a more rational way. However, few studies had been done to develop comprehensive reconstruction policies supporting building back better. As the outcomes of these decisions would have a long-term impact on the hazard resilience, financial healthiness, and sustainability of communities, optimal reconstruction decisions should consider both the resilience and sustainability performance. It started with the introduction of post-hazard reconstruction decision-framework. Then, it extended the concept of life-cycle analysis to a cluster of buildings, which includes two key ingredients: 1) the length of building portfolio life-cycle and 2) the renewal rate of a building portfolio. It then formulated the life-cycle analysis of building portfolios in terms of the expected building portfolio life-cycle cost and cumulative prospect value, which could consider the risk averseness of decision-makers. The building portfolio life-cycle analysis and reconstruction decision-making have been applied to portfolios under seismic hazards. The example of rebuilding

Centerville after a severe earthquake has revealed that considering risk-averse of decision-makers (by utilizing cumulative prospect value) could lead to higher reconstruction level.

6.2 Conclusions

The thorough quantitative assessment of building portfolios' performance on both resilience and sustainability metrics, and the exploration of optimal decision-making strategies for building portfolios located in hazard-prone regions have provided some essential findings regarding decision-making in different stages, i.e. new construction, pre-hazard retrofitting, and post-hazard reconstruction. While it is recognized that these findings are preliminary due to limited data and case studies, however, they provide a basis for future inquiries and studies.

For New Construction Performance Criteria

1. In resilience-based design, not Life-safety (LS), but Immediate Occupancy (IO) is considered as the major performance objective for buildings, which should be related to the overall community resilience goals.
2. The links between the overarching community resilience goals and the performance objectives of individual buildings, could be built through a multilayered, cascading de-aggregation framework.
3. Through a lower-level de-aggregation methodology, it is possible to derive a group of minimum fragility parameters that are ready to be applied to the development of new prototypes of residential buildings from performance-based design and form the basis for a new generation of design codes.

4. The minimum performance criteria of buildings depend on the size of the community, in both tornado and seismic hazards, larger communities tend to have lower minimum performance criteria for individual buildings, given the same community-level resilience goal.

For pre-hazard retrofit decision-making

5. Resilience performance of portfolios in multiple aspects could be enhanced simultaneously by organized pre-hazard retrofitting strategies from a group of optimal strategies, from which decision-makers could select their strategy according to their preference over multiple performance metrics.
6. At moderate budget level, communities have more flexibility on optimal retrofit strategies, i.e. a large number of feasible strategies is available to give a wide range of trade-off between two performance levels.
7. Given a limited budget, optimal strategies tend to place the majority of retrofit actions in the zone with higher density under tornado hazards to maximize resilience performance.

For Post-hazard Reconstruction Decision-making

8. Post-hazard reconstruction should be planned from the perspective of the whole life-cycle of building portfolios to support building back better decisions that can enhance the performance of communities in future hazards.

9. Integrating the risk averseness into the portfolio life-cycle analysis will lead to higher reconstruction level and has the potential to unify the building portfolio resilience and sustainability requirements into one.
10. The optimal reconstruction strategy is sensitive to the life-cycle length of building portfolios. Traditional treatment of infinite life-cycle length will overestimate the life-cycle impact and be too conservative in reconstruction.
11. The optimal reconstruction decisions for individual buildings could be different from those for the portfolio as a whole. Such discrepancy may help communities develop financial incentives and policies.
12. For regions susceptible to characteristic earthquakes, it is important to consider their non-uniform annual occurrence rates, which can greatly affect the optimal reconstruction strategies.

6.3 Recommendations

The research conducted in this dissertation has identified several topics worth further investigation as listed below.

1. This study focused on the decision-making for individual buildings based on given cluster performance goals, thus skipped the upper-level risk de-aggregation and decision-making. Studies are needed to explore the risk management of functionality clusters (e.g. building, transportation, utility

network), which would need a thorough understanding of the performance of each cluster as well as the interdependencies between them.

2. While the decision-making framework for communities subjected to single hazard has been developed in this study, the proper consideration of multiple hazards (e.g. earthquake and flood) is in great need to better understand the interaction of multiple hazards, and their impact on optimal strategies.
3. One assumption of this study is that the external hazards are stationary, which is problematic in some cases. For instance, due to climate change, the number and intensity of extreme hurricanes are increasing, thus assuming stationary hazard intensity and frequency becomes inappropriate. Proper treatment of such non-stationary hazards in the decision-framework is needed.
4. One limitation of the portfolio life-cycle analysis in this study that it assumes the number of buildings within the communities to be invariable. However, communities in the real-world trend to expand in size due to population growth and economic development. Further studies are needed to integrate this into the portfolio life-cycle analysis and decision-making.
5. This study focused on how the decision-making of the physical built environment could help communities achieve their resilience and sustainability goals. More studies are needed to assess and design non-engineering measures in assisting communities to achieve their performance goals.
6. In the risk de-aggregation under seismic hazards, one assumption is that the failure probability of structural and non-structure components is independent.

More researches are needed to better model the correlation of failure mode between components and its effect on risk de-aggregation results and performance-based design of individual buildings.

References

Agyeman, J., R. Bullard, and B. Evans. (2002). Exploring the nexus: Bringing together sustainability, environmental justice and equity. Space and Polity 6 (1): 77-90.

Amini, M. O., & van de Lindt, J. W. (2013). Quantitative insight into rational tornado design wind speeds for residential wood-frame structures using fragility approach. Journal of Structural Engineering, 140(7), 04014033.

Anagnos, T., & Kiremidjian, A. S. (1984). Stochastic time-predictable model for earthquake occurrences. Bulletin of the Seismological Society of America, 74(6), 2593-2611.

ANSI. (1972). American National Standard: Building Code Requirement for Minimum Design Loads in Buildings and other Structures.

Arup. (2014). City Resilience Index. City Resilience Framework. New York. https://www.arup.com/perspectives/city-resilience-index

ASCE. (2013). Report Card for America's Infrastructure. http://www.infrastructurereportcard.org

ASCE. (2016). Minimum design loads for buildings and other structures. ASCE 7-16, Reston, VA.

ASCE. (2017). Developing Resilience-Based Performance Standards for Buildings and Lifeline Systems: Final Draft for IRD Review.

Atkinson, G. M., & Boore, D. M. (1995). Ground-motion relations for eastern North America. Bulletin of the Seismological Society of America, 85(1), 17-30.

Ayres, R. U., van den Bergh, J. C. J. M., and Gowdy, J. M. (1998). Viewpoint: Weak versus strong sustainability. Tinbergen Institute Discussion papers.

Bellman, R., 1954. The theory of dynamic programming. Bulletin of the American Mathematical Society, 60 (6): 503–516, doi:10.1090/S0002-9904-1954-09848-8, MR 0067459.

Bertero, R. D., & Bertero, V. V. (2004). Performance-Based Seismic Engineering: Development and Application of a Comprehensive Conceptual Approach to the Design of Buildings. In Earthquake engineering: from engineering seismology to performance-based engineering, Bozorgnia, Y., & Bertero, V. V. (Ed). CRC press.

Bocchini, P., & Frangopol, D. M. (2010). Optimal resilience-and cost-based postdisaster intervention prioritization for bridges along a highway segment. Journal of Bridge Engineering, 17(1), 117-129.

Bocchini, P., Frangopol, D. M., Ummenhofer, T., & Zinke, T. (2014). Resilience and sustainability of civil infrastructure: Toward a unified approach. Journal of Infrastructure Systems, 20(2), 04014004.

Building Research Establishment (BRE). (2010). BREEAM Offices 2008 Assessor Manual.

Brooks, H. E. (2013). Severe thunderstorms and climate change. Atmospheric Research, 123, 129-138.

Brundtland, G. H. (1987). Our common future: Brundtland-report, Oxford University Press, Oxford.

Bruneau, M., Chang, S. E., Eguchi, R. T., Lee, G. C., O'Rourke, T. D., Reinhorn, A. M., ... & Von Winterfeldt, D. (2003). A framework to quantitatively assess and enhance the seismic resilience of communities. Earthquake spectra, 19(4), 733-752.

Campbell, K. W. (2003). Prediction of strong ground motion using the hybrid empirical method and its use in the development of ground-motion (attenuation) relations in eastern North America. Bulletin of the Seismological Society of America, 93(3), 1012-1033.

Cha, E. J., & Ellingwood, B. R. (2012). Risk-averse decision-making for civil infrastructure exposed to low-probability, high-consequence events. Reliability Engineering & System Safety, 104, 27-35.

Changnon, S. A. (2009). "Tornado losses in the United States," Natural Haz. Rev., 10.1061/(ASCE)1527-6988(2009)10:4(145), 145–150.

City and County of San Francisco. 2013. Ordinance 66-13: Building Code – Mandatory Seismic Retrofit Program – Wood-Frame Buildings, 2013.

Cimellaro, G. P., Reinhorn, A. M., & Bruneau, M. (2010). Framework for analytical quantification of disaster resilience. Engineering structures, 32(11), 3639-3649.

Cimellaro, G. P., Renschler, C., Reinhorn, A. M., & Arendt, L. (2016). PEOPLES: a framework for evaluating resilience. Journal of Structural Engineering, 142(10), 04016063.

City of Moore, 2014: Ordinance No. 768 (14). www.cityofmoore.com/sites/default/files/main-site/high- winds-codes-passed.pdf.

Cornell, C. A., & Krawinkler, H. (2000). Progress and challenges in seismic performance assessment. PEER Center News, Spring 2000.

Crowther, K. G., & Haimes, Y. Y. (2005). Application of the inoperability input—output model (IIM) for systemic risk assessment and management of interdependent infrastructures. Systems Engineering, 8(4), 323-341.

Cutler, H., Shields, M., Tavani, D., & Zahran, S. (2016) Integrating engineering outputs from natural disaster models into a dynamic spatial computable general equilibrium model of Centerville, Sustainable and Resilient Infrastructure, 1:3-4, 169-187, DOI: 10.1080/23789689.2016.1254996

Czajkowski, J. (2016, February). Moving from risk assessment to risk reduction: An economic perspective on decision making in Natural Disasters'. In Frontiers of Engineering: Reports on Leading-Edge Engineering from the 2015 Symposium. National Academies Press.

Deb, K. 2001. Multi-objective Optimization Using Evolutionary Algorithms. John Wiley and Sons: Chichester.

Ellingwood, B. R., & Wen, Y. K. (2005). Risk - benefit - based design decisions for low - probability/high consequence earthquake events in Mid - America. Progress in Structural Engineering and Materials, 7(2), 56-70.

Ellingwood B. R., Cutler, H., Gardoni, P., Peacock, W. G., van de Lindt, J. W. & Wang, N. (2016) The Centerville Virtual Community: A Fully Integrated Decision Model of Interacting Physical and Social Infrastructure Systems. Sustainable and Resilient Infrastructure. 1(3-4), 95-107.

Estes, A. C., & Frangopol, D. M. (1999). Repair optimization of highway bridges using system reliability approach. Journal of structural engineering, 125(7), 766-775.

FEDM. (2016). Florida Residential Construction Mitigation Program (RCMP). http://www.floridadisaster.org/Mitigation/RCMP/index.htm

FEMA. (1997). NEHRP guidelines for the seismic rehabilitation of buildings. FEMA 273.

FEMA/NIBS. (2003). Multi-hazard Loss Estimation Methodology Earthquake Model (HAZUS-MH MR4): Technical Manual. Federal Emergency Management Agency, Washington, D.C.

FEMA. (2006). Techniques for the Seismic Rehabilitation of Existing Buildings. FEMA 547.

FEMA, P. 695 (2009) Quantification of seismic performance factors. FEMA P-695 report, the Applied Technology Council for the Federal Emergency Management Agency, Washington, DC.

FEMA. (2010). Wind Retrofit Guide for Residential Buildings. Report No. FEMA P-804, Washington, D.C.

Galanis, P., Sycheva, A., Mimra, W., & Stojadinović, B. (2018). A framework to evaluate the benefit of seismic upgrading. Earthquake Spectra, 34(2), 527-548.

German Sustainable Building Council. (2009). DGNB system. https://www.dgnb.de/en/index.php

Gencturk, B., Hossain, K., & Lahourpour, S. (2016). Life cycle sustainability assessment of RC buildings in seismic regions. Engineering Structures, 110, 347-362.

Ghosh, J., Tapia, C., and Padgett, J. E. (2011). Life-cycle analysis of embodied energy for aging bridges subject to seismic hazards. Appli- cations of statistics and probability in civil engineering, M. Faber, J. Köhler, and K. Nishijima, eds., CRC Press, Boca Raton, 562–569.

Goda, K., & Hong, H. P. (2008). Application of cumulative prospect theory: Implied seismic design preference. Structural Safety, 30(6), 506-516.

Goliger, A. M., and Milford, R. V. (1998). A review of worldwide occur- rence of tornadoes. J. Wind Eng. Ind. Aerodyn., 74–76, 111–121.

Gutenberg B., Richter C.F.. Frequency of earthquakes in California, Bull. seism. Soc. Am., 1944, vol. 34 (pg. 185-188).

HCIDLA. 2015. The Seismic Retrofit Work Program. http://hcidla.lacity.org/seismicretrofit

Holling, C. S. (1973). “Resilience and stability of ecological systems.” Ann. Rev. Ecol. Syst., 4(1), 1–23.

Housner G. (1956). Limit design of structures to resist earthquakes. Proc 1st World Conference on Earthquake Engineering. Berkeley California June 1956.

Hunt, R. G., Franklin, W. E. (1996). LCA—How it came about. The international journal of life cycle assessment, 1(1), 4-7.

HWANG C and YOON K, 1981. Multiple Attribute Decision Making: Methods and Applications. Berlin/Heidelberg/New York: SpringerVerlag.

Intemational Atomic Energy Agency (IAEA) (2009). lNES: The international nuclear and radiological event scale user's manual (2008 Edition). lAEA, Vienna.

Ishibe, T., & Shimazaki, K. (2012). Characteristic earthquake model and seismicity around late Quaternary active faults in Japan. Bulletin of the Seismological Society of America, 102(3), 1041-1058.

IRC. (2015). International Residential Code for One- and Two-family Dwellings. International Code Council.

ISO. (1997). ISO 14040: Environmental management - Life cycle assessment - Principles and framework.

Jara, J. M., & Rosenblueth, E. (1988). The Mexico earthquake of September 19, 1985—probability distribution of times between characteristic subduction earthquakes. Earthquake Spectra, 4(3), 499-529.

Jayaram and Baker, 2010. Efficient sampling and data reduction techniques for probabilistic seismic lifeline risk assessment. Earthquake Engng Struct. Dyn. 2010; 39:1109–1131.

Jennings, E., van de Lindt, J., & Peek, L. (2015). Multi-objective community-level seismic retrofit optimization for resiliency using engineering and socioeconomic variables. In 12th International Conference on Applications of Statistics and Probability in Civil Engineering (pp. 1-10).

Kajikawa, Y. (2008). Research core and framework of sustainability science. Sustain. Sci. 3, 215e239.

Kanda, J., & Ellingwood, B. R. (1991). Formulation of load factors based on optimum reliability. Structural Safety, 9, 197–210.

Kennedy, J., & Eberhart, R. C. (1995). Particle swarm optimization. In Proceedings of the 1995 IEEE International Conference on Neural Networks, pages 1942–1948, Piscataway, New Jersey. IEEE Service Center.

Kiremidjian, A. S., & Anagnos, T. (1984). Stochastic slip-predictable model for earthquake occurrences. Bulletin of the Seismological Society of America, 74(2), 739-755.

Klein, R. J. T., Nicholls, R. J., and Thomalla, F. (2003). Resilience to natural hazards: How useful is this concept? Global Environ. Change Part B: Environ. Hazards, 5(1–2), 35–45.

Larsen, R. J., & Marx, M. L. (2011). An Introduction to mathematical statistics and applications (6^{th} edition). Pearson.

Laskari, E. C., Parsopoulos, K. E., & Vrahatis, M. N. (2002). Particle swarm optimization for integer programming. In Proceedings of the 2002 Congress on Evolutionary Computation. CEC'02 (Cat. No. 02TH8600) (Vol. 2, pp. 1582-1587). IEEE.

Lee, J. Y., & Ellingwood, B. R. (2015). Ethical discounting for civil infrastructure decisions extending over multiple generations. Structural Safety, 57, 43-52.

Lee, J. and Ellingwood, B. (2017). A decision model for intergenerational life-cycle risk assessment of civil infrastructure exposed to hurricanes under climate change. Reliability Engineering and System Safety 159 (2017) 100–107.

Lin P and Wang N. (2016). Building portfolio fragility functions to support scalable community resilience assessment. Sustainable and Resilient Infrastructure, 2016. http://dx.doi.org/10.1080/23789689.2016.1254997

Lin, P., Wang, N., & Ellingwood, B. R. (2016). A risk de-aggregation framework that relates community resilience goals to building performance objectives. Sustainable and Resilient Infrastructure, 1(1-2), 1-13.

Lin, P., and Wang, N. (2017). Stochastic post-disaster functionality recovery of community building portfolios I and II. Structural Safety. DOI: 10.1016/j.strusafe.2017.05.004 and 2017.05.002

Lu, D. (1995). Ph.D. Dissertation. A statistically rigorous model for tornado hazard assessment. Texas Tech University.

Luco, N., Ellingwood, B.R., Hamburger, R.O., Hooper, J.D., Kimball, J.K., & Kircher, C.A. (2007): Risk-targeted versus current seismic design maps for the conterminous United States. Structural Engineers Association of California 2007 Convention Proceedings, 26-29 Sep 2007, Lake Tahoe CA, 163-175

Maloney, T., Ellingwood, B., Mahmoud, H., Wang, N., Wang, Y., & Lin, P. (2018). Performance and risk to light-framed wood residential buildings subjected to tornadoes. Structural safety, 70, 35-47.

Masoomi, H., & van de Lindt, J. (2017): Restoration and functionality assessment of a community subjected to tornado hazard, Structure and Infrastructure Engineering, DOI: 10.1080/15732479.2017.1354030

Matthews, M. V., Ellsworth, W. L., & Reasenberg, P. A. (2002). A Brownian model for recurrent earthquakes. Bulletin of the Seismological Society of America, 92(6), 2233-2250

McGuire, R. K. (2004). Seismic hazard and risk analysis. Earthquake Engineering Research Institute.

Meadows, D. H., Meadows, D. L., Rander, J., and Behrens, W. W. (1972). The limits to growth: A report for the Club of Rome's project on the predicament of mankind, Universe Books, New York.

Mieler, M., Stojadinovic, B., Budnitz, R., Comerio, M., and Mahin, S. (2015). A framework for linking community resilience goals to specific performance targets for the built environment. Earthquake Spectra, 31, 1267–1283.

National Institute of Standards and Technology. (NIST). (2015a). Disaster Resilience Framework: 75% draft for San Diego, CA Workshop. https://www.nist.gov/sites/default/files/documents/el/building_materials/resilience/Framework_LineNumbered_75-25_11Feb2015.pdf

National Institute of Standards and Technology. (NIST). (2015b). Community Resilience Planning Guide for Building and Infrastructure Systems: draft for public comment. (http://dx.doi.org/10.6028/NIST.SP.1190v1)

National Oceanic and Atmospheric Administration. (NOAA). (2015). Severe Weather Database Files (1950-2015): U.S. TORNADOES. (http://www.spc.noaa.gov/wcm/#data)

Nishenko, S. P., & Buland, R. (1987). A generic recurrence interval distribution for earthquake forecasting. Bulletin of the Seismological Society of America, 77(4), 1382-1399.

Nishijima, K., Straub, D., and Faber, M. H. (2007). "Inter-generational distribution of the life-cycle cost of an engineering facility." Journal of Reliability of Structures and Materials, 1(3): 33-46.

National Oceanic and Atmospheric Administration. (NOAA). (2015). Severe Weather Database Files (1950-2015): U.S. TORNADOES. http://www.spc.noaa.gov/wcm/ - data

Oregon. Seismic Safety Policy Advisory Commission (OSSPAC). (2013). The Oregon resilience plan: Reducing risk and improving recovery for the next Cascadia earthquake and tsunami. The Commission.

Otto, S. (2007). Bedeutung und Verwendung der Begriffe nachhaltige Entwicklung und Nachhaltigkeit: Eine empirische Studie, Dissertation, Jacobs Univ. Bremen, Jacobs Center on Lifelong Learning and Institu- tional Development, Germany.

Padgett, J. E., & Tapia, C. (2013). Sustainability of natural hazard risk mitigation: Life cycle analysis of environmental indicators for bridge infrastructure. Journal of Infrastructure Systems, 19(4), 395-408.

Padgett, J.E., & Li, Y. (2014). Risk-Based Assessment of Sustainability and Hazard Resistance of Structural Design. J. Perform. Constr. Facil., 04014208.

Pepper, D. (2005). Modern environmentalism: An introduction, Routledge, London.

Petersen, M. D., Cao, T., Campbell, K. W., & Frankel, A. D. (2007). Time-independent and time-dependent seismic hazard assessment for the State of California: Uniform California Earthquake Rupture Forecast Model 1.0. Seismological Research Letters, 78(1), 99-109.

Porter, K. A. (2016). Safe enough? A building code to protect our cities and our lives. Earthquake Spectra, 32(2), 677-695.

Rackwitz, R., Lentz, A., and Faber, M. H. (2005). "Socio-economically sustainable civil engineering infrastructures by optimization." Structural Safety, 27(3): 187-229.

Raiffa, H., & Schlaifer, R. (1961). Applied statistical decision theory. Harvard University.

Reddy, M. J., and Kumar D. N. (2007). Multi-objective particle swarm optimization for generating optimal trade-offs in reservoir operation. Hydrol. Process. 21, 2897–2909. (9)

REDi. (2013). Resilience-based Earthquake Design Initiative (REDi) Rating system.

Reid, H. F. (1911). The elastic-rebound theory of earthquakes. Univ. Calif. Publ. Bull. Dept. Geol., 6(19), 413-444.

Reinhold, T. A., and Ellingwood, B. (1982). Tornado damage risk assess- ment. NUREG-CR-2944/BNL-NUREG-51586 AN, RD—Center for Building Technology, National Bureau of Standards, Washington, DC.

Rose, A. (2004). Defining and measuring economic resilience to disasters. Disaster Prevention and Management: An International Journal, 13(4), 307-314.

Rose, A. (2011). Resilience and sustainability in the face of disasters. Environ. Inno. Soc. Trans., 1(1), 96–100.

Rosowsky, D. V., & Ellingwood, B. R. (2002). Performance-based engineering of wood frame housing: Fragility analysis methodology. Journal of Structural Engineering, 128(1), 32-38.

Saaty, T L., 1977. A Scaling Method for Priorities in Hierarchical Structures, Journal of Mathematical Psychology, 15: 57-68.

Schaefer, J. T., Kelly, D. L., and Abbey, R. F. (1986). A minimum assump- tion tornado-hazard probability model. J. Clim. Appl. Meteorol., 25(12), 1934–1945.

Sen, P. & Yang, J. B. (1998). Multiple Criteria Decision Support in Engineering Design", SpringerVerlag, London.

Simmons, K., Kovacs, P., & Kopp, G. (2015). Weather, Climate, and Society. Vol. 7, April. DOI: 10.1175/WCAS-D-14-00032.1

Simonen, K. (2014). Life cycle assessment. Routledge.

SPUR. (2009). “The resilient city: Defining what San Francisco needed from its seismic mitigation policies”.

Standohar-Alfano, C. and van de Lindt, J. (2014). Empirically Based Probabilistic Tornado Hazard Analysis of the United States Using 1973-2011 Data. Nat. Hazards Rev., 10.1061/(ASCE)NH.1527-6996.0000138, 04014013.

Stein, M. (1987). Large sample properties of simulations using Latin hypercube sampling. Technometrics, 29(2), 143-151.

Strader, S. M., Pingel, T. J., & Ashley, W. S. (2016). A Monte Carlo model for estimating tornado impacts. Meteorological Applications, 23(2), 269-281.

Stewart, M. G., & Li, Y. (2010). Methodologies for economic impact and adaptation assessment of cyclone damage risks due to climate change. Australian Journal of Structural Engineering, 10(2), 121-135.

Takahashi, Y., Kiureghian, A. D., & Ang, A. H. S. (2004). Life‐cycle cost analysis based on a renewal model of earthquake occurrences. Earthquake engineering & structural dynamics, 33(7), 859-880.

Texas Tech University. (2011). A recommendation for an Enhanced-Fujita Scale. Lubbock, TX.

Timmerman, P. (1981). “Vulnerability. Resilience and the collapse of society: A review of models and possible climatic applications.” Environmental monograph, Institute for Environmental Studies, Univ. of Toronto, Canada, 1.

Toro, G. R., & Silva, W. J. (2001). Scenario Earthquakes for Saint Louis, MO, Memphis, TN, and Seismic Hazard Maps for the Central United States Region: Including the Effect of Site Conditions (p. 247). Boulder, Colorado: Risk Engineering.

Turner, R. K. (1992). Speculations on Weak and Strong Sustainability. Centre for Social and Economic Research on the Global Environment (CSERGE).

Tuttle, M. P., Schweig, E. S., Sims, J. D., Lafferty, R. H., Wolf, L. W., & Haynes, M. L. (2002). The earthquake potential of the New Madrid seismic zone. Bulletin of the Seismological Society of America, 92(6), 2080-2089.

Tversky, A., & Kahneman, D. (1992). Advances in prospect theory: Cumulative representation of uncertainty. Journal of Risk and uncertainty, 5(4), 297-323.

Von Neumann, J., & Morgenstern, O. (1944). Game theory and economic behavior.

United Nations (UN). (1998). Kyoto protocol to the United Nations Framework Convention on Climate Change. United Nations, 〈http:// unfccc.int/resource/docs/convkp/kpeng.pdf〉 (Jan. 4, 2012).

U.S. Green Building Council (USGBC). (2012). LEED 2009 for New Construction and Major Renovations.

van de Lindt, J. W., Pei, S., Dao, T., Graettinger, A., Prevatt, D. O., Gupta, R., & Coulbourne, W. (2012). Dual-objective-based tornado design philosophy. Journal of Structural Engineering, 139(2), 251-263.

Wang, M., & Takada, T. (2005). Macrospatial correlation model of seismic ground motions. Earthquake Spectra, 21, 1137–1156.

Wang, Y. and Wang, N. (2017). Retrofitting Building Portfolios to Achieve Community Resilience Goals under Tornado Hazard. 12th Int. Conf. on Structural Safety and Reliability, 2416-2422.

Wang, Y., Wang, N., Lin, P., Ellingwood, B., Mahmoud, H., & Maloney, T. (2018). De-aggregation of Community Resilience Goals to Obtain Minimum Performance Objectives for Buildings under Tornado Hazards. Structural Safety, 70, 82-92.

Wen, Y., and Kang, Y. (2001). Minimum building life-cycle cost design criteria. I: Methodology. J. Struct. Eng., 10.1061/(ASCE)0733-9445(2001)127:3(330), 330–337.

Wesnousky, S. G., Scholz, C. H., Shimazaki, K., & Matsuda, T. (1984). Integration of geological and seismological data for the analysis of seismic hazard: A case study of Japan. Bulletin of the Seismological Society of America, 74(2), 687-708.

Wesnousky, S. (1994). The Gutenberg-Richter or characteristic earthquake distribution, which is it?. Bulletin of the Seismological Society of America, 84(6), 1940-1959.

Williams, P. R., Nolan, M., & Panda, A. (2014). Disaster Resilience Scorecard for Cities. UNISDR. https://www.unisdr.org/we/inform/publications/53349

Zhang, W., & Nicholson, C. (2016) A multi-objective optimization model for retrofit strategies to mitigate direct economic loss and population dislocation, Sustainable and Resilient Infrastructure, 1:3-4, 123-136, DOI: 10.1080/23789689.2016.1254995

Zhang, W., & Wang, N. (2017). Resilience-based Risk Mitigation for Road Networks. Structural Safety, 62, 57-65

Zhang, W., Lin, P., Wang, N., Nicholson, C.D. & Xue, X. (2018). Probabilistic Prediction of Post-disaster Functionality Loss of Community Building Inventories Considering Utility Disruptions. ASCE Journal of Structural Engineering, Special Issue on Structural Design and Robustness for Community Resilience to Natural Hazards. 144 (4), 04018015.

Appendix A. Fragility Parameters for Residential Buildings

Table A.1 Original fragility parameters (structural part) of each building type

Bld. ID	Fragility parameters							
	DS1		DS2		DS3		DS4	
	λ_1	ε_1	λ_2	ε_2	λ_3	ε_3	λ_4	ε_4
W1	0.32	1.01	0.80	1.05	2.47	1.07	6.05	1.06
W2	0.50	0.93	1.25	0.98	3.86	1.02	9.45	0.99
W3	0.50	0.84	1.25	0.86	3.86	0.89	9.45	1.04
W4	0.40	1.01	1.00	1.05	3.09	1.07	7.56	1.06
W5	0.86	0.97	2.14	0.90	6.62	0.89	16.2	0.99
W6	0.48	0.91	0.96	1.00	2.88	1.03	8.40	0.92

Table A.2 Original fragility parameters (non-structural drift sensitive) of each building type

Bld. ID	Fragility parameters							
	DS1		DS2		DS3		DS4	
	λ_1	ε_1	λ_2	ε_2	λ_3	ε_3	λ_4	ε_4
W1	0.50	1.07	1.01	1.11	3.15	1.11	6.30	1.14
W2	0.50	0.98	1.01	0.99	3.15	1.02	6.30	1.09
W3	0.50	0.89	1.01	0.91	3.15	0.90	6.30	1.04
W4	0.50	1.07	1.01	1.11	3.15	1.11	6.30	1.14
W5	0.86	1.01	1.73	0.97	5.40	0.93	10.80	1.03
W6	0.48	0.96	0.96	1.05	3.00	1.07	6.00	0.93

Table A.3 Original fragility parameters (non-structural acceleration sensitive) of each building type

Bld. ID	Fragility parameters							
	DS1		DS2		DS3		DS4	
	λ_1	ε_1	λ_2	ε_2	λ_3	ε_3	λ_4	ε_4
W1	0.16	0.72	0.32	0.70	0.64	0.67	1.28	0.67
W2	0.20	0.71	0.40	0.68	0.80	0.66	1.60	0.66
W3	0.25	0.73	0.50	0.68	1.00	0.67	2.00	0.64
W4	0.20	0.72	0.40	0.70	0.80	0.67	1.60	0.67
W5	0.20	0.67	0.40	0.67	0.80	0.70	1.60	0.70
W6	0.20	0.65	0.40	0.67	0.80	0.67	1.60	0.67

Table A.4 Fragility parameters (structural part) of two enhanced levels for each occupancy class

Occup. class	Code level	DS1		DS2		DS3		DS4	
		λ_1	ε_1	λ_2	ε_2	λ_3	ε_3	λ_4	ε_4
SF	E2	0.60	0.80	1.81	0.81	6.05	0.85	15.12	0.97
	E1	0.50	0.80	1.51	0.81	5.04	0.85	12.60	0.97
MF	E2	1.03	0.81	3.11	0.88	10.37	0.90	25.92	0.83
	E1	0.86	0.81	2.59	0.88	8.64	0.90	21.60	0.83
MH	E2	0.70	0.91	1.38	1.00	4.15	1.03	12.10	0.92
	E1	0.58	0.91	1.15	1.00	3.46	1.03	10.08	0.92

1. Assume the mean fragility parameter λ of E2 is 1.2 times that of E1

Table A.5 Fragility parameters (non-structural drift sensitive) of two enhanced levels for each occupancy class

Occup. class	Code level	DS1		DS2		DS3		DS4	
		λ_1	ε_1	λ_2	ε_2	λ_3	ε_3	λ_4	ε_4
SF	E2	0.50	0.85	1.01	0.88	3.15	0.88	6.30	0.94
	E1	0.50	0.85	1.01	0.88	3.15	0.88	6.30	0.94
MF	E2	0.86	0.87	1.73	0.89	5.40	0.96	10.8	0.94
	E1	0.86	0.87	1.73	0.89	5.40	0.96	10.8	0.94
MH	E2	0.48	0.96	0.96	1.05	3.00	1.07	6.00	0.93
	E1	0.48	0.96	0.96	1.05	3.00	1.07	6.00	0.93

Table A.6 Fragility parameters (non-structural acceleration sensitive) of two enhanced levels for each occupancy class

Occup. class	Code level	DS1		DS2		DS3		DS4	
		λ_1	ε_1	λ_2	ε_2	λ_3	ε_3	λ_4	ε_4
SF	E2	0.36	0.73	0.72	0.68	1.44	0.68	2.88	0.68
	E1	0.30	0.73	0.60	0.68	1.20	0.68	2.40	0.68
MF	E2	0.36	0.73	0.72	0.68	1.44	0.68	2.88	0.68
	E1	0.30	0.70	0.60	0.67	1.20	0.67	2.40	0.68
MH	E2	0.36	0.73	0.72	0.68	1.44	0.68	2.88	0.68
	E1	0.30	0.65	0.60	0.67	1.20	0.67	2.40	0.67

1. Assume for E1 and E2, λ is 1.2 and 1.44 times that of W2

Appendix B. Capacity Parameters for Residential Buildings

Table B.7 Original capacity parameters of each structural type

Bld. ID	Yield capacity point		Ultimate capacity point	
	D_y (in)	A_y (g)	D_u (in)	A_u (g)
W1	0.16	0.10	2.35	0.25
W2	0.24	0.20	4.32	0.60
W3	0.36	0.30	6.48	0.90
W4	0.24	0.20	4.32	0.60
W5	0.16	0.10	2.35	0.25
W6	0.18	0.15	2.16	0.30

Table B.8 Capacity parameters for enhanced performance of each structural type

Occu. class	Code level	Yield Capacity Point		Ultimate Capacity Point	
		Dy (in)	Ay (g)	Du (in)	Au (g)
SF	E2	0.60	0.50	13.81	1.50
	E1	0.48	0.40	11.51	1.20
MF	E2	0.95	0.60	15.00	1.50
	E1	0.63	0.40	12.53	1.00
MH	E2	0.30	0.25	3.50	0.50
	E1	0.24	0.20	3.00	0.40